personal buildup for

Force Motors Ltd.

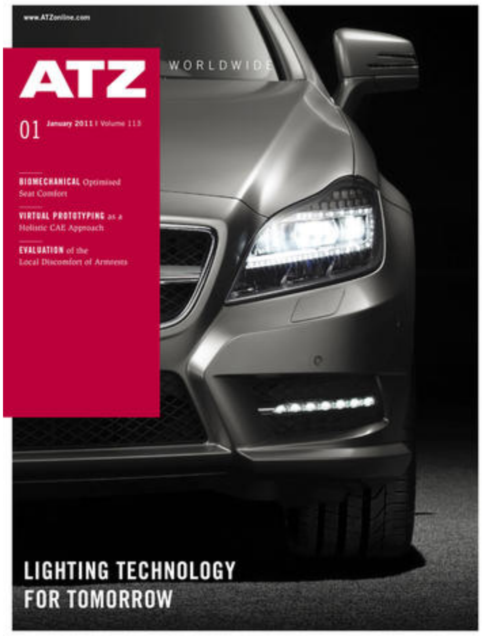

ATZ .worldwide 1/2011, as epaper released on 22.12.2010
http://www.atz-worldwide.com

content:

page 1: Cover. p.1

page 2: Contents. p.2

page 3: Confidence. p.3

page 4: Michael Hamm: Innovative Light Sources for Vehicles. p.4-9

page 10: Stephan Preussler, Rainer Neumann, Vladimir Kubena: Full LED Front Lights with Adaptive High Beam. p.10-15

page 16: Gerhard Silber, Christophe Then, Torsten Gaertner: Increasing Crash Safety Through Biomechanical Optimised Seat Comfort. p.16-19

page 20: Fouad El Khaldi, Raymond Ni, Peter Ullrich, Carlos Terres Aboitiz: Advantages of Virtual Prototyping as a Holistic CAE Approach. p.20-25

page 26: Hans-Peter Schöner, Wolfgang Hurich, Jürgen Luther, Ralf Guido Herrtwich : Coordinated Automated Driving for the Testing of Assistance Systems. p.26-31

page 32: Sebastian Eulert, Georg Lührs, Jan Bräunig, Holger Kunze: Active Noise Reduction for Rear Axle Gear Units. p.32-37

page 38: Wolfgang Schreiber, Holger Westendorf, Bernd Emmermann, Nicole von Wieding : The New VW Caddy ? A Car for Every Occasion. p.38-43

page 44: Peer Review. p.44-45

page 46: Uwe Janoske, Hauke Gregor, Michael Schrodt, Hermann Schwameder : Experimental and Numerical Methods for the Evaluation of the Local Discomfort of Armrests. p.46-51
page 52: Lutz Eckstein, René Göbbels, Martin Goede, Tino Laue, Roland Wohlecker: Analysis of Secondary Weight Reduction Potentials in Vehicles. p.52-60

www.ATZonline.com

ATZ WORLDWIDE

01 January 2011 | Volume 113

BIOMECHANICAL Optimised Seat Comfort

VIRTUAL PROTOTYPING as a Holistic CAE Approach

EVALUATION of the Local Discomfort of Armrests

LIGHTING TECHNOLOGY FOR TOMORROW

CONTENTS

COVER STORY

LIGHTING TECHNOLOGY FOR TOMORROW

4, 10 I The frequency of road traffic accidents by darkness is still twice as high as that by daylight. To bring light into the darkness, ATZ presents advanced developments of lighting engineering for tomorrow. Automotive Lighting uses LED-based headlights in order to variably and adaptively divide the light on the road. For the year 2050, Visteon has designed a car whose LED headlights have the first bending light with adaptive high beam that is ready for series production.

COVER STORY

LIGHTING TECHNOLOGY

4 Innovative Light Sources for Vehicles
Michael Hamm [Automotive Lighting]

10 Full LED Front Lights with Adaptive High Beam
Stephan Preussler, Rainer Neumann, Vladimir Kubena [Visteon]

INDUSTRY

INTERIOR

16 Increasing Crash Safety Through Biomechanical Optimised Seat Comfort
Gerhard Silber, Christophe Then [University of Applied Sciences Frankfurt/Main], Holger Doepner [Tecosim]

DIGITAL PRODUCT DEVELOPMENT

20 Advantages of Virtual Prototyping as a Holistic CAE Approach
Fouad El Khaldi, Peter Ullrich, Carlos Terres Aboitiz [ESI]

TESTING TECHNOLOGY

26 Coordinated Automated Driving for the Testing of Assistance Systems
Hans-Peter Schöner, Wolfgang Hurich, Jürgen Luther, Ralf Guido Herrtwich [Daimler]

POWERTRAIN

32 Active Noise Reduction for Rear Axle Gear Units
Sebastian Eulert, Georg Lührs [Volkswagen], Jan Bräunig, Holger Kunze [Fraunhofer IWU]

NEW CARS

38 The New VW Caddy – A Car for Every Occasion
Wolfgang Schreiber, Holger Westendorf, Bernd Emmermann, Nicole von Wieding [Volkswagen Nutzfahrzeuge]

RESEARCH

44 Peer Review

COMFORT

46 Experimental and Numerical Methods for the Evaluation of the Local Discomfort of Armrests
Uwe Janoske, Hauke Gregor [University of Wuppertal], Michael Schrodt [Gratz Simulation], Hermann Schwameder [University of Salzburg]

LIGHTWEIGHT DESIGN

52 Analysis of Secondary Weight Reduction Potentials in Vehicles
Lutz Eckstein, René Göbbels [RWTH Aachen University], Martin Goede, Tino Laue [Volkswagen], Roland Wohlecker [fka]

RUBRICS I SERVICE

3 Editorial
45 Imprint, Scientific Advisory Board

COVER FIGURE, FIGURE ABOVE © Mercedes-Benz

CONFIDENCE

Dear Reader,

This weekend, we heard the news – at last, one is tempted to say – that the countries organised in the "United Nations Framework Convention on Climate Change" in Cancun have agreed on a target to limit anthropogenic global warming to two degrees Celsius. The (smaller) group of those states who had consented to comply with the Kyoto Protocol even passed a resolution in Mexico that a reduction in CO_2 emissions by between 25 and 40 % by 2020 is necessary.

"Reduction" — that sounds like being forced to give up something. But let us not fool ourselves: even if we dramatically limit ourselves, people in emerging economies will not be deterred from wanting to achieve our level of affluence. Today, around two billion people on this planet live without an electricity supply. And only about half a billion own a car. In 2050, when my oldest son will be 52 years old, the world's population will be between nine and ten billion people, with the fewest of them living in Europe. These people will want the same rights to have internet access, a car, good food and comfortable accommodation as we have. And they will do everything they can to achieve it.

A reason for resignation? I say: no! Let us recall the founders of our prosperity. Inventors like James Watt, Rudolf Diesel or Werner Siemens. They liberated us in the industrialised nations from arduous physical tasks by providing machines to perform our work. Often, they had to battle against tremendous resistance.

Modern engineering generations have to master the challenge of designing energy production and conversion in such a way that our planet does not suffer irreparable damage. The human mind is capable of addressing such challenges. We therefore have every reason to look forward to the future with confidence and to play a part in designing it.

In the hope that you share my confidence, I wish you a Happy New Year!

JOHANNES WINTERHAGEN, Editor-in-Chief
Frankfurt/Main, 12 December 2010

INNOVATIVE LIGHT SOURCES FOR VEHICLES

New light sources conquer the exterior vehicle lighting. LED-based headlamps and taillights offer an attractive design but also the possibility to make lighting functions more variable. Automotive Lighting explains how adaptive distribution of portions of light on the road – related to vehicle speed, oncoming traffic and environmental conditions – become possible now.

AUTHOR

DR.-ING. MICHAEL HAMM
is Head of the Lighting Technology Development and Innovation department at Automotive Lighting in Reutlingen (Germany).

TECHNOLOGY	REFLECTION	LIGHT GUIDE	COMBINATION
FUNCTIONAL PRINCIPLE	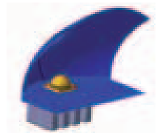	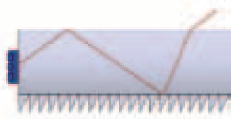	
DIRECT EFFICIENCY (WITHOUT OTHER ELEMENTS)	40 – 60 %	10 – 20 %	40 – 50 %
EXAMPLE	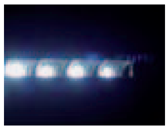		

❶ Technical options for the modern light source LED daytime running the example; efficiency can vary considerably depending on geometric and optical conditions

ONE CENTURY OF BULBS

It is a gradual process, but no one really wants to stop it: the time of the bulbs is coming to an end. After Thomas Alva Edision filed the key patent in 1879, bulbs served all functions of lighting and vehicle lighting for more than a century.

LEDs were first introduced in the 1990s in taillights. This at that time expensive technology was the ultimate solution for space problems or for in those times extremely challenging styling variations. In the headlamps, first "hybrid" models were seen in 2004. This technology leap was supplemented since the late 1980s by the high intensity discharge lamps (HID lamps, called Xenon lights in Germany) for the low beam and high beam function. From 2003 they were also used as curve light.

PHYSICS AND DESIGN POSSIBILITIES OF LED

The properties of the new light source LED are fundamentally different than those of incandescent lamps with tungsten filaments inside. In HID lamps, a plasma is generated. This is created in cherry pit sized burner, where AC voltage drives an ion mixture that produces light via recombination radiation.

But LED light is produced directly in the semiconductor crystal. After the application of a forward voltage the LED emits light direct from the semiconductor material. The resulting colour is defined by the gap between valence and conductive ban. The colour "yellow" originates directly in the LED by using Aluminum-Indium-Galliumphosphid (AlInGaP) based material. The most effective way to generate white colour from the LED is the phosphor conversion process. A blue emitting diode or Indium-Gallium-Nitrite (InGaN) generates in combination with a phosphor layer above the semiconductor the mixture of blue and yellow colour, thus white light.

The surfaces that create luminance in LED have become smaller in comparison to the old bulbs, they are quasi point sources. A single LED used for signal function comes with a side length of the semiconductor crystal of 0.2 mm. A small drawback, however, is this: Even LED not convert all the electrons into photons, a large portion is converted into heat (currently heat losses around 70 %, in four to six years the losses could be reduced to 50 %). The small semiconductor must therefore connected to heat sinks and cooling systems in order not to be damaged irreparably. CO_2 emissions can be reduced by LED [1].

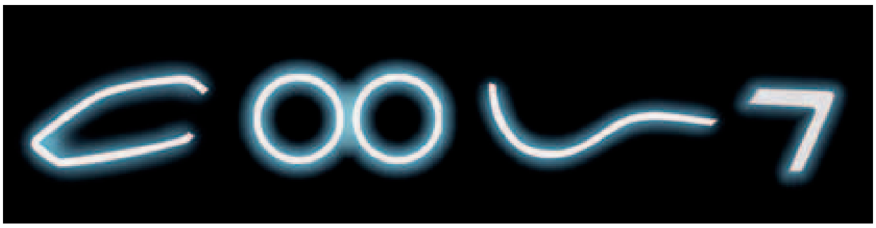

❷ Customized specific day and night styling in the functions daytime running light / position light will more and more be see on our streets (f.l.t.r.: N. N., BMW, Audi, Opel)

LIGHTING TECHNOLOGIES IN THE VEHICLE

The light on the car is subject to legal regulations in order to ensure that the driver or other road users get unambiguous information and to increase traffic safety [2]. Generally, three different technologies and their mixture for light generation can be named:

: Reflection with reflective surfaces (for example aluminum vapor-coated reflectors)
: Projection with optical imaging (for example cylindrical lenses or spherical lenses, which project a virtual light source / light distribution)
: Light guide (optically transparent media, the light is transported inside without losses)
: Combinations of the three basic techniques.

In ❶, the functional principle, the direct efficiency and an example are presented.

LIGHT GUIDES

The characteristic feature of the light guidance through an optical system is the total internal reflection (TIR) that means the rays are 100 % reflected at a surface between an optical medium with high refractive index and the air with low refractive index.

For outcoupling from the light guide again, the beam direction must be changed in order to exit the TIR conditions. Light guides, no matter if tubular, thin or thick, 3-dimensional or free shaped, need on the back side a series of prisms (or general outcoupling elements) that redirect the light in the desired and technically feasible direction, ①. Additionally the prescribed light distribution is produced.

The customer's demand is to have a homogeneous appearance. It should be as evenly lit from many angles of observation, not only in the angular zones that are intended by legislature. The light guides achieve this quite well, but at the expense of efficiency in terms of pure function. Daytime running lights (DRL) with light guides, ❷, however, are still more efficient than conventional incandescent bulbs. Depending on the design and contour significant reductions can be achieved. With a power of 10 to 15 W per headlamp this is just half of the consumption compared to 25 to 35 W of a conventional bulb driven DRL solution.

MAIN LIGHTING FUNCTIONS: LOW BEAM AND HIGH BEAM

In the modern headlamps several submodules jointly generate the light pattern. This means also additional adjustment operations during the production of the complete low beam module. Two sub-modules create a broad, symmetrical basic light distribution. The Mercedes CLS modules were designed in reflection technology around the spot module, in the Audi A7 this are projection modules aside the spot. The spread is about 40° and the maximum of about 10 lux. The spot is a narrow but powerful light distribution with 10° spread and a high maximum of around 65 lux.

In most LED lamps you usually can find a fourth, mostly hidden LED light module. It is the static curve light, also called the cornering light. The purpose is to extend the lateral spread, but is used not only in junctions or turning situations.

ALL-ELECTRONICS HEADLAMP FUNCTIONS

The new all-LED headlamp generations are equipped with adaptive lighting functions. Tthat means the low beam and high beam is controlled automatically to different driving and external parameters to the traffic and weather situations by using electronics control.

Curve light, all-weather lights with integrated fog function, the camera-controlled automatic leveling on rural roads (> 75 km/h) and motorway light (> 115 km/h) are ensuring under all driving conditions an optimal illumination of the road. As described above, modern headlamps today are equipped with several high-power LED modules. Each LED sub-module provides a certain area of road with light. In contrast to the conventional technologies, the light can be "redistributed" electronically depending on the ambient conditions.

ALL-WEATHER FUNCTION

Via a rain sensor or a manual fog light switch the headlamp receives the command to activate the all-weather function. The LED spot module, which is responsible to create a superb range, is reduced in both headlamps to about 60 % of its original power. Thus, the two static cornering light modules are activated, ❸.

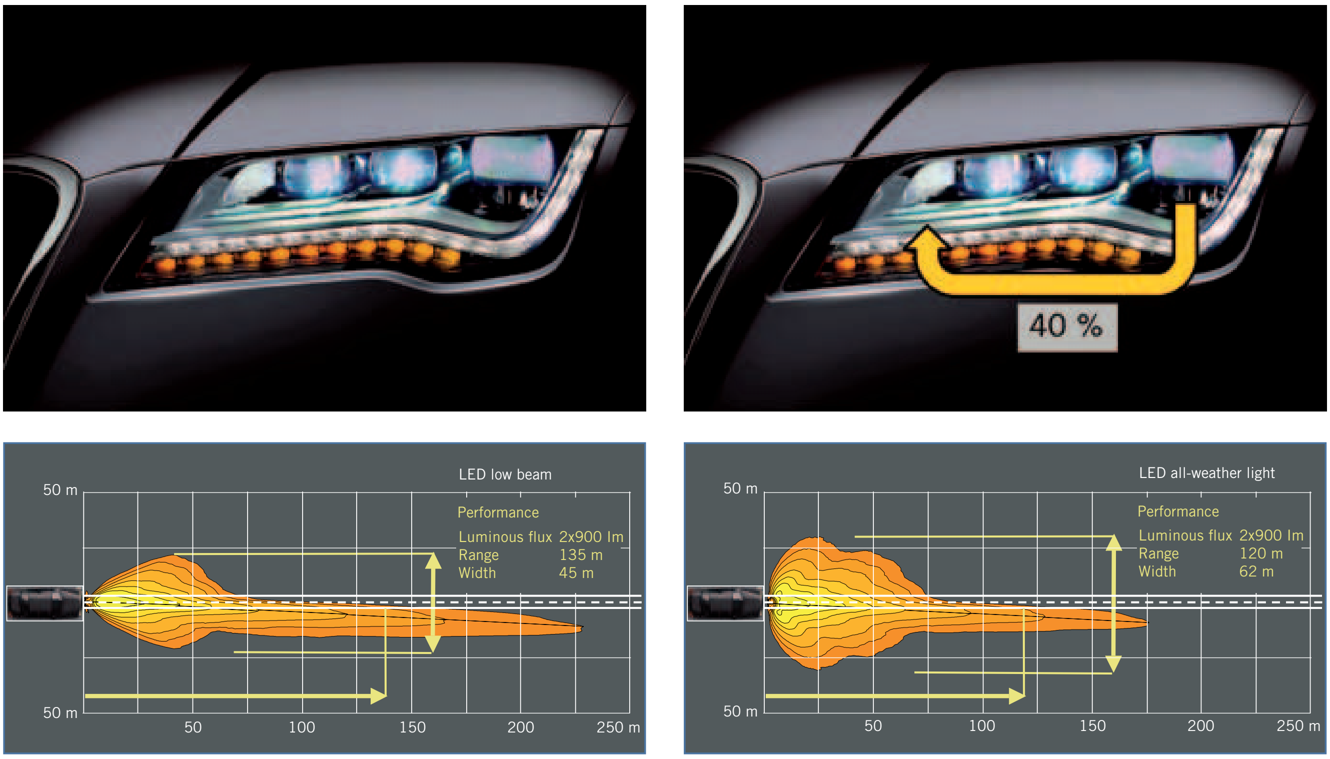

❸ Adaptive LED all-weather light produced by the redistribution of power in the LED headlights; the side illumination is increased and the scope is withdrawn

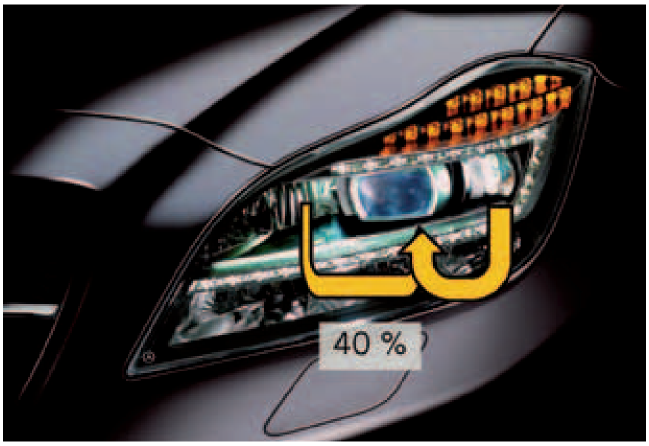

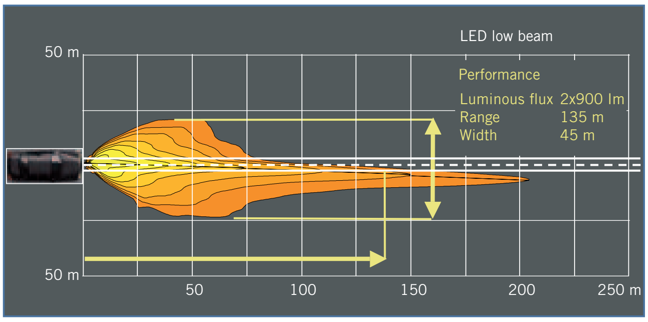

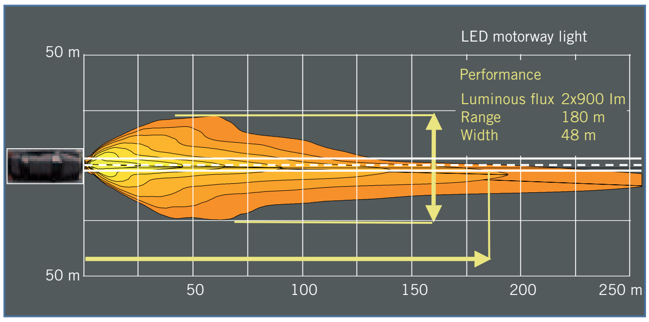

❹ Adaptive LED motorway light produced by the redistribution of power in the LED headlights; range and visibility is increased and side illumination is reduced

The total power consumption in the vehicle remains the same. However, an entirely different light distribution is generated: In adverse weather conditions and low vehicle speeds the light is distributed on the lateral side roadway and increases the orientation on the road. Additionally the redirection of light from the front to the sides reduces both self-glare in fog or glare of oncoming traffic.

By using the navigation system, a predictive light control is possible. In the mode city light, a widened light distribution and a better side illumination in populated areas significantly increase and enhance the driving comfort.

MOTORWAY FUNCTION

Via the navigation system and the speed signal the headlamp receives signals to activate the motorway light function, ❹. The two basic light reflectors that produce a widespread side illumination are reduced in performance. The spot module, which is responsible for creating an outstanding range, is operated in both headlamps with 40 % more power.

The total power consumption in the vehicle remains the same with a completely different light distribution as before: At high speeds on the highway the light distribution enables increased detection distance and more comfortable viewing conditions. The adaptive leveling function on rural roads and highway driving is controlled electronically. Depending on traffic conditions and driving dynamics, the cut-off limit is additionally raised and helps increasing the range of the motorway function.

CURVE FUNCTION

Steering angle and navigation system information indicate that the car is approaching a curve. If the headlights would only look straight ahead, the visibility distance

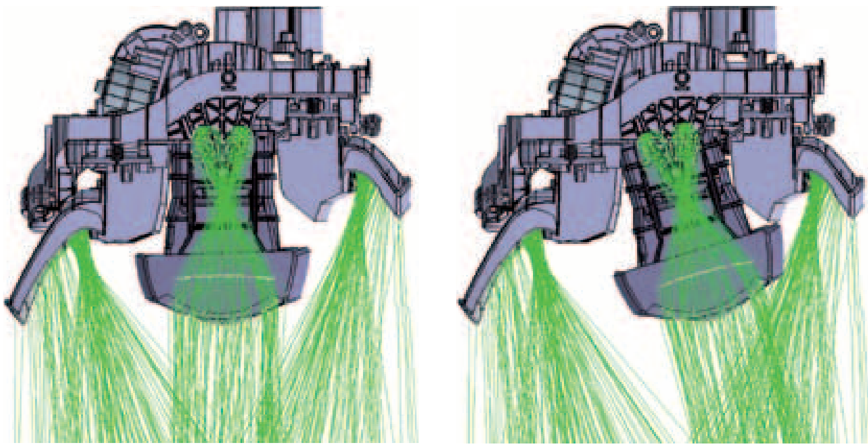

❺ Adaptive LED curve light in the Mercedes-Benz CLS is produced by pivoting the spot module within the complete low beam module; no need to move the two basic light reflectors to the left and the right on the street would be reduced in this particularly dangerous situation. A new developed curve light module allows the ideal adjustment of the central far distance light to follow the course of the road, ❺. Within the module the spot pivots to follow the road, without the need to move the whole system.

In the lower area of its headlamps Mercedes CLS offers an active night-vision system. This function is realized first with a two-dimensional array in infrared technology. An infrared sensitive camera in the vehicle detects the radiated of the street scene and provides the corresponding image on a monitor in the cockpit.

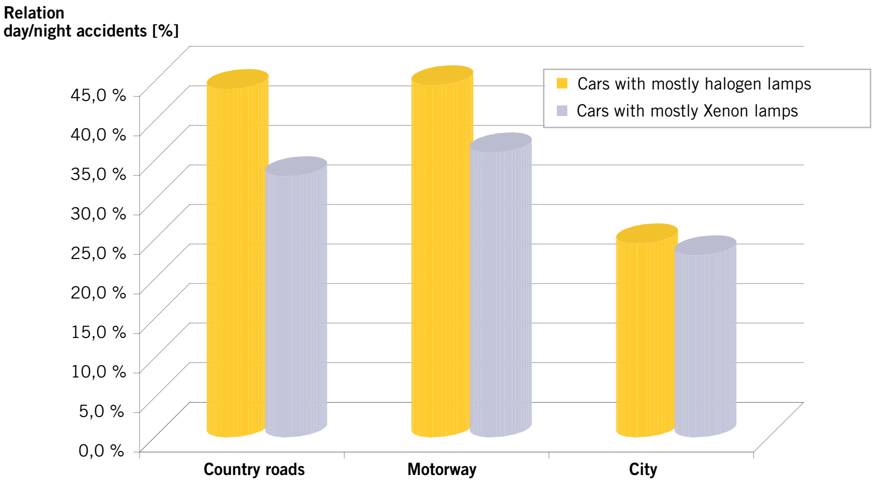

❻ Results of the study by TÜV Rheinland [3]: 30% fewer accidents on highways for vehicles with good light compared to conventional halogen light

PRACTICAL RESULTS FOR TRAFFIC SAFETY

The theoretical potential of a good lighting was so far only a rough guess, although every driver with the "dim light" illumination of a 6-V system remembers the old Bilux lights. Additionally, only a rough separation in light performance could be done. For the first time a study by TÜV Rheinland [3] has proven in 2007 that vehicles equipped with HID light (that means with a performant illumination) in comparison to halogen light (that means with rather minimal conventional illumination) show reduced accident rates at night.

The accident ratio day/night was compared by two different vehicle test groups, ❻. The results show that cars equipped predominantly with HID lights (which are a synonym for good lighting) produce about 30 % fewer accidents on rural roads and motorways [4, 5]. The accident ratio of day / night in city traffic was still the same in the two test groups, however. This increases the reliability of the study and correlates well with the lighting conditions in urban compared to rural roads. Out of town's own lights are often the only light for orientation and there good lighting matters.

If all vehicles in Europe were equipped with such powerful lights, according to the investigations 3970 fatalities and more than 46,000 accidents could have been avoided. The performance of the today's modern LED headlamps has reached or exceeded the HID lights level investigated here – so it is a good perspective those lamps can help reducing accidents. Results will be available most probably in three or five years.

SUMMARY

The electronic headlight is no dream any more. Today navigation, sensor and camera information control the headlamp. They turn, adjust the distribution of light and operate the automatic high beam lamps. The result is together with a good LED module a good light. Good lighting reduces accidents and can prevent fatalities.

The innovative light sources have made a real upheaval in the headlights. Styling and function, attractive appearance and safety are no contradictions any more.

REFERENCES

[1] Hamm, M.: Down with CO_2 Emissions – Ecologic Potential and Limits with Lighting Functions. In: ISAL Proceedings, pp 1 – 10, Darmstadt, 2009

[2] Hamm, M.; Rosenhahn, E.-O.: System Strategies and Technology for Improved Safety and Comfort with Adaptive Headlamps. In: SAE Society of Automotive Engineers World Conference 2001-01-0299

[3] TÜV Rheinland: Studie Lebensretter Xenonlicht. 25. September 2007, http://www.tuv.com/de/news_xenonlicht.html

[4] Schäbe, H.; Schierge, F.: Investigation on the Influence of Car Lighting on Nighttime Accidents in Germany. In: ISAL Proceedings, pp 1 – 5, Darmstadt, 2007

[5] Schöttler, T.; Nehmzow, J.; Otte, D.: Influence of Headlamps for Accident Avoidance. Gidas Study, Hannover, Accident Research Unit of Medical University Hannover, 2010

FULL LED FRONT LIGHTS WITH ADAPTIVE HIGH BEAM

Prototypes are connecting many concept ideas of the future to series production developments of today. Visteon changed over a series production model to its latest demonstration vehicle C-Beyond. Chief among them is the front lighting system capable of meeting the most recent European legislation. It is the first series-production ready full LED application for automatically changing between high and low beam as well as static bending light.

AUTHORS

STEPHAN PREUSSLER
is Leader Advanced Trends Analysis at Visteon in Kerpen (Germany).

DR. RAINER NEUMANN
is Director Global Lighting Business Development at Visteon in Kerpen (Germany).

VLADIMIR KUBENA
is Manager Exterior Lighting at Visteon-Autopal in Novy Jicin (Czech Republic).

ADVANTAGES OF LED TECHNOLOGY

LED light sources are becoming increasingly popular in automotive industry. The stop/tail function of rear lamps, as well as the centre high mounted stop lamp, is an already well known LED application – also due to their quicker response behavior. But the use of LEDs for the main functions of front lighting is fairly recent. The advantages of LEDs include low power consumption, leading to reduced fuel consumption and CO_2 emissions, and a very long product life time – much longer than the expected life cycle of a typical passenger car. Another factor driving the growth in LED applications is the upcoming mandatory requirement for a separate daytime running lamp (DRL) which is ideally suited for the energy efficient, white LED light sources, ❶.

If all main functions in exterior automotive lighting applications are equipped with LED light sources, it is expected that CO_2 emissions can be reduced by 2 to 3 g/km. LEDs also provide a high degree of styling flexibility, offering new options for the appearance and shape of front and rear lamps.

Today, there are only around eight vehicle models on the global market equipped with LED front lighting functions. This modest penetration is mainly due to cost but volumes are likely to increase in the next few years as light source manufacturers introduce increasingly effective LEDs.

Importantly too, the increased efficiency combined with lower power consumption helps to reduce the overall temperature load in the vehicle. The need for active cooling, which currently is handled by fans to remove the heat from the LED chips, will therefore be eliminated offering the additional benefits of reduced weight, packaging space and cost.

LIGHTING TECHNOLOGY IN THE CONCEPT VEHICLE C-BEYOND

Regarding the mentioned aspects cost decreasing and emission reduction, Visteon developed its C-Beyond concept vehicle [1] with a special lighting system. It is the first series-production ready full LED application for automatically changing between high and low beam as well as static bending light. The vision for LED headlamps

scenario in the vehicle model year 2015 confirms as follows:

- LEDs light guides will be more effective.
- Required power consumption will drop.
- Life time will be reliably long.
- Styling flexibility will increase (fewer modules necessary to get same light output).
- Heat load will be reduced (no active cooling necessary).
- Overall costs for headlamps will decrease.
- LED headlamps will be seen in premium segment and electrical/hybrid vehicles.

The C-Beyond front light is equipped with the Visteon's development LED projector module that provides all main beam patterns. The camera-driven, adaptive high-beam system automatically switches between high and low beams according to the flow of passing and oncoming traffic. In addition, the system offers a 'glare-free' mode that enables the lamps to continuously operate in high-beam mode with programmable shutters that reduce the light pattern for oncoming vehicles.

As the first production ready full LED application, the C-Beyond features a Visteon proprietary high intensity LED headlamp which provides all main beam patterns as prescribed by the most recent European regulation (ECE-R-123; also known as AFS-2 functionality). The design of the headlamps draws attention to the main themes of the concept vehicle – sustainability, connectivity and enhanced driving experience – through their advanced functions. All lighting functions in the headlamp are powered solely by light-emitting diodes light sources.

In addition to the main unit, the headlamp also utilizes LEDs for the front position light, static bending, DRL and the turn indicators, ❷. The DRL encircle all functions of the front lights with low powered LEDs which are used as a supplementary styling element to support the outline/real estate of the front lights and create the unique identity of the vehicle.

Sequential turn indicators running fore to aft are placed in between the DRL. The 3D physicality of the individual arrow-shaped segments is distinctive and allows for easy recognition by other traffic partners. A smooth transition towards the static bending cavity is incorporated into the ending of these turn indicators.

	STYLING AND ATTRACTION	WEIGHT	PACKAGING	POWER CONSUMPTION	CO_2 EMISSIONS
LED HEADLAMP LOW BEAM	+	+	+	+	+
LED HEADLAMP HIGH BEAM	+	+	+	+	+
LED DAYTIME RUNNING LIGHT	+	○	+	+	+
LED REAR LAMP	+	○	○	+	+

❶ Trends in automotive lighting – more efficiency with LED light sources

❷ Full-LED headlamps provide packaging flexibility for brand differentiation and reduced depth, while reducing power consumption

Position lamps are divided into three sections and make use of vacant space on the dark grey frosted bezel, again enhancing the distinctive styling of the lights. The position lamps draw attention to the main component of the front lamps – the adaptive high beam unit with its unique mechatronics.

The headlamps' performance is on par with today's high intensity discharge (HID, called Xenon in Germany) technology with low beam demonstrating an improvement over current HID projector unit performance with lumen output of the low beam of more the 1000 lm, ❸. In addition to this headlamp's optical performance, the compact dimensions and low weight makes the module an ideal building block for future full LED headlamp applications.

THERMAL MANAGEMENT

The thermal design of the headlamp eliminates the need for active cooling and the concept employs a unique passive cooling concept for all functions. This approach increases the reliability of the system by reducing the risk of mechanical movement inside of the headlamp assembly which might otherwise cause failure or spread dust inside the lamp.

To enable the elimination of the active cooling system very efficient driving electronics are needed. Each watt of electrical power saved has a positive impact on the weight of the lamp but also helps to ensure that the thermal design is supporting the electronics components inside of the lamp. The overall efficiency of the LED driving module exceeds 87 % meaning that just 13 % is transformed (lost) by heat dissipation. The highly efficient driving electronics for the C-Beyond head lamps are using a microprocessor based buck boost approach and allow to exceed the lighting performance of standard HID lamps.

CAMERA-DRIVEN ADAPTIVE HIGH BEAM SYSTEM

Incorporating a camera-driven adaptive high beam system, the car is capable of automatically adapting its lighting to stay on full beam without dazzling oncoming traffic. The system automatically switches between high and low beam according to the flow of the proceeding and oncoming traffic and also offers a glare-free mode. This feature enables the lamps to continuously operate in high-beam mode with programmable shutters employed to reduce the light pattern for oncoming vehicles.

The system works by using an integrated camera to detect vehicles and adapt the beam pattern in such a way that other road users are not glared. This feature gives the driver the added advantage of having more light on both sides of oncoming or proceeding traffic while the performance is close to high beam, ❹.

The position of the dark spot (the area that is calculated to avoid dazzling oncoming traffic) is determined by the camera. This automation offers real safety as well as a comfort benefits for the driver. There is no need to operate the high beam / low beam lever to change the beam pattern when proceeding or oncoming traffic appears. The system is also capable of detecting public illumination systems and automatically switches high beam back to low beam

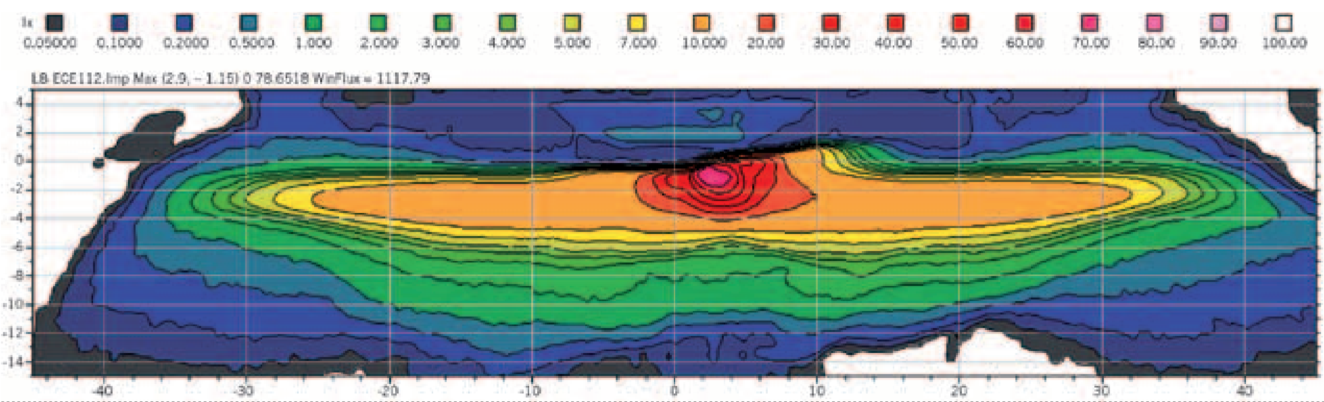

❸ The full-LED headlamps' performance is on par with today's high intensity discharge technology with low beam demonstrating an improvement over current high intensity discharge projector unit performance with light output of the low beam of more the 1000 lm or town mode, depending on the speed of the vehicle. As a result, the high beam mode is typically used three times more than on conventional systems. That improves the driver's visibility when driving at night.

PREDICTIVE ADAPTIVE FRONT LIGHTING

To improve the driver's visibility and awareness when driving at night, headlamp direction is synchronized with the navigation system. The state-of-the-art predictive advanced front lighting concept uses global positioning data to predict the road ahead and adapts the beam pattern of the headlamps to the road scenario before steering input occurs.

Unlike conventional adaptive front lighting systems, which calculate the beam pattern of the headlamps based on the steering-wheel angle and vehicle speed, the predictive advanced front lighting concept is connected to the navigation system by utilizing an advanced driver assistance system (ADAS) with artificial horizon provider. Processing vehicle and navigation information, this interface determines the road shape and the most likely path of the road ahead. This information is used by a new algorithm to calculate the most likely driving path of the vehicle and enables the predictive advanced front lighting system to adapt the beam pattern of the headlamps accordingly, ❺.

❹ The camera-driven adaptive high beam lighting system automatically switches between high and low beam to match the actual traffic situation. The system also offers a glare-free mode that reduces the light pattern for oncoming vehicles.

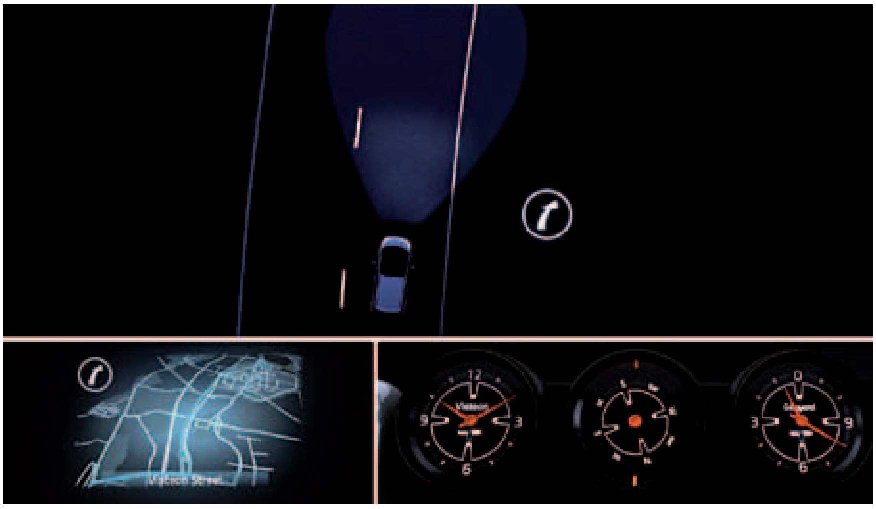

❺ The adaptive full-LED headlamps are a projector-based solution that satisfies legislation according to regulation ECE-R-123

SEQUENTIAL LED TURN INDICATOR

Additional advanced features include a unique sequential LED turn indicator, which provides distinctive features for front and rear turn indicator functionality. Using mid power LEDs and incorporating a unique sequential switching pattern, arrow shaped LED segments create the sequential turn indicator for easy signal recognition and a distinctive design feature.

The sequential turn signal points outboard of the vehicle. The LEDs are illuminated with a small time delay to the previous one to achieve a clearly visible sequential turning signal, ❻.

SOLID LED LIGHT GUIDES

The LED light guide, when used as DLR's accentuated the outline of the headlamp and provide an easily recognized brand signature for the vehicle. Numerous low power LEDs are distributed along the outline shape of the headlamp and achieve a homogenous appearance by a frosted surface on top of the optical filter.

Solid light guides for C-Beyond offer additional styling options with reduced power consumption through the efficient optical design and use of LEDs. The design of the front position light is achieved by using numerous low power LEDs together with a volume filter. The high number of low power LEDs allows the automotive designer to fill in unused space inside the headlamp with lighting features and guarantee efficient power consumption to keep the overall cost of the system in a reasonable range. The white LEDs can also be used as an attractive styling differentiator – with the additional benefit of improving visibility.

The C-Beyond headlamps also incorporate a unique LED static bending functionality using a two or four chip LED array. Static bending functionality helps the driver to illuminate the bend on curvy roads and improves the visibility other road users such as cyclists and pedestrians at night. Visteon's headlamp demonstrates a very good colour match between the LED low beam and the LED static bending light enlarging the side dispersion

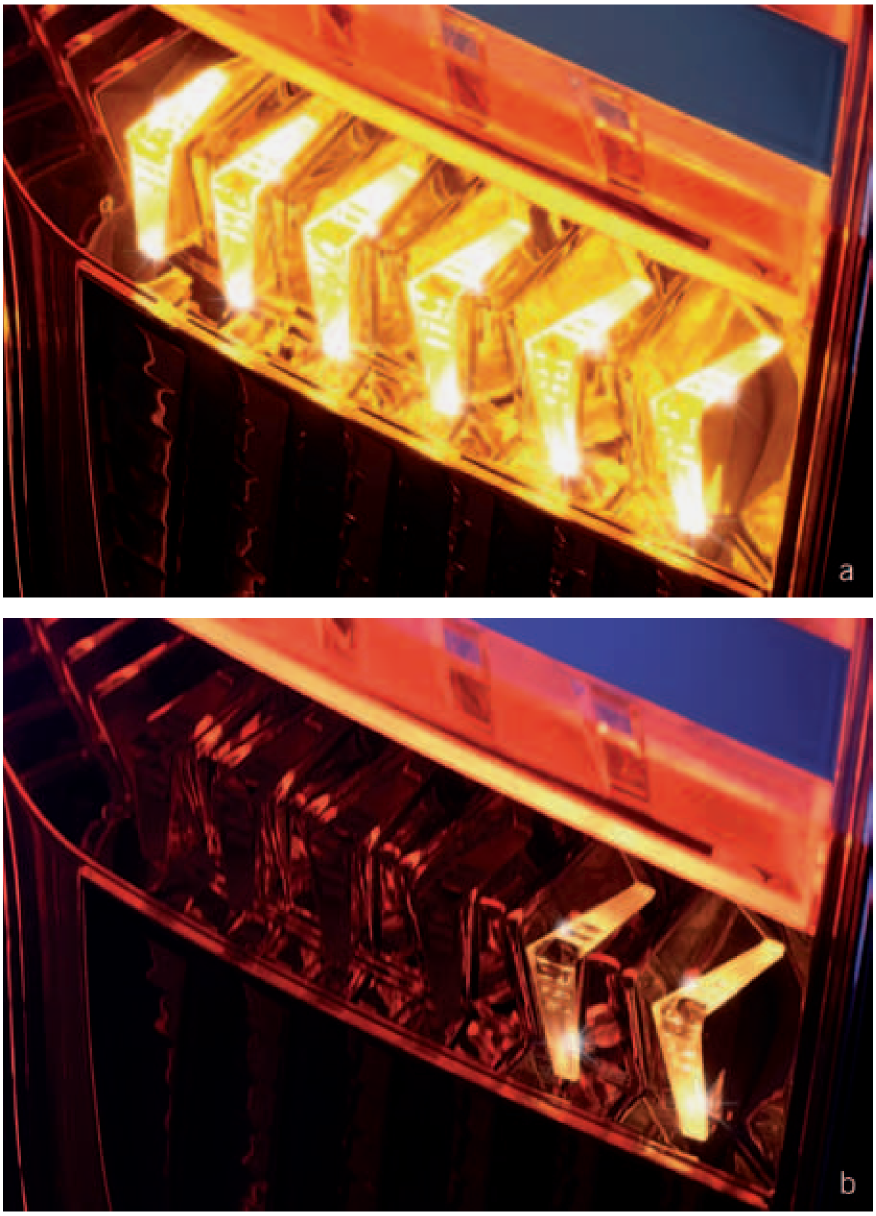

❻ Unique lighting feature for front and rear: sequential LED turn indicator with full (a) and partly (b) illumination

of the main beam. The compact and modular approach highlights Visteon's competence at developing and delivering modules which can be widely used across many different vehicle OEM platforms.

REAR LIGHT IN LED TECHNOLOGY

The C-Beyond rear lamps are also equipped with full LED light sources in combination with thick light guides and blocks for styling purposes; no halogen or incandescent bulbs are used. The LED rear lights incorporate light guides to build a frame for the lamp and to enhance the instantly recognizable character of the design. In addition to the rear sequential turn indicators, numerous 3D physical objects are used for tail light, fog light and stop light functions.

The full LED rear light includes tail, stop, turn and rear fog functionality and incorporates a lit to the edge tail light. This is a unique flat planar light guide with a small amount of low power LEDs which are capable of illuminating closely to the edge of the lamp. This is very close to the welding edge – a technology that has not been possible before.

The rear lamp also features a sensor which can be programmed to function as ambient lighting and a dirt sensor. The ambient lighting function uses the sensor to change the intensity of the tail lamp to suit day or night conditions by decreasing illumination during the night and increasing during day light to avoid glaring of other backer drivers (standing at traffic lights). The dirt sensor function detects if the lens is covered by dirt or grime and automatically increases the illumination intensity within the values defined by regulation.

The stop lamp is achieved by using the same thick light blades as in the rear fog lamp. The light blades are manufactured by using a unique over molding plastics injection method which ensures an excellent surface quality and avoids shrinkage of the plastic material which may impair the light distribution.

MARKET ACCEPTANCE

Visteon represents with the C-Beyond concept vehicle its vision of modern lighting technology and sustainable mobility. The vehicle and its technology has received very positive reviews from vehicle manufacturers at demonstrations throughout Europe, Japan and China. The C-Beyond represents a vision of how seamless connectivity and sustainable mobility may influence the way consumers use and interact with the next generation of vehicles.

Using results from intensive market studies and research methodologies, the visionary car incorporates insights gathered from consumers and vehicle manufacturers around the world. The concept is a working demonstration of Visteon's core strengths – regarding in-vehicle technology integration in its core product lines of climate, electronics, interiors and lighting. In addition, enhanced personalization and individual comfort features for all occupants promote new ways of enjoying and connecting to the vehicle.

REFERENCE

[1] Pudenz, K.: Neue Mobilitätsszenarien im C-Beyond-Konzeptfahrzeug von Visteon. In: www.ATZonline.de from 24th June 2010

INCREASING CRASH SAFETY THROUGH BIOMECHANICAL OPTIMISED SEAT COMFORT

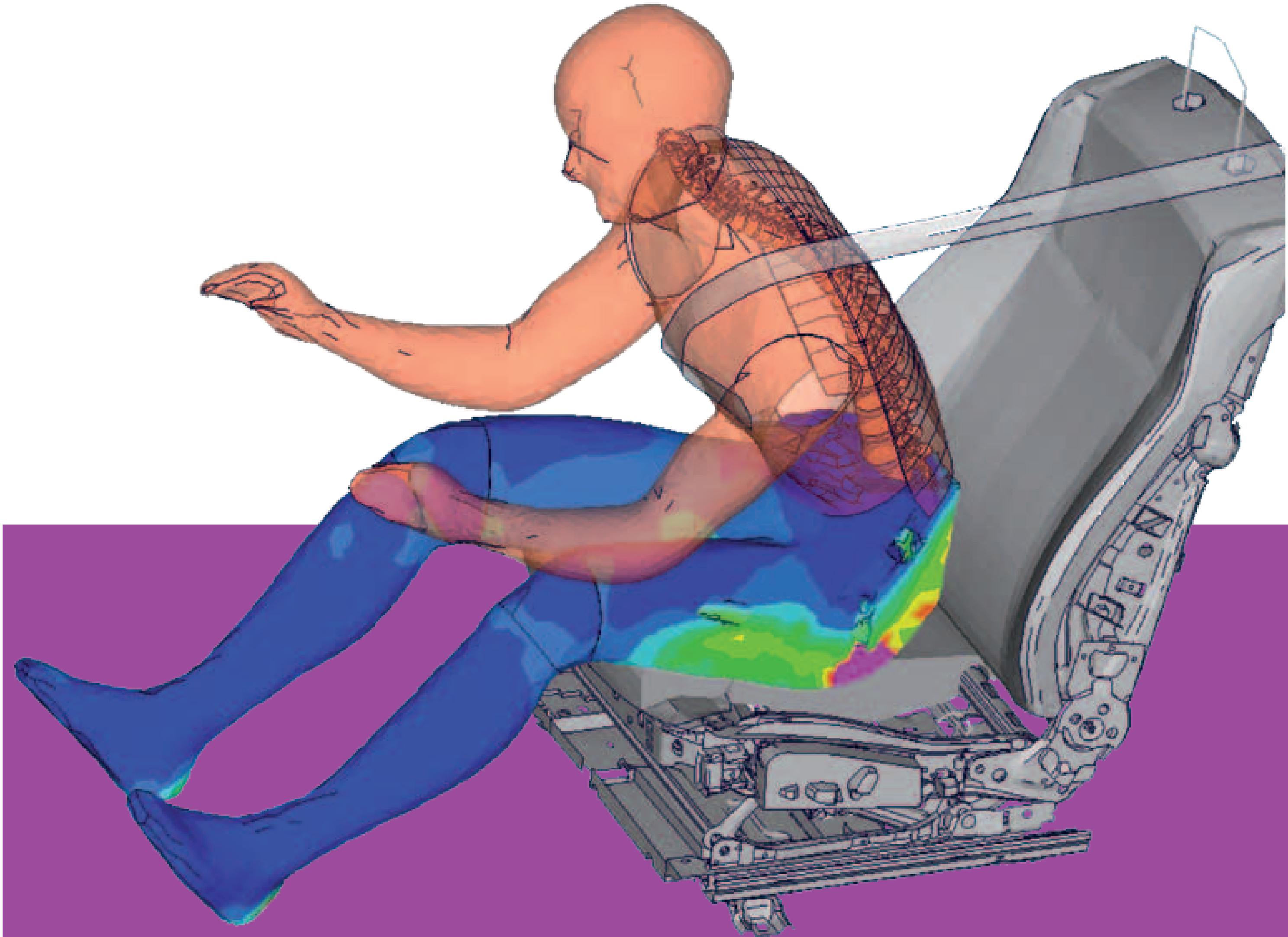

personal buildup for Force Motors Ltd.

For years, crash safety of passenger car seats are in advanced development and optimisation with simulation tools. Vice versa, the comfort is investigated as far as possible by empirical measurement techniques. Using the Boss method, developed by Tecosim Technische Simulation GmbH and University of Applied Sciences Frankfurt/Main, for human model-based optimization, safety and comfort can be increased in parallel.

AUTHORS

PROF. DR.-ING. HABIL. GERHARD SILBER
is Managing Director of the Institute for Materials Science (ifm) at the University of Applied Sciences Frankfurt/Main (Germany).

DIPL.-ING. MENG CHRISTOPHE THEN
is project leader Biomechanics/ Soft Tissue at the Institute for Materials Science (ifm) at the University of Applied Sciences Frankfurt/Main (Germany).

DIPL. ING. HOLGER DOEPNER
is Technical Specialist for Crash Interior Pedestrian at Tecosim Technische Simulation GmbH in Rüsselsheim (Germany).

COMPROMISE OF SAFETY AND COMFORT

In the development of modern vehicle seats, especially for automobiles, both the comfort and safety are equally important key aspects: The aim is high comfort level and maximum safety. Both aspects are not to be strictly separated from each other; most likely comfort can have a strong impact on safety aspects.

To determine and optimize seat characteristics in crash situations, simulation methods are already being used and models are verified by crash tests with dummies. In contrast, the optimization of the comfort of vehicle seats is largely empirical and is therefore dependent on the subjective impression. Further comfort enhancements are made in isolation and often subordinated in crash safety aspects, which are strictly regulated by law.

In a research project by Tecosim Technische Simulation GmbH and the Institute for Materials Science of the University of Applied Sciences Frankfurt/Main a method is developed for optimizing the crash safety of car seats, which includes, in particular, the comfort evaluation in the process.

CURRENT STATE OF SEAT DEVELOPMENT

In the development of modern vehicle seats, a large number of required product characteristics have to be considered. Besides the integration of further functions they should comply with requirements for crash safety at a minimum weight.

The development is to a large extent using numerical simulations for front-, rear- and side crashes, and luggage retention. Comfort aspects cannot be detected in these simulations and therefore must be examined in a separate step.

HUMAN MODEL-BASED PROCESS

The currently developed process is, on one hand, intended to evaluate and optimize the crash performance of vehicle seats in dynamic simulations. On the other hand, comfort properties will be evaluated with the so-called Boss method (Body Optimization and Simulation System). For both parts of the process it is necessary to create each considered seat as a FE simulation model. This normally is done based on CAD-data or, in case of further development of an existing seat, through changes on existing seat models. Conceivable, of course, is pure comfort evaluation of an existing seat. In this case, CAD data can also be determined in a reverse engineering process [1]. In any case it is important to know all material properties, especially of the stiffness of the seat foams. Possibly material tests are necessary which take into account the higher strain rates occurring in crash tests.

In assessing the dynamic properties of the seat usually the front crash and rear crash as well as luggage retention are considered. In these test no fractures or sharp edges should occur and plastic strains should be limited to approximately 10 – 15 %. The usual approach is to initially consider only the system occupant, seat and belt. Due to the lack of interaction between occupant and vehicle interior, no injury values are calculated which would be used for the vehicle assessment, for example as per FMVSS and NCAP.

But in belted load cases a small pelvis forward motion is desired early to effectively couple the occupant to the vehicle during deceleration. Integrated seat ramps can help to reduce the pelvis forward motion, but may have a negative effect on comfort. In side crash a lateral guidance is advantageous to keep the occupant away from intruding side structures, especially in the rib area. The shape and stiffness of the seat foam and the underlying structure will be optimized to reduce injury values like pelvis forces and rib intrusions. However, such a crash-optimized seat often is not found comfortable so that there are further needs for optimization in terms of comfort.

After dynamic simulations, the model iterations of the seat, also created using common optimization tools, are directly examined in terms of comfort. For this a software environment is created where the seat model can be assessed relatively quickly with the Boss method. This includes in particular the derivation of a “comfort level” from the calculated tissue tension.

OBJECTIVE EVALUATION OF SUBJECTIVE COMFORT FEELING

To design lying, sitting or shoe systems still pressure sensor matts are used

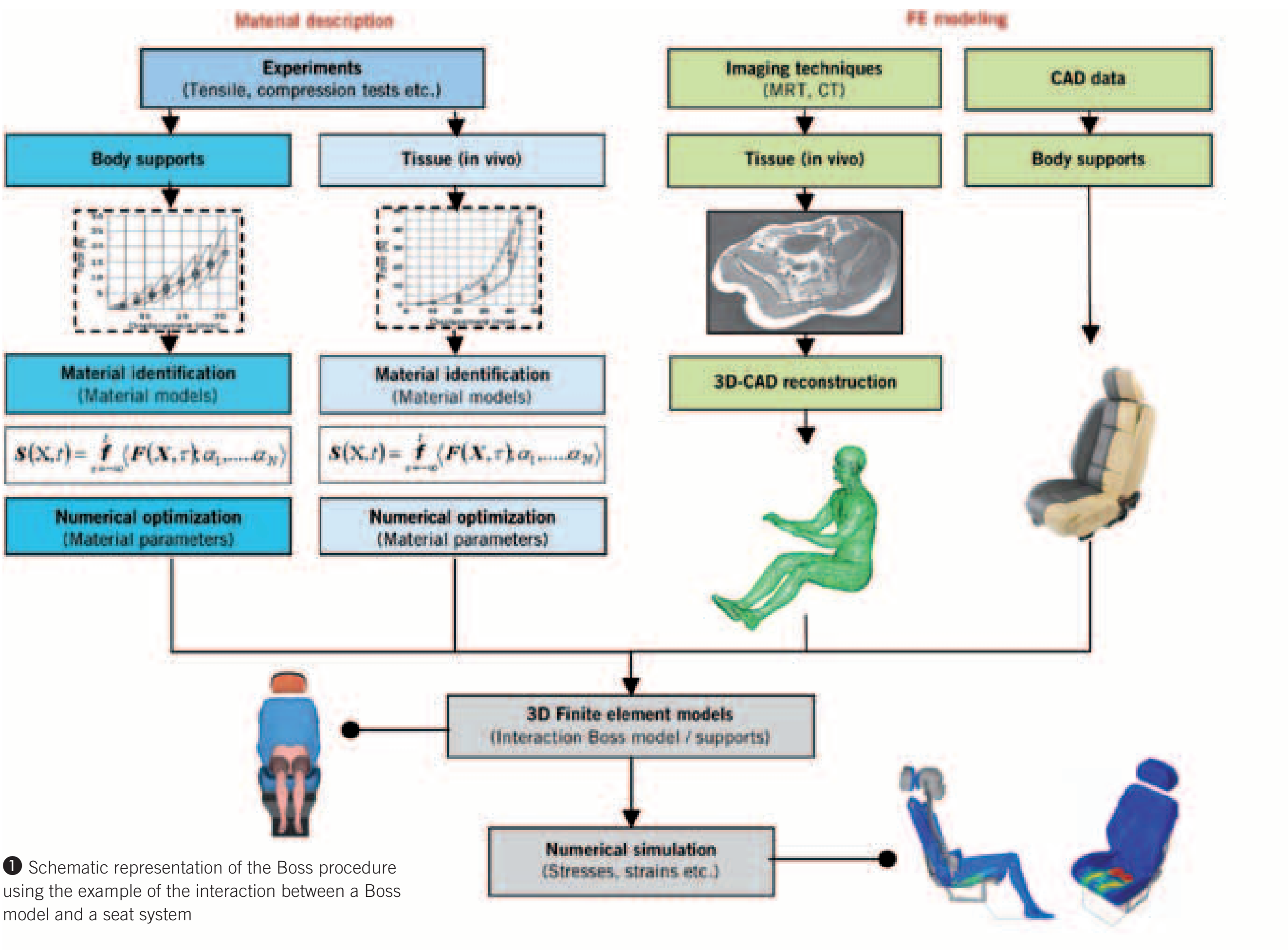

❶ Schematic representation of the Boss procedure using the example of the interaction between a Boss model and a seat system

today. However, these sensor matts provide only planar contact pressure between skin surface and technical body support (t_{SK}) – therefore they capture only extremely limited the very complex three-dimensional interaction between human and body support. In this way it is not possible to sense shear forces as well as stresses in deeper tissue layers to the bone. Until now an adequate method was missing, which is able to quantify and qualify the mechanical interactions in an objective way.

The newly developed Boss method combines engineering methods with modern medical technology and focuses not only on the technical description of the body supports, such as vehicle seats, but also lying systems, sports shoes and health shoes. Rather, the Boss method is characterized by the combination of all data describing the process: This includes experimental methods for determining the mechanical properties of the body support materials and the biomechanical in-vivo properties (in-vivo = in the living) of the human (soft) tissue (fat-muscle-associations) as well as the ex-vivo properties (ex-vivo = outside of the living) of tendons, ligaments or blood vessels. The method also includes the digitizing of shape and geometry of the body support. This follows to the representation of human anatomy and generation of adequate human models (Boss models) by means of imaging techniques such as magnetic resonance imaging (MRI) and 3D reconstruction tools for subsequent overpass the two-dimensional MR images into three-dimensional structures.

In this procedure the in-vivo mechanical characterization of human (soft) tissue has a central position. It represents the major challenge because it has to be strictly non-invasive in contrast to technical materials. This non-invasive method is carried out with tensile tests on the respective region of interest on the body of a living person using MRI environment. The result of this test is a force-displacement characteristic. At the same time the

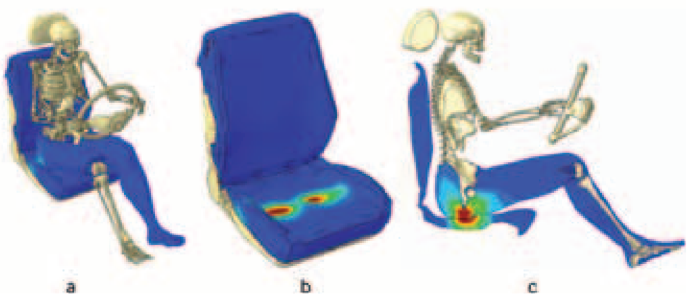

❷ Interaction of a finite element Boss model with a vehicle seat; a: Interface stresses on the seat surface; b and c: Stress distribution in the tissue and seat material in the sagittal section at the level of the ischial tuberosity

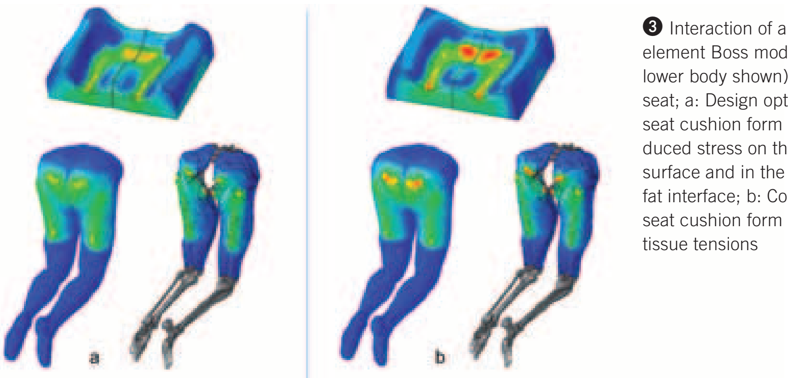

❸ Interaction of a finite element Boss model (only lower body shown) with a seat; a: Design optimized seat cushion form with reduced stress on the skin surface and in the muscle-fat interface; b: Commercial seat cushion form with high tissue tensions

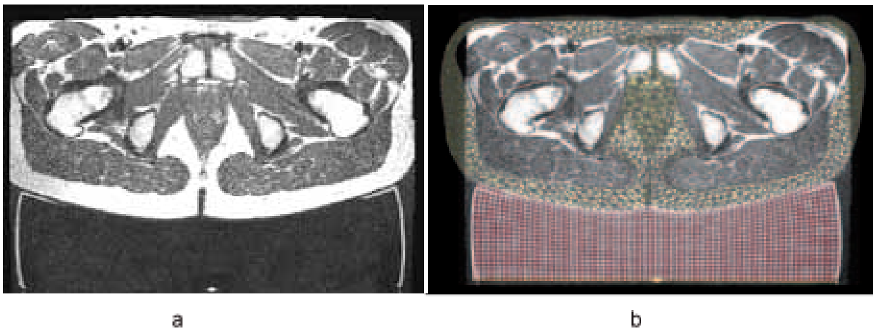

❹ Verification experiment to assess the quality of the model; a: MRI scan of the loaded buttocks; b: Visual match with the corresponding simulation model

necessary geometry information of the deformed tissue is recorded by means of the MRI device. All digitized data lead to a numerical tool in the form of a finite element model of the interacting system Boss model / body support, ❶, on whose basis the analysis of complex interactions in the form of stress and deformation is possible.

Using the FE method, the stress distribution in the region of tailbone and ischium due to interaction between Boss model and vehicle seat is calculated, ❷. It can be shown that depending on the anatomic position, completely different tensions in the body tissues may occur, ❸.

To verify the material parameters of tissue and body support it is necessary to generate loading situations in experiment and simultaneously simulate them with FEM. Such a verification test is shown in ❹. In this case the buttocks tissue was deformed with a cushion and the deformation in turn recorded by MRI (④ a, cut image). The comparison of the sectional view with the simulation result is shown in ④ b. For this section there is a good correlation between deformed fat- and muscle tissue and the cushion.

Using FE simulation the regions with increased stresses in the tissue are determined and in iterative optimization steps geometry and material of the seat structure is changed, until a reduction of maximum stresses and strains in the tissue is found (biomechanical hypothesis) [2 – 7].

VERIFICATION BY MEANS OF PROBAND STUDY

To verify the optimized seat geometry a study with volunteers will be done to assess the subjective perception of comfort. Here a comparison is made between physical reality and numerical simulation and a correlation between the objectively quantified results and the subjective sensation is created.

The verification process is iterative and recursive and should serve as a basis for re-optimization. An important criterion is to use the same physical key data, such as size and weight of the volunteers and the numerical dummy models.

OUTLOOK

The creation of the necessary software environment and the implementation of the Boss method in the process of human model-based optimization are in progress. A completion is scheduled for early 2012. It is expected that with this new process crash performance and comfort can be objectively evaluated in combination at an early stage of the development.

REFERENCES

[1] Müller-Bechtel, M.: TecBench – Virtual Benchmarking: Comparing Products with CAE Methods. IABC International Automotive Body Congress, Vaals, The Netherlands, 2008

[2] Schrodt, M.; Benderoth, G.; Silber, G.: Hyperelastic Description of Polymer Soft Foams at Finite Deformations. In: Technische Mechanik, Bd. 25, Heft 3/4, 2005

[3] Silber, G.; Schrodt, M.; Benderoth, G.; Abolmaali, N.; Vogl, T. J.: An In-vivo Method to Determine the Mechanical Behaviour of Human Soft Tissue. In: Proceedings Cadfem Users Meeting, Zurich, Switzerland, 2005

[4] Silber, G.; Schrodt, M.; Then, C.; Benderoth, G.; Balzer, J. O.; Vogl, T. J.: Mechanical Interaction Between Human Soft Tissue and Elastic Supports: In: 5th World Congress of Biomechanics, 2006, Journal of Biomechanics, Vol. 39, Suppl. 1, 2006

[5] Silber, G.: Ein neuartiges Verfahren zur Gestaltung, Bewertung und Prüfung von Anti-Dekubitus-Systemen. In: Orthopädie-Technik, Nr. 8, 2007

[6] Then, C.; Menger, J.; Benderoth, G.; Alizadeh, M.; Vogl, T. J.; Hübner, F.; Silber, G.: A Method for a Mechanical Characterisation of Human Gluteal Tissue. In: Tech Health Care, 15:385-398, 2007

[7] Then, C.; Menger, J.; Benderoth, G.; Alizadeh, M.; Vogl, T. J.; Hübner, F.; Silber, G.: Analysis of Mechanical Interaction Between Human Gluteal Soft Tissue and Body Supports. In: Tech Health Care, 15:1-16, 2007

FIGURE © Volkswagen

ADVANTAGES OF VIRTUAL PROTOTYPING AS A HOLISTIC CAE APPROACH

The efficient integration of the different CAE processes is a key factor for the automotive industry to reach the development goals in the given time and cost limits. The ESI Group together with Volkswagen Group bets on the right horse to use a single core model for different domains. Thus, crash simulation over NVH considerations to lightweight design investigations can use the same data with implicit code.

AUTHORS

FOUAD EL KHALDI
is Manager Industry Marketing and Solution Strategy at ESI Group in Paris (France).

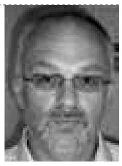

PETER ULLRICH
is Product Line Manager for Virtual Performance Solution of ESI Group in Eschborn (Germany).

CARLOS TERRES ABOITIZ
is Technical Director with the main objective of developing the End to End Virtual Prototyping Strategy of ESI Group in the Spanish Industry at ESI Group in Madrid (Spain).

INTEGRATION OF THE DIFFERENT CAE PROCESSES

Automotive developers are permanently confronted with new challenges. One of many examples is the development of 'green vehicles', which is highly topical. For achieving the defined goals a significant weight reduction is inevitable. An objective that only can be achieved with the usage of new design and production methods in combination with advanced or new materials as it was shown in the European research program "Super Light Car" coordinated by Volkswagen, ❶.

The development of innovative products within short development cycles and at low costs is mostly incompatible with costly and time intensive tests with physical prototypes. For a leaner and more effective vehicle development right before going to mass production automotive developers more and more use Computer Aided Engineering (CAE) methods to get a holistic approach and for reducing physical tests to a minimum and avoiding iteration loops ("Get it right the first time").

The success of such measures highly depends from the efficiency of the implemented CAE processes. In recent times the focus clearly is on the integration of the different CAE processes. ESI Group has strongly concentrated on the multi-domain and production-oriented simulation and is pursuing three main topics:

1. Optimized simulation by using a single core model
2. Integration of manufacturing simulation for more realistic virtual prototypes
3. Practice-oriented content management and process automation.

FIRST CRASH INVESTIGATIONS AT VOLKSWAGEN

Already since the middle of the 1980s there was a close relation between ESI Group and Volkswagen. Even at the development of new CAE methods ESI Group intensively cooperates with a number of enterprises of the Volkswagen Group and took several suggestions/experiences for its software tool development.

In the beginning it was a crash simulation (VW Polo) on a quite simple vehicle structure, but meanwhile the different brands are emphatically following a simulation driven car development on the base of Virtual Prototyping and an integrated manufacturing simulation. By using ESI's Virtual Performance Solution with its integration of different simulation solutions referencing on only one core-model for crash and the analysis of different load cases they could strongly increase their efficiency in different project stages and gain a decisive competitive edge.

INTEGRATION OF MODELS FROM DIFFERENT DOMAINS

Automotive structures have to meet performance targets in different domains. In conventional development processes this causes the application of different software solutions for crash, safety, noise, vibration and harshness (NVH), chassis, lightweight design etc. They not only have a specific input and output format but they even need different pre- and postprocessors, modeling methods and a lot of application specific know-how. For the interactions between the single domains additional processes and resources are necessary. Therefore companies are forced to define rigid workflows with corresponding modeling methods, interfaces and solver-specific programs. These measures cause losses in respect of the

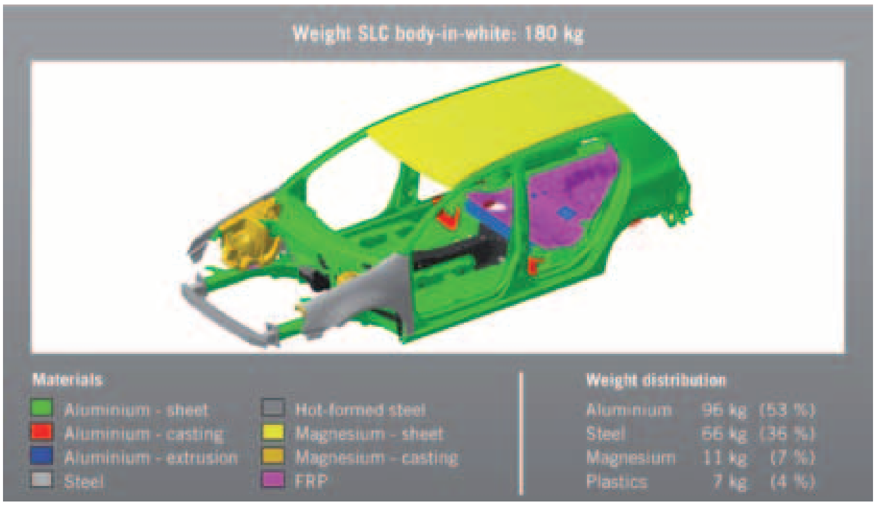

❶ Weight savings at the Super Light Car by using modern materials [1]

availability of engineering resources as well as for the available development time.

The current trend is to adopt "end-to-end" software solutions that enable sharing a common core compute model across multiple domains, at the level of components, products, or enterprise. They allow an efficient and easy management of computer models for different load cases, ❷. Beyond merely sharing node and element data, such solutions allow sharing across domains comprehensive content such as material models, connections, or contact interfaces.

The needed technology has been developed by ESI Group for such an approach and was created to a virtual solution that has been specified and validated with strong involvement of industrial partners, in particular Volkswagen Group companies. With such an integrated solution it is possible to develop a single data set for a problem, for example a seat belt anchorage simulation, on which the simulation models of the different domains can reference.

In a conventional process the original model, created for crash-tests, has to be used even for quasi-static stiffness analyses with crash codes due to different reasons. Using the new approach allows engineers to stay within the same core built for crash tests and switch an implicit code to perform the quasi-static simulation. Such an approach has significant advantages since implicit codes need much less compute time and enable a much easier set up, ❸. The car manufacturer Seat spent a lot of effort to intensively investigate integrated processes with the intention to merge a larger set of static/modal analyses with their crash models.

IMPACT ON IT COSTS

The diversity of applications in a conventional CAE environment has a direct impact on the information technology (IT) costs, as each solution needs service, validation of updates, specific solutions for the model data management, and last but not least training expenditures. In addition, an increasing number of applications even lets the hardware costs grow because they may have quite different system requirements.

Whereas for example explicit models require a high amount of compute power, implicit codes mainly need a high memory volume. With a modern Distributed Memory Parallel (DMP) Computing an analysis can be strongly parallelized on many computers. As a result the simulation of a large implicit model can be performed with the same memory size that is needed for a crash simulation. Such a utilization of the same hardware configuration for crash and linear analyses can substancially reduce the hardware costs.

By using an identical hardware configuration for crash and linear analyses the hardware cast can be reduced significantly. Furthermore these new technologies offer the capability to automate processes or to perform multi-domain optimizations. The benefits from cost reduction will allow companies to raise or shift resources in order to amplify additional innovations.

INTEGRATION OF MANUFACTURING MODELS

The quality of the information available to build models, like actual geometry, material properties or loading conditions, has a major impact on the quality of the simulation results. In this context the term "actual" covers two different aspects:

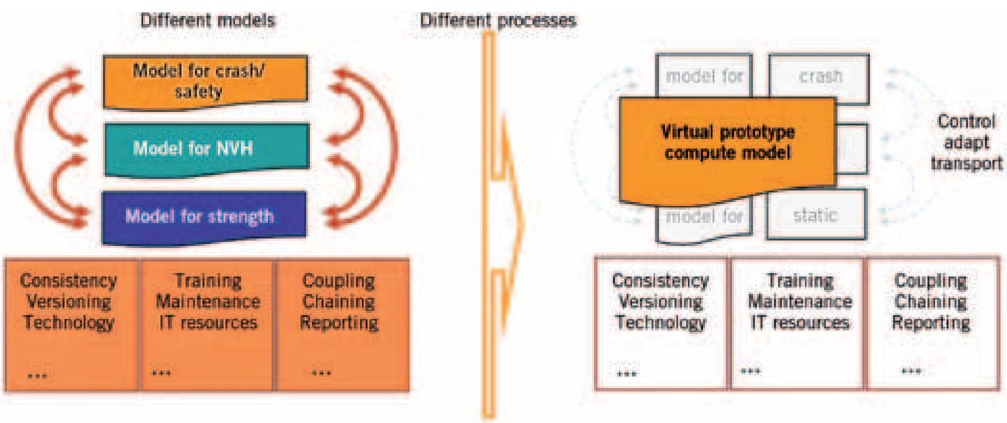

❷ Migration from single applications to an integrated CAE solution with a common database

: The properties should correspond to the most current design stage.
: Geometry and material data should reflect realistic, "as built" conditions, and not ideal or nominal properties.

Manufacturing and assembly processes have a major influence on the ideal component geometry, for example assembly distortion or thinning from stamping, ❹, or the material properties (for example strain hardening from stamping, reorientation of fibres during the composite forming processes) and should therefore taken into account during Virtual Prototyping, ❺. From a technological point of view the implementation of such simulation scenarios is reasonably well developed, but in real the integration of manufacturing aspects is confronted with two challenges:
: Manufacturing information is relatively late available in the project cycle, while product design analyses are ideally carried out in early design stages.
: Manufacturing and performance simulation solutions are generally in different software environments, and are not designed to communicate.

ESI Group has a great experience in manufacturing simulation and has especially developed methods for the evaluation of particular stamping and weld-assembly effects by the approximation of the actual geometry, material properties, and initial deformations on virtual prototypes in an early process phase.

For example, the welding and assembly process is simulated using technology developed in collaboration with the company Inpro which accounts for residual stress and distortion. This methodology is particularly adapted to preliminary design phase assessment. For metal stamping, inverse solvers are the typical technology of choice. For assembly, approximate distortions can be derived from thermo-mechanical analyses.

MANAGING AND CONTROLLING SIMULATION PROCESSES

Automotive projects are largely collaborative and normally distributed to multiple locations, ❻. It is essential for model quality and relevance to track model changes and properly propagate them from their different sources across the

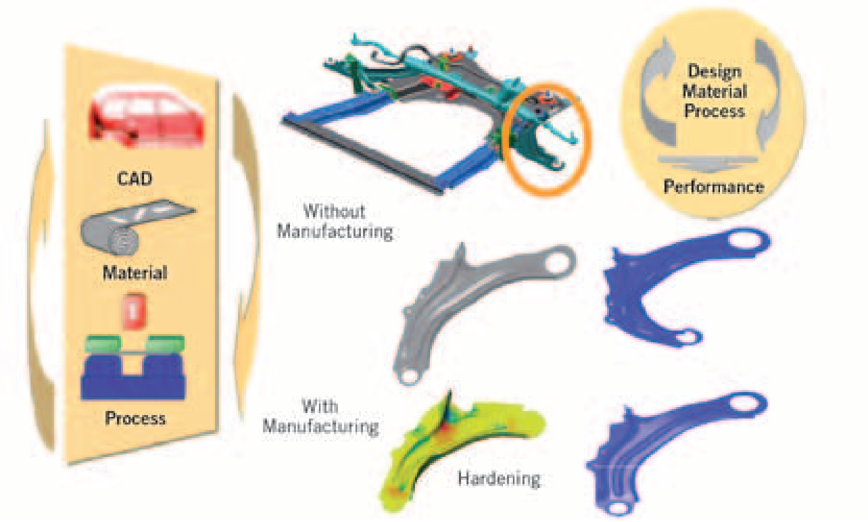

❸ Comparison of the component strength with and without the influence of manufacturing

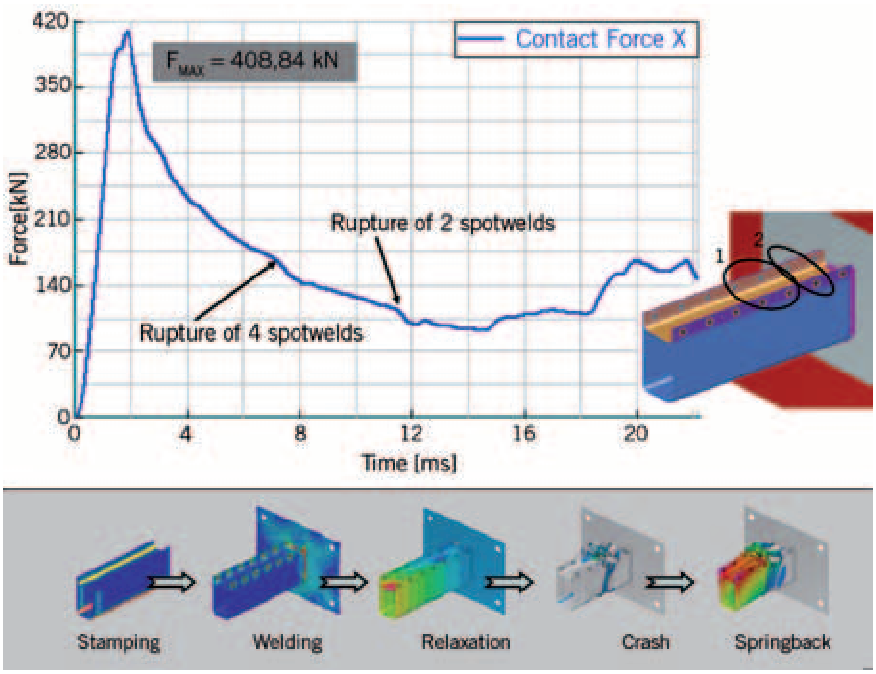

❹ Combination of explicit and implicit calculation for the simulation of different process steps

❺ Deviations from design data are nearly identical for explicit (left) and implicit (right) calculation (figure: © Seat)

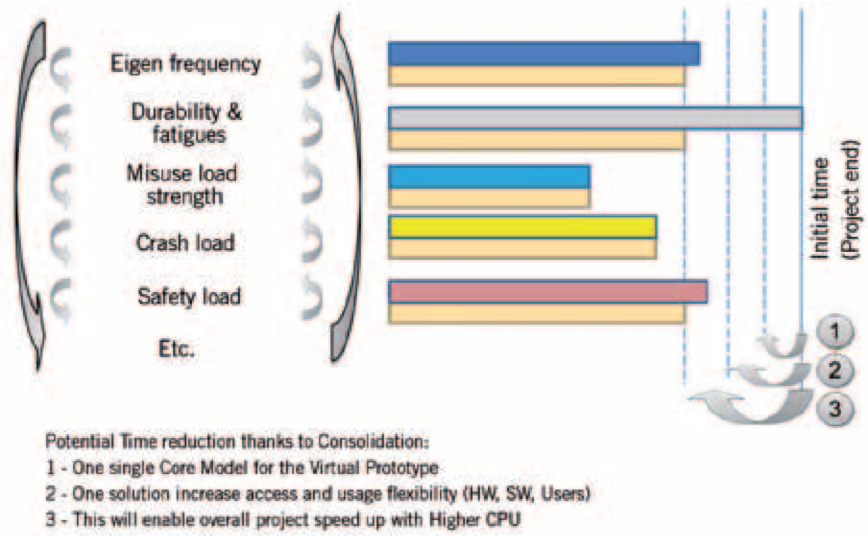

❻ Influence on project times by using a common simulation model

project organization. The potential time reduction in caused by three following consolidations:
1. One single core model for the virtual prototype
2. One solution increases access and usage flexibility (hardware, software, users)
3. This will enable overall project speed-up with higher CPU performance.

All teams/engineers involved in the development process have to be capable of using up-to-date data that is synchronized with the PDM/ERP information: they have a visibility and access to the latest approved CAD model and its design and engineering changes. They are also notified when their work is impacted by design or engineering changes. Before being approved and leading to design updates, the changes made by engineering teams have to be validated for the different domains. Visibility and notification mechanisms become critical as projects become larger and more distributed.

All these communication and data management tasks have to be addressed quickly and properly by the engineering platform which includes data and process management systems. The synchronization and approval processes for all different domains should be scalable. The integration of data management and simulation can in particular be supported by the solvers that shall carry, use, and pass meta-data regarding product or process information.

CONCLUSIONS AND OUTLOOK

Virtual Prototyping has become crucial for development projects in automotive industry like at Volkswagen and Seat to reach increasing performance targets on time and within tight budgets. Auto makers have recognized that the integration of the available technologies into increasingly competitive environments is necessary to realize the benefits of Virtual Product Development under industrial conditions.

ESI Group has already started integrating its different technologies, for multi-domain applications, process and content management as well as calculation models. Smart project management will be the next integration step: engineers will receive just-in-time data, tools, and instructions to accomplish their tasks as effectively as possible, while focusing on value creation through domain expertise rather than tools.

REFERENCE

[1] Sahr, Chr.; Berger, L.; Lesemann, M.; Urban, P.; Goede, M.: Systematic Material Selection for the SuperLight-Car's Body-in-White. In: ATZ Worldwide 112 (2010), No. 5, pp. 20 – 26

THANKS

This article is a team work development of several persons. The authors like to thank Pierre Culiere, Leader of the Crash-Safety Center of Excellence of ESI Group in Shanghai (China), and Dr. Raymond Ni, Director of Developments in Structural Mechanics at ESI Group in Paris (France), for their important part during preparation.

COORDINATED AUTOMATED DRIVING FOR THE TESTING OF ASSISTANCE SYSTEMS

Driver assistance systems need to master complex traffic situations and must be able to distinguish between potential accidents and non-critical circumstances. This poses an engineering challenge for the test technology, which has to ensure that these systems are reliable. Daimler's research department has developed a testing methodology that allows the precise, reproducible and safe testing of Mercedes assistance systems.

AUTHORS

DR.-ING. HANS-PETER SCHÖNER
is Head Testing and Workshops department in the Corporate Research and Advanced Development division of Daimler AG in Böblingen (Germany).

DIPL.-ING. WOLFGANG HURICH
is Head of the Testing and Metrology specialist area in the Testing and Workshops department at Daimler AG in Böblingen (Germany).

DIPL.-ING. JÜRGEN LUTHER
is Head of the Driverless Vehicles specialist area in the Testing and Workshops department at Daimler AG in Böblingen (Germany).

PROF. DR.-ING. RALF GUIDO HERRTWICH
has been Head of the "Driver Assistance and Chassis Systems" Centre in Daimler AG's Corporate Research and Advanced Development division since 2010 and is Head of the Daimler Centre for Automotive IT Innovations at Berlin Technical University (Germany).

TESTING OF ASSISTANCE SYSTEMS

Despite the constantly increasing use of virtual development methods for testing and validating driver assistance systems, there remains an important need for real-life trials of the system as a whole in a real-life environment. Quantitative validation of the systems requires a broad parameter range. Covering this range both completely and effectively presents a challenge when testing these systems.

Unlike the testing of dynamic drive control systems, which react to status variables inside a vehicle, testing assistance systems also requires status variables outside the vehicle to be taken into account. For example, the vehicle's position relative to a traffic lane is an important factor in lane departure warning systems, and the relative speeds and distances between several vehicles are decisive elements in adaptive cruise control systems. Whenever these systems do not merely provide warnings but intervene actively by supporting driver reactions or even independently in the vehicle's behaviour, these control systems need to be validated in a variety of traffic and environmental situations in order to obviate subsequent risks to vehicle occupants and to allow the systems to be certified for use [1].

The systematic testing of these systems means, from a technical point of view, that a test vehicle must be precisely controlled to follow a predetermined path, maintaining a specified speed along each section of the route. If several vehicles are involved, their movements must also be synchronized. Human drivers are still capable of meeting these conditions with sufficient accuracy in a single vehicle. However, this method rapidly reaches its limits when trying to simultaneously coordinate several vehicles in time and space. Although the statistical variation in the driving manoeuvres produced by test drivers may be thoroughly desirable for part of the test, greater precision and exact reproducibility of the tests is however essential for a systematic and effective study of compliance with specifications, for an objective comparison of different system variants and particularly when carrying out safety-critical manoeuvres.

Methods have been developed for improving the accuracy and repeatability of tests for particular individual assistance systems [2 – 5]. However, analysis of their applicability to the types of accidents to be addressed by future assistance systems showed that solutions were still needed for some problem areas. The task was therefore to design a test system that could coordinate and carry out even potentially dangerous manoeuvres by several vehicles safely and precisely.

ROBOTS FOR CONTROLLING VEHICLES

Mercedes-Benz and Anthony Best Dynamics Ltd. have jointly developed a system that provides a flexible solution for this task, ❶. It is described below [6].

Actuators capable of operating the accelerator, brake pedal and steering just like human drivers are installed in the test vehicles, replacing the human drivers, ❷. Robots like these (accelerator and brake robots) have been in use for some time for operating vehicles on roller test benches in test cycles or for controlling reproducibly complex steering manoeuvres (steering robots) in studies of drive dynamics.

❶ Automated vehicle in front of the control stand on the urban scenario test site in Sindelfingen

To control a vehicle's movement precisely, with the stipulation that it must, at a certain point at a certain time, be travelling in a specific direction at a specified speed, it is absolutely essential to be able to measure these variables exactly. This is achieved by using an inertial navigation system (INS), which is supported by a differential GPS and which transmits the required data to the robotic controls at a repetition rate of 100 Hz. The system's time drift is constantly corrected by correction data transmitted by radio to the INS by a local GPS base station at 1 s time intervals, allowing the vehicle's position to be measured to a typical accuracy of ±2 cm. Even if the GPS signal fails, the inertial sensors continue to indicate the vehicle's position for approximately 30 s with an accuracy better than 10 cm, which is good enough to allow a vehicle to be driven under a bridge, for example.

In addition to indicating position, the differential GPS also provides a highly accurate time reference signal. This signal is uniformly available to every vehicle and is used for synchronisation tasks.

The driving manoeuvres are controlled and monitored by the control system installed in the vehicle. This control computer receives a detailed schedule of the location and speed of the test drive and the precise start time via a WLAN link from a control stand. The complete test schedule (including action in the event that the test is aborted) is known in every vehicle before the manoeuvre starts. This ensures that the WLAN link, which may be only intermittently available, does not form part of the control loop and thus cannot have an adverse effect on safety.

Each vehicle is fitted with an independent safety controller and a spring-loaded emergency braking system. A system failure or any impermissibly excessive control deviation will bring the vehicles to a halt without the need for any external control intervention. The test can, of course, be aborted at any time via the WLAN link from the control stand.

The system in the control stand is capable of planning, operating and monitoring manoeuvres with up to five vehicles simultaneously, to be operated on an exclusive test area. This should enable the system to perform, with regard to complexity, any future foreseeable driving test scenario.

PLANNING OF MANOEUVRES

There are several options when it comes to the planning of test manoeuvres.

Although fitted with robots for operating the pedals and steering, the vehicles can still be driven by human drivers. This allows a learning mode in which the control system records a vehicle trajectory and stores it in the manoeuvre catalogue for subsequent automatic re-use. Some parameters, such as the scaling of speeds, the lateral displacement of the manoeuvre or the starting time, can be selectively varied.

For coordinated manoeuvres by several vehicles, trajectories can be compiled more efficiently using the graphical editor. A complete manoeuvre, made up of prefabricated parameterisable segments (straight stretches, arcs, lane changes, sinus curves, etc.), is planned and simul-

❷ Robots control the accelerator, brakes and steering in the test vehicle

❸ The vehicle tracks illustrate the precision and reproducibility achieved under automated control

taneously illustrated on the test area road layout. The course of the manoeuvre is simulated in order to verify that the dynamic driving limits can be adhered to. The ability to coordinate several vehicles is also simulated to check that there will be no collisions and that minimum safety margins between vehicles will be maintained.

LATERAL AND TIMING ACCURACY

In order to validate the control system, a measurement procedure independent of the differential GPS was used to examine the desired accuracy and reproducibility of the driving tests. This was able to verify that the standard measurement accuracy of ±2 cm achieved by the differential GPS, given adequate satellite visibility, also translates to the accuracy for driving past fixed obstacles with little clearance. High deceleration force tests (for example 0.75 *g*) involving bringing the vehicle to a halt in front of a specific obstacle achieved a ±3 cm reproducibility of the stopping point. However, such accuracy presumes that the controller has been adjusted to match the relevant vehicle type and that the vehicles can be driven a sufficient distance for settling of control errors. Very dynamic manoeuvres produce brief deviations of as much as one decimetre from the planned trajectory. However, if the same manoeuvre is executed several times, these deviations are reproducible and thus can be taken into account.

The long-term stability of positional accuracy was also verified by regularly driving past reference points on the test area. The driving pattern, which was repeatedly followed in fresh snow for several hours, impressively illustrates the reproducibility of the vehicle control system, ❸. Overall, the lateral track-following accuracy required for many manoeuvres of better than ±10 cm was easily achieved. In particular, reproducibility was significantly better compared to test drivers.

The longitudinal accuracy requirements depend on the vehicle's speed and are different for each of the functions being tested. The specification for this test system was determined as the ability to pass waypoints at specified times with an accuracy of 40 cm (at a speed of 20 m/s). This equates to reaching a waypoint within a reproducible time slot of ±20 ms. Longitudinal accuracy can be affected by an automatic transmission's shift points, for example. Factors such as this need to be taken into account when planning manoeuvres requiring high precision.

TESTING WITHOUT DRIVERS

There are applications for "automated driving" even for tests involving single vehicles.

For example, certain assistance systems are activated when a specific lateral acceleration is reached. By carrying out an automated driving manoeuvre at a specified speed and with a specified path radius, the lateral acceleration can be adjusted extremely reproducibly and, if required, at a continuous rate of increase. Executing manoeuvres in this way is considerably more efficient than using test drivers.

❹ Driverless validation manoeuvre: leaping over a ramp at up to 70 km/h

Validating occupant protection systems requires situations involving large longitudinal and vertical acceleration forces to be tested in which the airbag actuators must only be initiated under certain conditions. This includes vehicles having to leap over ramps at up to 70 km/h, ❹, drive over simulated curb stones while executing emergency braking forces or ram into realistic models of wild animals. Furthermore, rough road testing to validate vehicle durability can expose both vehicles and test drivers to extreme stress. These manoeuvres can now be executed in automated mode by robot-controlled vehicles without subjecting test drivers to any stress.

COORDINATING SEVERAL VEHICLES

The benefits of "coordinated automated driving" can be exploited to the full when conducting tests involving several vehicles. A large proportion of the testing of collision prevention or collision mitigation systems involves validating situations similar to actual accident scenarios but where the emergency braking system must definitely not be triggered. These situations mostly require vehicles to pass at very close range with, for example, an evading manoeuvre being executed at the last moment.

With robot-controlled vehicles, these tests can be carried out precisely, reproducibly and without posing any risk to test drivers or equipment. Parameters such as approach speed and angle, minimum spacing, etc. can be easily adjusted. A new software version or a new sensor variant can be tested using exactly the same manoeuvres, producing a test result which is both reproducible and meaningful.

The supreme test of vehicle coordination is cross-traffic at intersections at high speed and at very close proximity. Research projects such as "Aktiv" [7] stress the importance of this sort of traffic scenario. Traffic at intersections poses the highest requirements for precision with regard to both time and space. In contrast, longitudinal traffic scenarios (overtaking and oncoming traffic) often only demand spatial precision. Another consideration is the major damage that results from faulty execution of the manoeuvre. For health and safety reasons, close overtaking at speed is not carried out using test drivers. Coordinated automated vehicles allow cross-traffic manoeuvres to be carried out safely at up to 70 km/h and with minimum spacing of approximately one metre, ❺.

VIRTUAL GUIDE RAILS AND SELF-DRIVING CRASH TARGETS

Automated vehicles also permit assistance systems that intervene actively to be safely tested while hardware and software is still under development. The essential feature here is to give the systems room to react to the situations with which they are faced. Following a precisely pre-determined route would be counterproductive in such instances.

By using the so-called virtual guide rail function of the robot vehicle, a corridor can be defined within which braking or steering interventions by the assistance system can be tested. If the vehicle is about to depart from this corridor, due to the assistance system intervening either insufficiently or too strongly, only then will the robotic system intervene, either bringing the vehicle back on course or bringing it to a halt.

A further extension of the "coordinated automated driving" concept is the use of a self-driving soft crash target, ❻, for testing accident scenarios that do not end in near misses but in a crash. This vehicle, which is deliberately designed for crash scenarios, consists of a narrow, electrically-driven chassis and, just like the robotic vehicles, it can drive precisely along pre-planned trajectories. The vehicle is also equipped all-round with deformable air cushions which, when a crash occurs, reduce the speed differential using a damping characteristic of the collision force. This disperses the crash forces uniformly throughout the entire duration of the crash, thus minimizing their effect.

The self-driving soft crash target allows tests of collisions between moving vehicles to be carried out. The target can be used with radar and camera-based assistance systems because both its radar signature and visual appearance are similar to those of a vehicle. Its freely programmable trajec-

❺ Extremely close crossing manoeuvre at an intersection at 70 km/h

tories and its overall similarity in appearance to a vehicle make it suitable for use in every conceivable traffic scenario.

SUMMARY

The concept of “coordinated automated driving” offers the prospect of executing manoeuvres with hitherto unknown precision and reproducibility when testing assistance systems. Consequently, it is now possible for systems to be tested in safety-critical traffic scenarios and to be quantitatively validated more effectively. “Coordinated automated driving” makes a significant contribution to the comprehensive and robust testing and validation of future generations of assistance systems.

At the same time, the automated handling of test procedures makes it possible for the effective handling of officially agreed standard tests, such as those which might be necessary for a thorough comparison of similar assistance systems designed by different manufacturers or which might be used for a future active safety systems rating system. Active safety systems could then also be subjected to the same sort of systematic examination and assessment that has been carried out for years on passive safety crash systems. “Coordinated automated driving” opens the door to this possibility.

REFERENCES

[1] ISO 26262 (and DIN-ISO 61508): Road Vehicles Functional Safety (Draft International Standard)
[2] Hoffmann, J.; Winner, H.: Evita – das Untersuchungswerkzeug für Gefahrensituationen. 3. Tagung Aktive Sicherheit durch Fahrerassistenz, München, 2008 [Evita – The Experimental Tool for Hazardous Situations. 3rd Conference, Active Safety through Driver Assistance, Munich, 2008]
[3] Huber, B.; Resch, S.: Methods for Testing of Driver Assistance Systems. SAE Paper 2008-28-0020, January 2008
[4] Bock, T.; Maurer, M.; Färber, G.: Vehicle in the Loop (VIL) – A New Simulator Set-up for Testing Advanced Driving Assistance Systems. Driving Simulation Conference, Iowa City, IA (USA), 2007
[5] Gulde, D.: So testet AMS. Teil 9: Assistenzsysteme. Auto-Motor-Sport, 17-2010 [This is How AMS Tests: Part 9: Assistance Systems]
[6] Schöner, H. P.; Neads, S.; Schretter, N.: Testing and Verification of Active Safety Systems with Coordinated Automated Driving. ESV Conference, Stuttgart, 2009
[7] Aktiv: Adaptive und kooperative Technologien für den intelligenten Verkehr – Projektübersicht. [Adaptive and Cooperative Technologies for Intelligent Traffic – Project Summary.] www.aktiv-online.org, 2010

❻ The driverless soft crash target permits hazard-free collisions

THANKS

The authors would like to express their thanks to Hans-Georg Metzler, for many years head of Corporate Research and Advanced Development for Mercedes-Benz assistance systems, for many fruitful discussions during the design of the system presented here and for his support during its implementation.

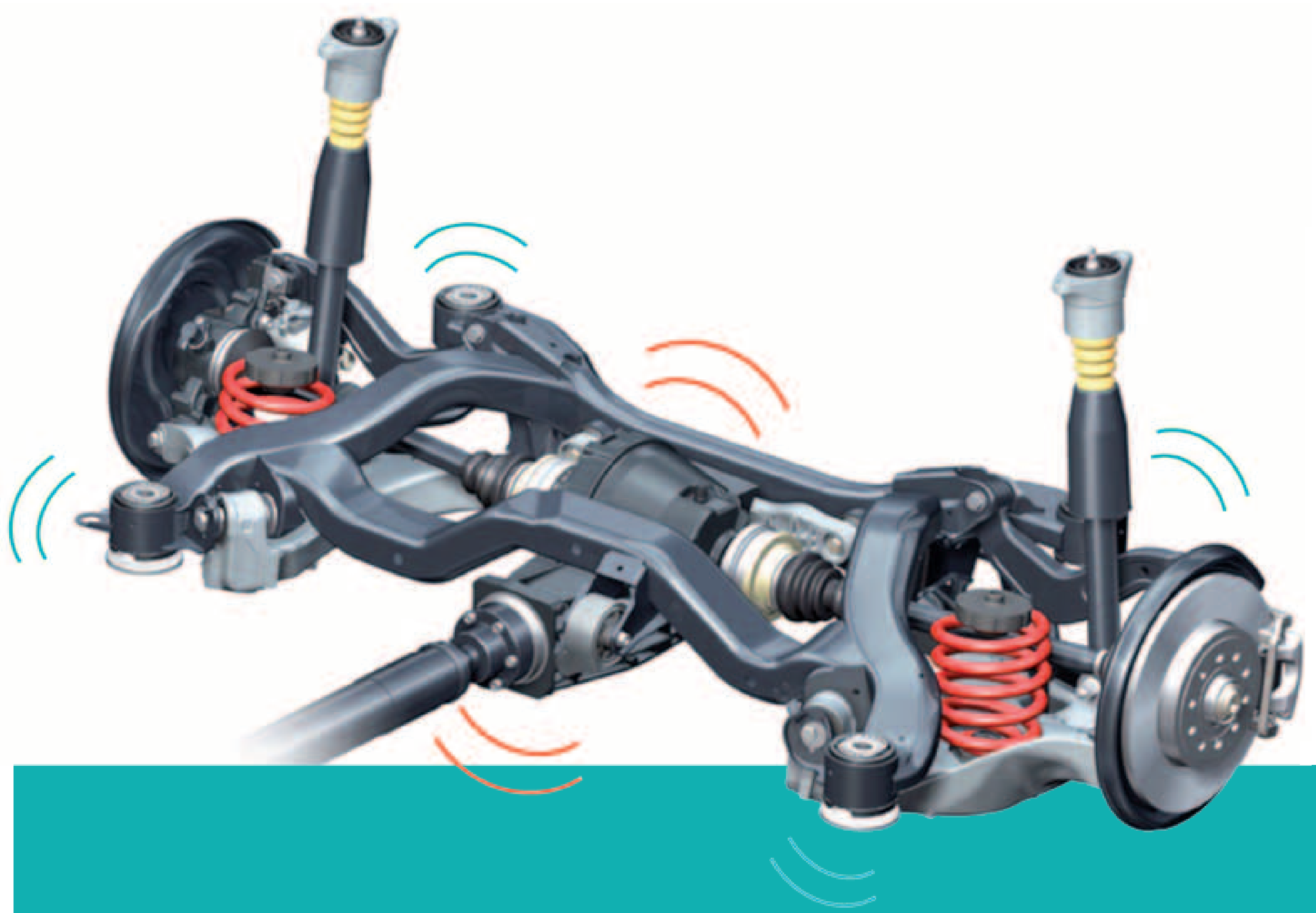

ACTIVE NOISE REDUCTION FOR REAR AXLE GEAR UNITS

The requirements on NVH behavior of passenger cars significantly increased. Volkswagen AG and Fraunhofer IWU show in a collaborative project new ways in the development of active mass damper for rear axle gear unit applications. With the presented system, consisting of an inertial mass actuator and a virtual absorber, the noise in the interior caused by the gear mesh could be reduced above 5 dB.

AUTHORS

DIPL.-ING. DIPL. WIRTSCH.-ING. SEBASTIAN EULERT
is Testing and Calculation Engineer in the Development Transmissions Components department at Volkswagen AG in Kassel (Germany).

DR.-ING. GEORG LÜHRS
is Head Acoustics Calculation in the Development Transmissions Components department at Volkswagen AG in Kassel (Germany).

DIPL.-ING. JAN BRÄUNIG
is Scientific Assistant in the Adaptronics and Acoustics department at Fraunhofer Institute for Machine Tools and Forming Technology (IWU) in Dresden (Germany).

DIPL.-ING. HOLGER KUNZE
is Head of the Adaptronics and Acoustics department at Fraunhofer Institute for Machine Tools and Forming Technology (IWU) in Dresden (Germany).

NOISE PHENOMENON REAR AXLE GEAR WHINE

In recent years the requirements on acoustic properties of passenger cars significantly increased. Due to environmental restrictions, comfort aspects and competition the car manufacturers have to match strict acoustic limits.

Due to this development, modern rear axle gear units (RAG) have to fulfill rigorous acoustic requirements, too. Usually their acoustical behavior is dominated by single tones which are unpleasant and should not be audible. Four-wheel-drive cars are very sensitive for vibrations in the powertrain; this property often leads to the so called rear axle gear whine. Gear mesh vibrations in the powertrain are leading to noise in the passenger compartment.

Experimental and computational modal analysis revealed a resonance of the powertrain at a frequency of 430 Hz. When excited by the gear mesh of the rear axle gear unit, ❶, at a certain speed of the test car this resonance leads to vibrations and noise. This effect can be measured in the vertical acceleration of the RAG and the interior sound pressure level of the car, ❷.

By using a scanning vibrometer the movement of the RAG has been investigated. These measurements revealed a rigid body movement of the RAG. While the back of the RAG shows almost no movement, the front part swings up and down with the frequency of 430 Hz. Transfer-path-analysis revealed that the vibration is mainly transmitted via the front elastomer of the RAG and the two front elastomers of the rear subframe into the vehicle body from which it is radiated as airborne noise into the passenger compartment (①, red labeled).

Within the research project the airborne noise reduction inside the car by using an active controlled system for damping the vibration of the RAG has been the main focus for Volkswagen AG and Fraunhofer Institute for Machine Tools and Forming Technology (IWU).

CONCEPTION AND LAYOUT OF THE ACTIVE SYSTEM

Considering the most effective actuator crosspoints erasing the first mesh-harmonic at the rear axle gear unit two positions have been preferred within the research project: The direct connection to the RAG (“A” in ①) and the rear subframe (RSF) interface close to the front RAG bearing (“B” in ①). The difference between these two connections is only measurable in the acceleration amplitude of the occurring vibrations within the relevant frequency range of the test vehicle and the necessary dependant regulating forces.

The direct actuator connection at the RAG is perfectly suited for the complete extermination of resonance vibrations. Furthermore force and displacement show their maximum at this position. A complete compensation of the rigid body vibration inducted to the bodywork is rather not possible. The reason therefore is that a minor part of the relevant structure-borne sound is being transmitted via the rear RAG-elastomer supports. The first objective of the research project was to investigate whether the advantages according to this position – low regulation force and displacement – allow an acceptable vibration reduction. The relevant elastomer support between RAG and RSF therefore causes an absorption by factor 3.

An electro-dynamic shaker was used as a testing proof of effectively working as inertial mass. Based on the mentioned test- and evaluation results the parameters could be improved to reduce the amplitudes of the relevant vibration components. The

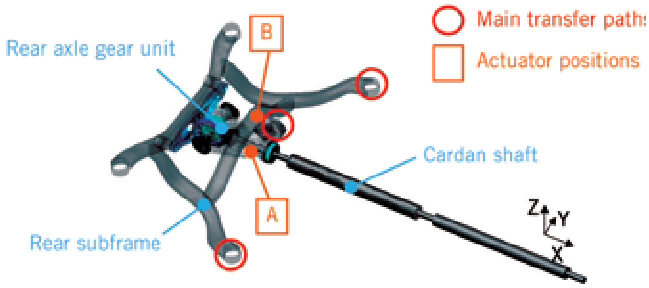

❶ Powertrain components of the test car

vehicle was tested on a rolling road test bench to set up the relevant driving conditions and constant speed. Acceleration measurements at the RAG as well as the acoustic feedback in the vehicle, recorded via microphones, verified the capabilities of the system.

FUNCTIONALITY OF AN INERTIAL MASS ACTUATOR

To generate compensation force an inertial mass actuator [2] was used. ❸ (top left) shows the corresponding mechanical circuit diagram for such system. The inertial mass m_A is connected to the structure with the stiffness c_A. The actuator, connected between the mass and structure, is generating the force F_A. The reaction force which is applied to the structure is labelled with F_R. The actuator with the frequency f_A is working above his resonance frequency f_{RA}. It reacts against his inertial mass and the generated force F_A applied to the structure has the same value, ③ (top right). Consequently the inertial mass actuator is an ideal power source if it is operating in the relevant frequency range. It is able to pass the necessary compensation force into the structure.

To keep the inertial mass as small as possible it is common to use a low spring stiffness cA in the system which causes a very low resonance frequency. Due to that electro-dynamic actuators which do not have any principle rigidity were selected. Later on the low stiffness was realised with leaf springs, ③ (down right).

The control concept of the inertial mass actuator is based on the functionality of a virtual absorber [3, 4]. For this purpose the acceleration at the actuator crosspoint to the structure is measured which allows establishing the force excitation of the actuator. This force-calculation occurs in a digitalised real-time system using a linear model which represents the behaviour of a real mechanical absorber. The coupling between absorber and structure is disconnected but the applied in force is equivalent to a real absorber in value and phase.

PRINCIPLE OF DAMPING VIBRATIONS

The principle of a mechanical absorber can be explained basing on a single-mass vibrator as shown in ❹ (top left) [5, 7]. This reduced system, presented in the diagram, ④ (top right), shows the amplitude response of the transfer function between force F and oscillation amplitude x. This diagram illustrates the characteristic increase of the amplitude which typically occurs by excitation in resonance frequency. Changing the system by coupling the absorber mass m_T with the coupling stiffness c_T (absorber spring) on top of the mass m results in the diagram as shown in ④ (green line). This curve progression shows one zero, which is defined by the absorber characteristics and whose frequency equates to the absorber eigenfrequency f_A. The absorber eigenfrequency is also defined as the ratio between absorber mass m_T and absorber stiffness c_T.

As a result of one additional mass and consequently one additional degree of freedom, ④ shows two secondary resonances (④, f_{R1} and f_{R2}) which are placed above and below the zero frequency. But a real zero only appears for a so called undamped absorber. In general minimizing the absorber damping d_T decreases the oscillation amplitude of the mass m at the absorber frequency but increases the secondary resonances. Increasing the absorber damping accordingly reverses these effects.

The mechanical absorber model is realised in a real time computer by the following transfer function $g_T(s)$:

EQ.

$$g_T\,(s) = \frac{F_R(s)}{a(s)} = \frac{d_T \cdot s + c_T}{s^2 + \frac{d_T}{m_T} \cdot s + \frac{c_T}{m_T}}$$

The advantage compared to an active absorber is the easy tunability of absorber parameters [6]. This means, that the absorber frequency can be calculative adjusted by changing the absorber mass m_T as well as the absorber stiffness c_T and absorber damping d_T.

The transfer function of the absorber is implemented in the real time system as an observable canonical form which allows changing several factors depending on the operating situation. The mass of the virtual absorber was chosen according to a valuation of the necessary inertial mass. For this purpose as well as for an active absorber the damping should be as low as possible. Hence this realisation is based on a real time calculation an undervalued damping could cause extreme amplitudes or even instability. The damping value was iteratively established to be as small as possible but as great as necessary to avoid instability.

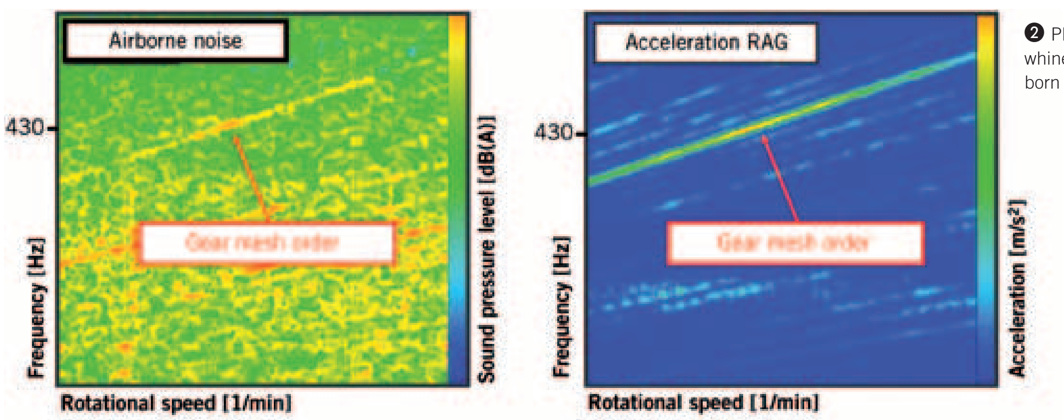

❷ Phenomenon of rear axle gear whine in the air (left) and structure-born noise spectrum (right)

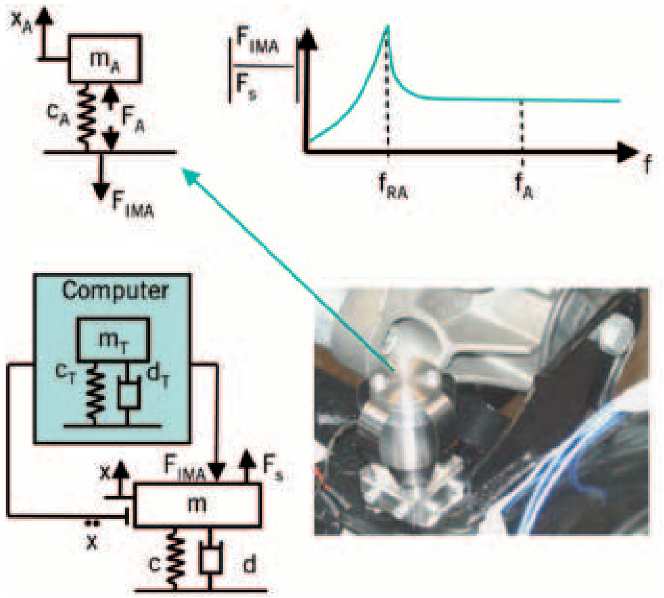

❸ Image of inertial mass actuator and computer absorber

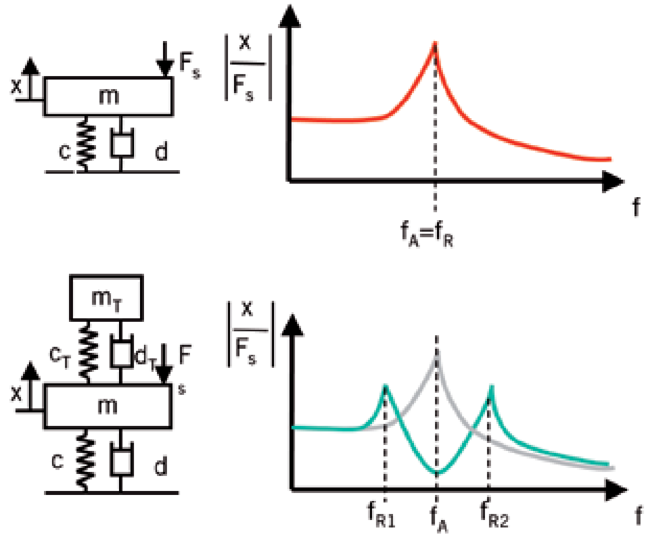

❹ Principle of mechanical absorber

ADAPTION OF STIFFNESS

To achieve an optimal vibration reduction actuator- and absorber frequency respectively should match with the trouble frequency [6]. This frequency is characterised by the tooth mesh of the RAG and so it depends on the driving speed. Due to that a continuous adaption of the absorber frequency is essential. To detect the frequency and the energy of the disturbing signal in real time several approaches were developed within this research project. The adaption of the absorber frequency can be realised via the interpretation of the phase relation between acceleration at the actuator cross point to the structure and the acceleration of the absorber mass.

ACTUATOR AND CONTROLLING IN PRACTISE

At Fraunhofer IWU a test rig has been constructed to figure out the optimal actuator position and to adjust the parameters of the control system. ❺ (left) shows the test rig which consists of the shaker and the components of the rear axle of the test car: the cardan shaft, the RAG with connecting rods and the RSF. The RSF is mounted by four load cells and stiff pillars to ground.

To simulate the excitation of the RAG an artificial sine-wave pulsation has been applied on the housing of the RAG by the electro dynamical shaker. The load cells and acceleration sensors at the elastomers have been used to monitor the performance of the active controlled system. ⑤ (right) shows an increasing acceleration when the system is shut off.

After verification on this test rig the active system was mounted in an experimental vehicle. The actuator has been installed to position B, ①. At the Volkswagen site in Kassel different tests have been carried out on a car roller test rig. Especially tests with constant velocity at the critical frequency revealed the functionality of the actuator. ❻ (left) shows a Campbell diagram of a sound pressure measurement in the vehicle interior. When the system is active the gear mesh order is significantly reduced. ⑥ (right)

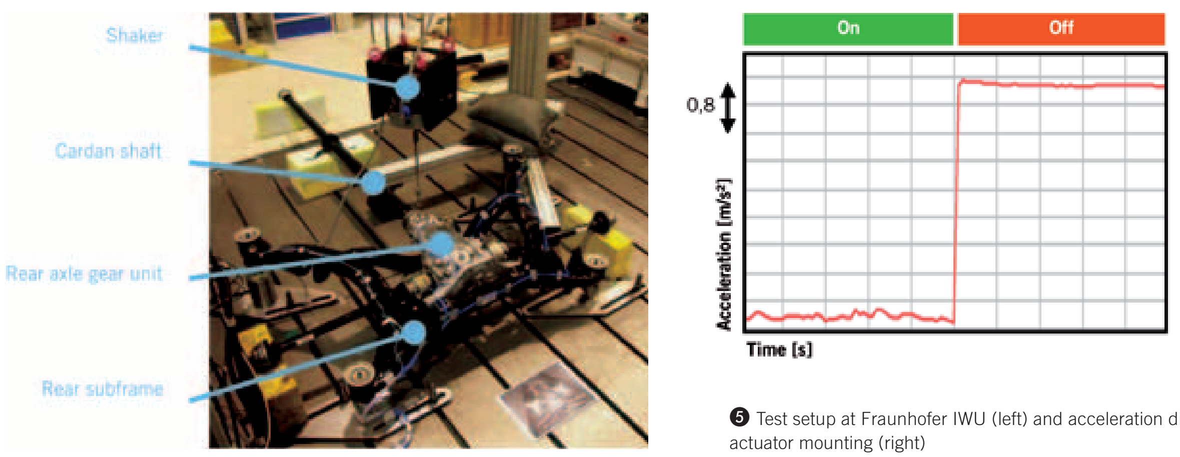

❺ Test setup at Fraunhofer IWU (left) and acceleration diagram of the actuator mounting (right)

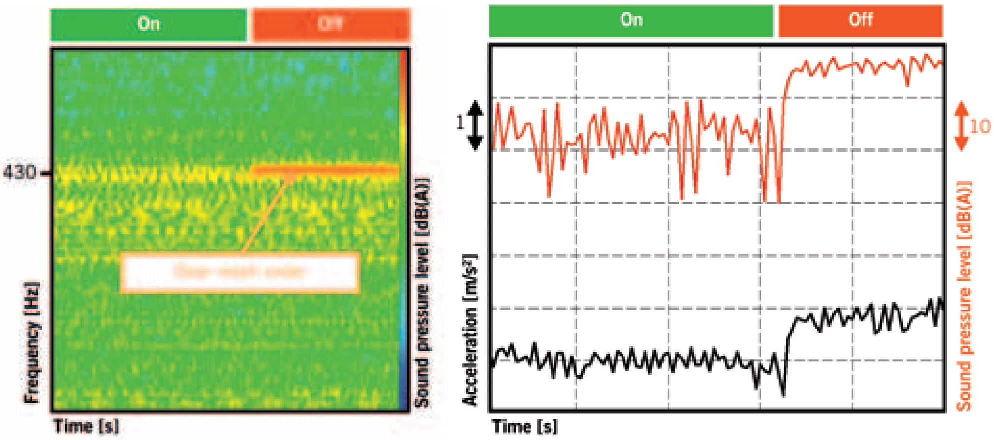

❻ Campbell diagram of a sound pressure measurement in the vehicle interior (left) and gear mesh order cut of the RAG acceleration and sound pressure level (right)

shows a gear mesh order cut of the RAG acceleration and sound pressure level. It is obvious that the amplitude rises when the system is shut off. This effect is considerably audible.

Beside the tests at constant velocity run ups and downs have been performed on the car roller test rig. These tests also reveal that the system works well.

FURTHER POSSIBILITIES AHEAD

The collaborative project of Volkswagen AG and Fraunhofer IWU showed new ways in the development of active mass damper for rear axle applications. With the presented active controlled system the sound pressure level of the gear mesh order could be reduced above 5 dB. Acoustic engineers judge this reduction by 2 BI on a scale of 10 which is used for the ranking of acoustic quality of cars. The functionality of the active system which consists of a inertial mass actuator and a virtual absorber has been proofed by the tests. The system is supplied by the cars energy system and operates with low battery consumption. On demand it can be switched on and off and fits into to the space available at the powertrain.

In future the importance of acoustic quality of cars will further increase which makes new ways of noise reduction interesting. This project has shown that an active controlled system can significantly reduce vibrations and noise. Motivated by the promising results further investigations about saving potentials in gearing process (for example lapping) and higher efficiency of the rear axle gear unit are in planning. Today these aspects are usually contrary to the acoustical behaviour of gear units.

REFERENCES

[1] Eulert, S.; Klaffke, S.; Lührs, G.; Martin, F.: Experimentelle und numerische NVH-Analyse verzahnungsinduzierter Biege- und Torsionsschwingungen – am Beispiel einer Hinterachse. In: Dynamisches Gesamtsystemverhalten von Fahrzeugantrieben (2008)

[2] Preumont, A.: Vibration Control of Active Structures An Introduction. Kluwer Academic Publisher, Dordrecht, 2002

[3] Bucht, A.: Energetische Untersuchungen am elektromechanischen Schwingungstilger. Master Thesis, PFH Göttingen, 2008

[4] Weyer, T.: Entwurf selbsteinstellender aktiver elektromechanischer Tilger. Dissertation, DLR Deutsches Zentrum für Luft- und Raumfahrt e. V., Braunschweig, 2007

[5] Illgen, A.; Drossel, W.-G.; Wittstock, V.; Schirmer, W.; Wiedemann, L.: Active Vibration Absorber for Gear Box Noise Reduction in Wind Turbines. In: Adaptronic Congress 2007, Göttingen, 23 and 24 May 2007

[6] Gelfert J.: Konzeption und Realisierung für die Regelung eines aktiven Schwingungstilgers. Diplomarbeit, TU Dresden, Fraunhofer IWU, Dresden, 2009

[7] VDI 3833 Blatt 1/2: Schwingungsdämpfer und Schwingungstilger. Beuth-Verlag, Berlin, 2006

THE NEW VW CADDY
A CAR FOR EVERY OCCASION

Volkswagen Commercial Vehicles has launched a new generation of the Caddy with wide-ranging updates. As the first city delivery vehicle and compact MPV in this class, it is equipped with ESP as standard equipment in all versions and has six new four-cylinder TDI and TSI engines with up to 21 % fuel economy improvement. The development objectives also included a highly precise styling that follows the Volkswagen design-DNA.

DEVELOPMENT GOALS AND POSITIONING

Safety must never be compromised for monetary reasons. That is why Volkswagen Commercial Vehicles decided to offer the new Caddy, the brand's entry-level model, with ESP as a 100 % standard feature – and it is the first vehicle in its class to offer this. Another objective was to meet the requirements of the EU5 emissions standard at all power levels. This has been achieved by a restructured engine range and the use of the first seven-speed dual clutch gearbox in this segment. Other, high-priority development goals were to optimise the vehicle's utility value and operating costs as well as improving reliability and comfort. As another first in the Caddy class, Hill Climb Assist has been introduced.

The equipment lines have also been reconfigured, ❶. On the Caddy, Volkswagen makes a basic distinction between commercial versions used as business vehicles and passenger car versions generally driven by private individuals. In the business line, panel van and kombi versions are still offered here, and they account for about 70 % of the total production volume. For the passenger car versions, three equipment lines will be available immediately: Startline, Trendline and Comfortline. The Trendline version replaces the Caddy Life. The more extensively equipped Comfortline version replaces the special Style model. The new exclusive model is the Caddy Comfortline Edition (previously Style Edition). Still in the programme are the Tramper camper version, which is especially popular among young globetrotters, and the Maxi (extended wheelbase) and 4Motion versions (four-wheel drive).

AUTHORS

DR. WOLFGANG SCHREIBER
is Speaker for the Board of Management of the Volkswagen Commercial Vehicles brand and Executive Vice President Product Development at Volkswagen Commercial Vehicles, Wolfsburg (Germany).

DR. HOLGER WESTENDORF
is Head of Product Development Model Lines at Volkswagen Commercial Vehicles, Wolfsburg (Germany).

BERND EMMERMANN
is Head of C-Model Lines at Volkswagen Commercial Vehicles, Wolfsburg (Germany).

NICOLE VON WIEDING
is Sub-Project Manager Technical Project Management C-Model Lines at Volkswagen Commercial Vehicles, Wolfsburg (Germany).

SIX NEW ENGINE VERSIONS

Six of the seven engines offered on the Caddy are new to the range. Five of them follow a downsizing principle. Engine displacement is deliberately reduced and compensated for by supercharging and direct injection systems. Due to engine downsizing to just 1.2 l, the combined fuel consumption of the 63 kW and 77 kW petrol direct injection engines was reduced to 7.0 l of fuel (equivalent to 164 g/km CO_2). The turbodiesels output 55 kW, 75 kW, 81 kW and 103 kW. They all operate with common rail injection, which is both quiet and fuel-efficient. The 75 kW version with BlueMotion Technology (with a stop/start system and energy recuperation) consumes just 4.9 l per 100 km in the panel van (equivalent to 134 g/km CO_2). All TDIs engineered to the EU5 emissions standard are fitted with a diesel particulate filter as standard equipment. Like the previous generation model, the new Caddy is also being offered with an 80 kW 2.0-l four cylinder engine (Eco-

COMMERCE	PASSENGER CARS	LEISURE
	Comfortline Edition	
	Comfortline	
Kombi	Trendline	
Panel Van	Startline	Tramper

❶ The equipment lines of the new Caddy

Fuel) that was developed for natural gas operation ❷. The 75 kW TDI can be ordered with an optional seven-speed DSG. For the more powerful 103 kW TDI, a six-speed DSG is available.

1.2-L TSI WITH 77 KW

In all core markets, the 1.2-l TSI replaces the 1.6-l MPI with multi-point injection. The latest series of four-cylinder petrol engines from Volkswagen AG is characterised by a redesigned die-cast aluminium cylinder crankcase with cylinder liners in grey cast iron. Other engine features include the two diagonally mounted valves per cylinder head with a roller cam follower valve drive and timing chain. The piston assembly with a ring pack designed for lower tangential stresses also has a lightweight construction. This results in reduced friction and tangential forces. The crankcase vent with an oil separator was integrated into the cylinder head and engine block. In sum, design modifications resulted in an engine that weighs 24.5 kg less than the engine at the next higher power level.

Just how efficiently the engine operates is evident in the combined fuel consumption value of the Caddy 1.2 TSI: 7.0 l/100 km. The equivalent previous model consumed 8.2 l/100 km or 17 % more. The engine attains its maximum power at 5,000 rpm. It can transfer its maximum torque of 175 Nm to the crankshaft from 1,550 rpm. The TSI accelerates the Caddy to 100 km/h in 12.4 s and attains a top speed of 169 km/h, ❸.

1.6-L TDI WITH 75 KW

After successful implementations of 2.0-l common rail engines in passenger cars, Volkswagen Commercial Vehicles is now presenting the second generation of this diesel series in the Caddy. Key development goals were improved fuel economy, acoustic comfort, smooth engine running and low exhaust emissions.

The TDI engines fulfil the requirements of the EU5 emissions standard and are equipped for future requirements – especially those related to the environment and sustainability.

The 1.6-l TDI is offered at a power level of 75 kW. The underlying objective in designing this completely new base engine was not just to reduce engine displacement. Based on experience from the first generation, details of all other components were revised and optimised with regard to friction losses, acoustics and emissions.

The cylinder crankcase made of lamellar graphite cast iron has a very strong and rigid construction. Bowed features and reinforcement ribs created high torsional and bending rigidity, minimised cylinder distortions and low acoustic wave emissions. Optimisation of the cylinder crankcase to design targets enabled a 10 % weight reduction compared to the first generation. The engine displacement of 1,598 cm³ is attained by a bore diameter of 79.5 mm and a stroke of 80.5 mm.

An evaluation of the cylinder head should consider modifications that were made to the induction air channels and valve diameters to adapt them to the lower displacement. Valve spring forces were lowered to reduce friction forces. The integrated channel for exhaust gas recirculation makes the component more compact.

The crankshaft drive was also redesigned. The forged connecting rod with a length of 152 mm reduces force components perpendicular to the cylinder walls. In addition, the almost square stroke/bore ratio decreases the mean piston velocity by 10 % and reduces internal engine friction.

The crankshaft is designed with four cheeks. This was a primary factor in making the crankcase drive 15 % lighter. Decreasing tangential forces at the piston rings has reduced the friction of the piston group while simultaneously attaining a low oil consumption and blow-by values. The optimised contour of the oil scraper ring improves its scraping effect and allows only minimal tangential forces. In conjunction with the optimised roundness of the cylinder liners, this also reduces friction power losses.

❷ Caddy EcoFuel for operation on natural gas

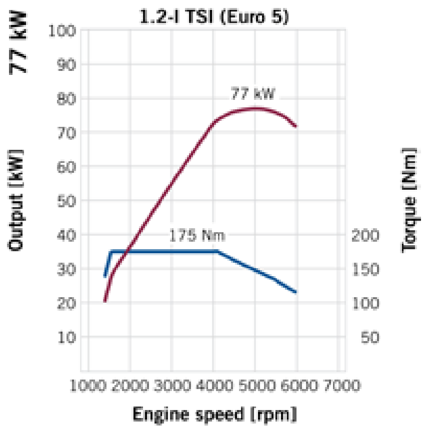

❸ Power curves of the 1.2-l TSI engine

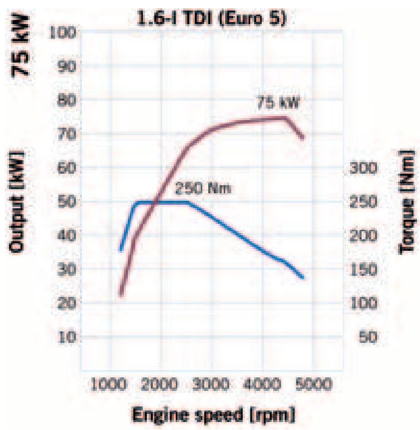

❹ Power curves of the 1.6-l TDI engine

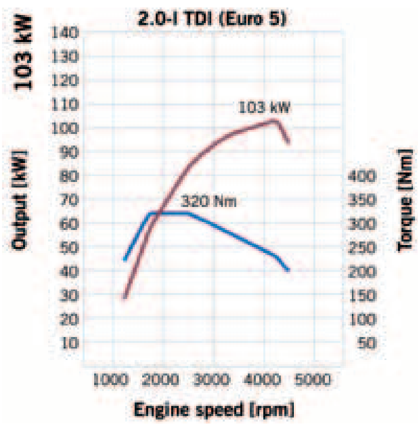

❺ Power curves of the 2.0-l TDI engine

The camshaft drive and the drive for the ancillary components were also optimised to improve their acoustics and reduce friction power losses. Making a significant contribution here is the narrower toothed belt, whose width was reduced by 25 mm, as well as a self-tensioning flexible belt for driving the generators and one toothed belt for driving the oil pump.

In conjunction with BlueMotion technology, this engine makes the new Caddy one of the most fuel-efficient models in the model series. Its combined fuel consumption of 4.9 l per 100 km (equivalent to 129 g/km CO_2) contrasts with its dynamic driving performance: The Caddy 1.6 TDI accelerates from 0 to 100 km/h in 12.9 s, and its top speed is 170 km/h. It outputs its peak power at 4,400 rpm and already develops its maximum torque of 250 Nm at 1,500 rpm, ❹.

2.0-L TDI WITH 103 KW

The second generation 2.0-l TDI is based on the engine of the 1.6-l TDI, and it systematically supports modular construction methods. The crankcase bearing block was reinforced for higher power. The bore diameter is 81 mm. With a stroke of 95.5 mm, this results in a stroke volume of 1,986 cm³.

The diameters of the intake and exhaust valves of the cylinder head were enlarged by 1.5 mm to cover increased air flow requirements. For optimal air induction into the combustion chamber, the inlet channels were also modified. The injection system and turbocharger were tuned to the higher power level as well.

The Caddy 2.0 TDI in the panel van version consumes 5.9 l/100 km (equivalent to 155 g/km CO_2). This contrasts with a top speed of 186 km/h and an acceleration time of 10.0 s for the sprint to 100 km/h. In addition, the TDI has an impressive torque reserve at practically every engine speed, developing its maximum torque of 320 Nm from a low 1,500 rpm. Its reaches its maximum power at 4,200 rpm, ❺.

❻ 4Motion four-wheel drive system in the new Caddy

THE CADDY'S FOUR-WHEEL DRIVE SYSTEM

In introducing the Caddy 2.0 TDI 4Motion (81 kW), Volkswagen Commercial Vehicles is the only manufacturer to offer a city delivery van or compact MPV with permanent four-wheel drive, ❻. In addition to the use of the fourth generation electronically controlled Haldex clutch, specific 4Motion features include a two-part cardan shaft, exhaust system modifications to adapt it to the rear differential and cardan shaft, and reinforcements in the rear body side members. The electro-hydraulic Haldex clutch of the Caddy 4Motion operates in an oil bath. The multi-plate clutch system itself is flanged to the rear differential. Via an electric pump, a pressure reservoir is supplied with oil at a working pressure of 30 bar. An electronic control unit computes the ideal drive torque for the rear axle, and it regulates, via a valve, how much oil pressure is applied to the working piston of the multi-plate clutch. This increases the surface pressure on the clutch plates in proportion to the torque desired at the rear axle. The amount of pressure applied to the clutch plates can be varied continuously to adjust the amount of torque transfer. Activation of the 4Motion system is independent of slip, since the working pressure is always available. In extreme cases, up to 100 % of the drive torque can be directed to the rear axle.

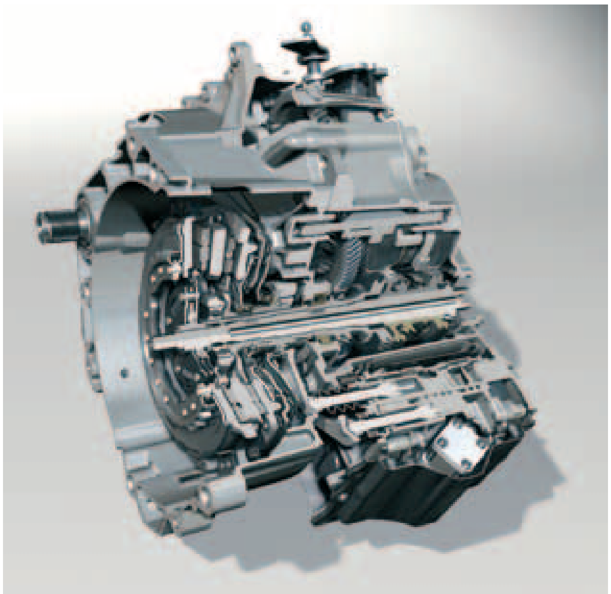

❼ Seven-speed DSG DQ 200

SEVEN-SPEED DUAL CLUTCH GEARBOX

The new Caddy is also the only city delivery vehicle and compact MPV in its class to be offered with an efficient dual clutch gearbox (DSG) as an option instead of a conventional automatic gearbox, ❼. For the first time in this model series, Volkswagen Commercial Vehicles is now implementing a seven-speed DSG in addition to the six-speed DSG. These gearboxes are offered in the 1.6-l TDI (75 kW) and 2.0-l TDI (103 kW). The two types of DSG differ in the maximum engine torque they can handle; the seven-speed DSG is used in the Caddy 1.6 TDI, while the six-speed DSG is used in the Caddy 2.0 TDI.

The dual clutch gearbox primarily consists of two independent gearbox units, each with a separate clutch. Functionally, each of these gearbox units is constructed like a manual transmission. One key property of the seven-speed DSG is its dry clutches. The dry clutch system offers numerous advantages which, in sum, lead to even further efficiency gains. For example, there is no need for a suction filter, oil cooler or pressurised oil lines in the gearbox housing, since no oil is needed to cool the clutch plates. What remains is the "normal" gearbox oil for lubrication and cooling of the gears and bearings. By eliminating clutch cooling oil, the total volume of oil was reduced from 6.5 l (six-speed DSG) to 1.7 l in the seven-speed DSG. The two DSG variants are specialists at their respective tasks. While the six-speed DSG is used in large and torque-strong engines (up to 350 Nm) due to its wide torque range, the seven-speed DSG is designed specifically for use with smaller engines (to 250 Nm torque).

The seven-speed DSG being used in the Caddy 1.6 TDI makes a significant contribution towards further reducing fuel consumption and emissions. In parallel, it offers a plus in agile performance. The reasons are obvious: in the seven-speed configuration, it was possible to lay out the first gear with a shorter gear ratio, thus improving drive-off performance. Despite the shorter gear ratio for drive-off, the gearbox is characterised by a very comfortable and tight sequencing of the gears and an overdrive. This long seventh gear has a positive effect on fuel economy, emissions and acoustic comfort.

Engine power is transferred to the dual clutch via the crankshaft and a dual-mass flywheel. The system has two dry friction clutches and one central plate. The latter transfers the torque to the drive shaft via the relevant clutch. Clutch I handles the odd-numbered gears, and clutch II the even gears plus reverse gear. The result of this sophisticated clutch management approach is that there are no gaps in propulsive power during shifting. The system's comfort and convenience are excellent, and the driver experiences an incomparably dynamic yet comfortable shifting feeling. Responsible for this – along with an intelligent electro-hydraulic transmission control (mechatronic system) – are two clutches, two drive shafts and three final drive shafts. This networked system makes it possible to continually "lie in wait", ready to go into action at the next higher driving level.

The "brains" of the Volkswagen dual clutch gearbox are the mechatronics. This electronic control unit regulates the rapid and complex shifting processes. The basic layout of the mechatronics includes an electronic control unit and what is known as a valve block with individual sensors and actuators. Specifically, the mechatronics module computes and controls data such as the data for controlling the clutches, the individual gears, pressures and various safety stages. Also used here are modulator valves, switching valves and a large number of hydraulic valve spools.

The mechatronics of the seven-speed DSG were designed as an autonomous unit with an oil circuit that is separate from the gearbox. This also yields advantages:

: The hydraulic fluid can be specially tuned to the needs of the mechatronics, while a normal oil such as that used for manual transmissions can be used for the gearbox. The low-temperature properties of the mechatronics are very good, since no compromises need to be made in terms of oil viscosity.
: The high purity of the hydraulic oil enables use of so-called cartridge valves with very small gap dimensions. They significantly reduce the amount of leak-

❽ Removable second row of seats

age, and the use of an electrically powered pump is economical.
: The pressure level can be elevated compared to an open hydraulic system. At the same time, the actuators can be made smaller due to the higher power density, and this reduces the overall weight of the gearbox.
: The mechatronics can be fully assembled and tested outside the gearbox.
: The dual clutch and gearshifting do not require an internal combustion engine. Theoretically, the system could be used together with a hybrid drive system with a stop/start function.

EXTERIOR – CLEAN AND PRECISE SHAPES

A new generation of Volkswagen commercial vehicles whose exterior bears the signature of the company's new design DNA is being launched on the market with the debut of the new Caddy. This is particularly apparent in the completely new front end design characterised by a horizontal organisation of elements. The radiator grille and headlights – available in two versions (H4 and H7, each with integrated daytime running lights) – form an integral unit with the lower bumper area. Fitted in the bumper are the new, optional front fog lights with optional cornering light functionality, which is available on all models.

In its side profile, the Caddy's two new alloy wheel choices (15 and 17-inch) and new distinctive body contour line catch the eye. This line runs from the headlights to the triangular windows of the A-pillars. Setting a benchmark in its class are the roof rails being offered for the first time on the Caddy, which are standard equipment from the Comfortline. They have a load capacity of 100 kg. New at the rear are the restyled signatures, rear lights and VW logo. Also revised are the lighting unit in the license plate frame and the now electrically actuating tailgate handle.

INTERIOR – IMPROVED FUNCTIONALITY AND EQUIPMENT

The new Caddy is distinguished by numerous detailed modifications. They include new user controls, as well as new three-spoke steering wheels and upholstery fabrics and the now fully trimmed interior – even on the Caddy Trendline. The colour of the interior trim in the side and floor areas was also changed from "Art Grey" to a darker "Anthracite." Another eye-catching feature is the redesigned controls for the manual air conditioning or automatic climate control system on the centre console. The now lockable glove box is cooled by one of these two air conditioning systems on the Trendline und Comfortline equipment lines.

In parallel, Volkswagen Commercial Vehicles also improved the versatility of the Caddy's seating system, which accommodates from two to seven seats depending on the version and equipment features. The most important innovation is that, in contrast to the previous model, the individual second row seats can now be completely removed, ❽. In addition, a new seat rail design has made it considerably easier to remove the third seating row. When the two rear seat rows are removed, this increases the MPV's maximum cargo length to 1,781 mm or 2,250 mm (Caddy Maxi). With this seat configuration, boot space volumes are 3,030 l and 3,880 l, respectively.

SUMMARY

The standard-equipment ESP of the new Caddy shows once again that Volkswagen Commercial Vehicles takes its responsibility towards customers very seriously. In addition, the optimised model takes a great leap forward in the competitive field with a unique line-up of engines. Fuel consumption and emission values are significantly better than those of the previous model. This has resulted in substantially lower operating costs. Its new TSI and TDI engines also offer improved comfort with reduced noise emissions. In the interior, new styling and an optimised seating system will reinforce the Caddy's position as market leader in Germany. The city delivery vehicle and compact MPV also has the potential to expand its position internationally. Last but not least, the vehicle's technical features, its styling that is characterised by timeless precision and further improved quality also contribute to making the new Caddy one of the best in its class in retaining its value.

PEER REVIEW ATZ | MTZ

PEER REVIEW PROCESS FOR RESEARCH ARTICLES IN ATZ AND MTZ

STEERING COMMITTEE

Prof. Dr.-Ing. Lutz Eckstein	RWTH Aachen University	Institut für Kraftfahrzeuge Aachen
Prof. Dipl.-Des. Wolfgang Kraus	HAW Hamburg	Department Fahrzeugtechnik und Flugzeugbau
Prof. Dr.-Ing. Ferit Küçükay	Technische Universität Braunschweig	Institut für Fahrzeugtechnik
Prof. Dr.-Ing. Stefan Pischinger	RWTH Aachen University	Lehrstuhl für Verbrennungskraftmaschinen
Prof. Dr.-Ing. Hans-Christian Reuss	Universität Stuttgart	Institut für Verbrennungsmotoren und Kraftfahrwesen
Prof. Dr.-Ing. Ulrich Spicher	Universität Karlsruhe	Institut für Kolbenmaschinen
Prof. Dr.-Ing. Hans Zellbeck	Technische Universität Dresden	Lehrstuhl für Verbrennungsmotoren

ADVISORY BOARD

Prof. Dr.-Ing. Klaus Augsburg
Prof. Dr.-Ing. Bernard Bäker
Prof. Dr.-Ing. Michael Bargende
Prof. Dipl.-Ing. Dr. techn. Christian Beidl
Dr.-Ing. Christoph Bollig
Prof. Dr. sc. techn. Konstantinos Boulouchos
Prof. Dr.-Ing. Ralph Bruder
Dr. Gerhard Bruner
Prof. Dr. rer. nat. Heiner Bubb
Prof. Dr. rer. nat. habil. Olaf Deutschmann
Dr. techn. Arno Eichberger
Prof. Dr. techn. Helmut Eichlseder
Dr.-Ing. Gerald Eifler
Prof. Dr.-Ing. Wolfgang Eifler
Prof. Dr. rer. nat. Frank Gauterin
Prof. Dr. techn. Bernhard Geringer
Prof. Dr.-Ing. Uwe Grebe
Prof. Dr.-Ing. Horst Harndorf
Prof. Dr. techn. Wolfgang Hirschberg
Univ.-Doz. Dr. techn. Peter Hofmann
Prof. Dr.-Ing. Bernd-Robert Höhn
Prof. Dr. rer. nat. Peter Holstein
Prof. Dr.-Ing. habil. Werner Hufenbach
Prof. Dr.- Ing. Roland Kasper
Prof. Dr.-Ing. Tran Quoc Khanh
Dr. Philip Köhn
Prof. Dr.-Ing. Ulrich Konigorski
Dr. Oliver Kröcher
Dr. Christian Krüger
Univ.-Ass. Dr. techn. Thomas Lauer
Prof. Dr. rer. nat. Uli Lemmer
Dr. Malte Lewerenz
Prof. Dr.-Ing. Markus Lienkamp
Prof. Dr. rer. nat. habil. Ulrich Maas
Prof. Dr.-Ing. Martin Meywerk
Prof. Dr.-Ing. Klaus D. Müller-Glaser
Dr. techn. Reinhard Mundl
Prof. Dr. rer. nat. Cornelius Neumann
Dr.-Ing. Lothar Patberg
Prof. Dr.-Ing. Peter Pelz
Prof. Dr. techn. Ernst Pucher
Dr. Jochen Rauh
Prof. Dr.-Ing. Konrad Reif
Prof. Dr.-Ing. Stephan Rinderknecht
Dr.-Ing. Swen Schaub
Prof. Dr. sc. nat. Christoph Schierz
Prof. Dr. rer.-nat. Christof Schulz
Prof. Dr. rer. nat. Andy Schürr
Prof. Dr.-Ing. Ulrich Seiffert
Prof. Dr.-Ing. Hermann J. Stadtfeld
Prof. Dr. techn. Hermann Steffan
Prof. Dr.-Ing. Wolfgang Steiger
Prof. Dr.-Ing. Peter Steinberg
Prof. Dr.-Ing. Christoph Stiller
Dr.-Ing. Peter Stommel
Prof. Dr.-Ing. Wolfgang Thiemann
Prof. Dr.-Ing. Helmut Tschöke
Dr.-Ing. Pim van der Jagt
Prof. Dr.-Ing. Georg Wachtmeister
Prof. Dr.-Ing. Jochen Wiedemann
Prof. Dr. techn. Andreas Wimmer
Prof Dr. rer. nat. Hermann Winner
Prof. Dr. med. habil. Hartmut Witte

Scientific articles of universities in ATZ Automobiltechnische Zeitschrift and MTZ Motortechnische Zeitschrift are subject to a proofing method, the so-called peer review process. Articles accepted by the editors are reviewed by experts from research and industry before publication. For the reader, the peer review process further enhances the quality of the magazines' content on a national and international level. For authors in the institutes, it provides a scientifically recognised publication platform.

In the ATZ | MTZ Peer Review Process, once the editors has received an article, it is reviewed by two experts from the Advisory Board. If these experts do not reach a unanimous agreement, a member of the Steering Committee acts as an arbitrator. Following the experts' recommended corrections and subsequent editing by the author, the article is accepted.

In 2008, the peer review process utilized by ATZ and MTZ was presented by the WKM (Wissenschaftliche Gesellschaft für Kraftfahrzeug- und Motorentechnik e. V./German Professional Association for Automotive and Motor Engineering) to the DFG (Deutsche Forschungsgemeinschaft/German Research Foundation) for official recognition.

IMPRINT

ATZ WORLDWIDE

www.ATZonline.com

Founded 1898 as „Der Motorwagen“

Organ of the VDI-Gesellschaft Fahrzeug- und Verkehrstechnik (FVT)

Organ of the Forschungsvereinigung Automobiltechnik e. V. (FAT) and of the Normenausschuss Kraftfahrzeuge (FAKRA) in the DIN Deutsches Institut für Normung e. V.

Organ of the Wissenschaftliche Gesellschaft für Kraftfahrzeug- und Motorentechnik e. V. (WKM)

01 I 2011 _ January 2011 _ Volume 112

Springer Automotive Media I Springer Fachmedien Wiesbaden GmbH
P. O. Box 15 46 · 65173 Wiesbaden · Germany I Abraham-Lincoln-Straße 46 · 65189 Wiesbaden · Germany
Amtsgericht Wiesbaden, HRB 9754, USt-IdNr. DE811148419

Managing Directors Dr. Ralf Birkelbach (Chairman), Armin Gross, Albrecht Schirmacher I **Senior Advertising** Armin Gross I **Senior Marketing** Rolf-Günther Hobbeling
Senior Production Christian Staral I **Sales Director** Gabriel Göttlinger

EDITOR-IN-CHARGE
Wolfgang Siebenpfeiffer

EDITORIAL STAFF

EDITOR-IN-CHIEF
Johannes Winterhagen (win)
phone +49 611 7878-342 · fax +49 611 7878-462
johannes.winterhagen@springer.com

VICE-EDITOR-IN-CHIEF
Dipl.-Ing. Michael Reichenbach (rei)
phone +49 611 7878-341 · fax +49 611 7878-462
michael.reichenbach@springer.com

CHIEF-ON-DUTY
Kirsten Beckmann M. A. (kb)
phone +49 611 7878-343 · fax +49 611 7878-462
kirsten.beckmann@springer.com

SECTIONS
Body, Safety
Dipl.-Ing. Ulrich Knorra (kno)
phone +49 611 7878-314 · fax +49 611 7878-462
ulrich.knorra@springer.com
Chassis
Roland Schedel (rs)
phone +49 6128 85 37 58 · fax +49 6128 85 37 59
ATZautotechnology@text-com.de
Electrics, Electronics
Markus Schöttle (scho)
phone +49 611 7878-257 · fax +49 611 7878-462
markus.schoettle@springer.com
Engine
Ruben Danisch (rd)
phone +49 611 7878-393 · fax +49 611 7878-462
ruben.danisch@springer.com
Online
Katrin Pudenz M. A. (pu)
phone +49 6172 301-288 · fax +49 6172 301-299
redaktion@kpz-publishing.com
Production, Materials
Stefan Schlott (hlo)
phone +49 8191 70845 · fax +49 8191 66002
Redaktion_Schlott@gmx.net
Research
Dipl.-Ing. (FH) Moritz-York von Hohenthal (mvh)
phone +49 611 7878-278 · fax +49 611 7878-462
moritz.von.hohenthal@springer.com
Service, Event Calendar
Martina Schraad (mas)
phone +49 611 7878-276 · fax +49 611 7878-462
martina.schraad@springer.com
Transmission
Dipl.-Ing. Michael Reichenbach (rei)
phone +49 611 7878-341 · fax +49 611 7878-462
michael.reichenbach@springer.com

ENGLISH LANGUAGE CONSULTANT
Paul Willin (pw)

PERMANENT CONTRIBUTORS
Richard Backhaus (rb), Dipl.-Reg.-Wiss. Caroline Behle (beh), Prof. Dr.-Ing. Stefan Breuer (sb), Dipl.-Ing. (FH) Andreas Fuchs (fu), Jürgen Grandel (gl), Prof. Dr.-Ing. Fred Schäfer (fs)

ADDRESS
P. O. Box 15 46, 65173 Wiesbaden, Germany
redaktion@ATZonline.de

ADVERTISING

HEAD OF SALES MANAGEMENT
Britta Dolch
phone +49 611 7878-323 · fax +49 611 7878-140
britta.dolch@best-ad-media.de

KEY ACCOUNT MANAGEMENT
Elisabeth Maßfeller
phone +49 611 7878-399 · fax +49 611 7878-140
elisabeth.massfeller@best-ad-media.de

SALES MANAGEMENT
Sabine Röck
phone +49 611 7878-269 · fax +49 611 7878-140
sabine.roeck@best-ad-media.de

MEDIA SALES
Heinrich X. Prinz Reuß
phone +49 611 7878-229 · fax +49 611 7878-140
heinrich.reuss@best-ad-media.de

DISPLAY AD MANAGER
Susanne Bretschneider
phone +49 611 7878-153 · fax +49 611 7878-443
susanne.bretschneider@best-ad-media.de

AD PRICES
Price List No. 54 (10/2010)

MARKETING I OFFPRINTS

PRODUCT MANAGEMENT AUTOMOTIVE MEDIA
Sabrina Brokopp
phone +49 611 7878-192 · fax +49 611 7878-407
sabrina.brokopp@springer.com

OFFPRINTS
Martin Leopold
phone +49 2642 9075-96 · fax +49 2642 9075-97
leopold@medien-kontor.de

PRODUCTION I LAYOUT
Kerstin Brüderlin
phone +49 611 7878-173 · fax +49 611 7878-464
kerstin.bruederlin@springer.com

YOUR HOTLINE TO ATZ

Editorial Staff
☎ +49 611 7878-341
Reader's Service
☎ +49 611 7878-151
Advertising
☎ +49 611 7878-269

SUBSCRIPTIONS
VVA-Zeitschriftenservice, Abt. D6 F6, ATZworldwide
P. O. Box 77 77, 33310 Gütersloh, Germany
Renate Vies
phone +49 5241 80-1692 · fax +49 5241 80-9620
SpringerAutomotive@abo-service.info

SUBSCRIPTION CONDITIONS
The eMagazine appears 11 times a year at an annual subscription rate 199 Euro for private persons and 299 Euro for companies. Special rate for students on proof of status in the form of current registration certificate 98 €. Special rate for VDI/ÖVK/VKS members on proof of status in the form of current member certificate 172 €. Special rate for studying VDI members on proof of status in the form of current registration and member certificate 71 €. Annual subscription rate for combination ATZworldwide (eMagazine) and ATZ (print) 398 €. The subscription can be cancelled in written form at any time with effect from the next available issue.

HINTS FOR AUTHORS
All manuscripts should be sent directly to the editors. By submitting photographs and drawings the sender releases the publishers from claims by third parties. Only works not yet published in Germany or abroad can generally be accepted for publication. The manuscripts must not be offered for publication to other journals simultaneously. In accepting the manuscript the publisher acquires the right to produce royalty-free offprints. The journal and all articles and figures are protected by copyright. Any utilisation beyond the strict limits of the copyright law without permission of the publisher is illegal. This applies particularly to duplications, translations, microfilming and storage and processing in electronic systems.

Springer Automotive Media is a brand of Springer Fachmedien. Springer Fachmedien is part of the specialist publishing group Springer Science+Business Media.

EXPERIMENTAL AND NUMERICAL METHODS FOR THE EVALUATION OF THE LOCAL DISCOMFORT OF ARMRESTS

AUTHORS

UNIV.-PROF. DR.-ING. HABIL. UWE JANOSKE
is Head of the Institute of Fluid Mechanics at the University of Wuppertal (Germany).

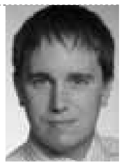

DIPL.-ING. HAUKE GREGOR
is Research Assistant at the Institute of Fluid Mechanics at the University of Wuppertal (Germany).

DR.-ING. MICHAEL SCHRODT
is Managing Director of Gratz Simulation GmbH in Weinsberg (Germany).

UNIV.-PROF. MAG. DR. HERMANN SCHWAMEDER
is in Charge of the "Interfakultärer Fachbereich Sport- und Bewegungswissenschaft/USI" at the University of Salzburg (Austria).

A simulation environment was developed at the University Wuppertal to predict the discomfort behavior in virtual prototypes for armrests. A coupled solution of the structural mechanics of the foam structure of the armrest and the fluid flow is capable to determine the local conditions. The discomfort behavior is estimated by a correlation matrix of experimental values. Extensive experiments were made to gain the correlation matrix for the discomfort behavior which could be given as a function of velocity and volume flow.

THE SEAL OF APPROVAL FOR SCIENTIFIC ARTICLES IN ATZ.
ATZ
PEER REVIEW
RECEIVED 2010-08-07
REVIEWED 2010-09-02
ACCEPTED 2010-11-16
REVIEWED BY EXPERTS FROM RESEARCH AND INDUSTRY.

1 INTRODUCTION
2 SIMULATION MODEL
3 EXPERIMENTS
4 NUMERICAL RESULTS
5 CONCLUSIONS

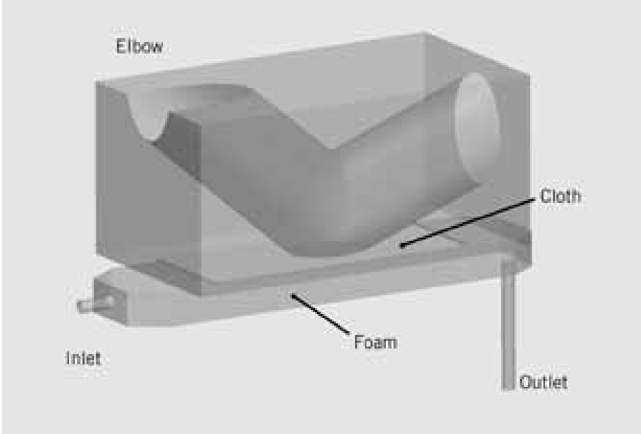

❶ Geometry of the simulation model

1 INTRODUCTION

Comfort issues are an important factor in the development of new products. In most cases, the evaluation of discomfort, like the discomfort of armrests in automotive applications, is done in late phases of the product development, i.e. a real prototype already exists. Changes or improvements of the discomfort behavior require new prototypes and extensive testing resulting in high costs. Currently, numerical tools like computational fluid dynamics are not capable of evaluating or indicating discomfort behavior. In this work, ventilated and tempered armrests which are used in trucks, cars and construction machines, are considered using a coupled simulation of fluid and structure to evaluate discomfort behavior. An evaluation or optimization of the ergonomics of the armrest, proposed by Murphy and Oliver [1], was not considered.

A definition of comfort and discomfort was described in the work of Zhang et al. [10]. Comfort and discomfort are not describing opposites but rather liking (comfort) or bearing (discomfort). In this work the discomfort according to the definition of Zhang et al. [10] will be evaluated.

In the past various works have been carried out to evaluate thermal comfort. Mezrhab and Bouzidi [5] use a network-model based on the solution of the energy balance to describe the temperature distribution in the compartment of a car. Zhang et al. [6] calculate the temperature distributions in a car using a CFD tool with giving a relationship between the thermal comfort and the values found by the CFD analysis. Works based on heating, ventilation and air conditioning in buildings, e.g. by Lin et al. [4] describe correlations for the thermal comfort as a function of flow velocities and temperatures. Similar results are obtained by Catalina et al. [2] used for the optimization of climate control strategies. Zhang et al. [8] describe very detailed the influence of temperature on 19 different positions of the body and the thermal comfort. The influence of flow velocities was neglected. Models for the thermoregulation describing heat fluxes in the human body can be found in the work of Tanabe et al. [3] or Fiala [9]. The cited papers determine factors for thermal comfort without a contact between the body and a support. Cengiz and Babalik [7] ran various road tests to evaluate the comfort behavior of different car seats. In this work, the thermal discomfort behavior where parts of a body (here: elbow) and a support (here: armrest) are in contact are described by numerical and experimental methods. The numerical methods shall be capable as a design tool to evaluate virtual prototypes concerning the thermal discomfort behavior.

2 SIMULATION MODEL

Numerical flow simulations offer only information about measureable quantities like pressure, velocity and temperatures. Information about discomfort, especially for applications where a contact between the body and a support takes place, cannot be predicted with these tools. Therefore, experimental methods are required to evaluate these sensations of discomfort. A simulation environment was developed to predict the discomfort behavior in virtual prototypes for armrests. A coupled solution of the structural mechanics of the foam structure of the armrest and the fluid flow is capable to determine the local conditions. The discomfort behavior is estimated by a correlation matrix of experimental values. Extensive experiments were made to gain the correlation matrix for the discomfort behavior which could be given as a function of velocity and volume flow. In further steps, this method will be extended to other applications where a contact between a body and a support takes place.

In the next sections, the geometry of the simulation model, the simulation procedure as well as the assumptions will be presented.

2.1 GEOMETRY

❶ shows the geometry used for the simulations. The elbow of a person will be positioned in the middle of a porous foam representing the armrest. The geometry of the elbow was reconstructed using a 3D-scanner (Optix 400M, 3D Digital Corp.). The porous foam is covered by a cloth. The conditions of the flow can be varied in respect of temperature and velocity at the inlet of the armrest. Depending on the mechanical pressure of the arm on the foam, different flow conditions at the contact point of the arm and the foam will be present resulting in different local comfort conditions.

2.2 SIMULATION PROCEDURE

Essentially for the evaluation of the thermal comfort behavior is the knowledge of the local flow situation, i.e. flow velocity and temperature. ❷ shows the simulation procedure for modeling the discomfort behavior. As the flow properties are dependent on the flow structures of the porous media, a structural simulation of the contact problem is done first. Depending on the resulting stress the porosity can be obtained by a sub-model explained in the section 2.4.3. The porosity distribution as well as the deformation of the geometry of the foam is taken into account in the CFD simulation.

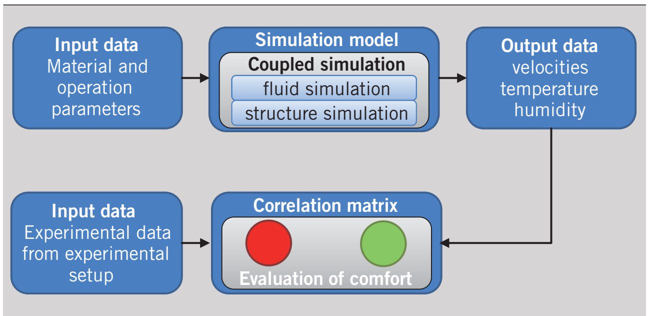

❷ Simulation procedure

The resulting velocities and temperatures are the input of a correlation matrix which will be obtained by experimental data (see section 3). The result will be the local discomfort behavior. The procedure can be integrated in a time loop for the simulation of time-dependent processes. Finally, the tool predicts discomfort symbolized by the traffic light in ②.

2.3 ASSUMPTIONS

To reduce the computational effort several assumptions have been made:

: The contact area between arm and armrest will be assumed constant.
: The flow is assumed to be compressible and turbulent. The turbulent flow will be described with a two-equation turbulence model (k-ε-Modell).
: The foam will be modeled approximately as a linear-elastic material.
: The foam will be modeled as a homogeneous porous media in the CFD simulations.

2.4 MODEL EQUATIONS

In the next section, the equations are summarized used for the simulation model.

2.4.1 STRUCTURE

The displacement v can be calculated using the momentum balance, Eq. 1, using a linear-elastic material behavior with a linear relationship of the strain ε_s and the stress σ_s given by Young's modulus E and the transversal contraction υ, Eq. 2 and Eq. 3, as a result of the external, volume related force f_s.

EQ. 1 $$\nabla \cdot \sigma_s + f_s = 0$$

EQ. 2 $$\sigma_s = \frac{E}{1+\upsilon}\varepsilon_s + \frac{\upsilon E}{(1+\upsilon)\ (1\text{-}2\ \upsilon)}\, tr\, \varepsilon_s\, I$$

EQ. 3 $$\varepsilon_s = \frac{1}{2}\,[\nabla\upsilon + (\nabla\upsilon)^T]$$

2.4.2 FLUID

The flow conditions, i.e. velocity v and pressure p can be calculated by the continuity, Eq. 4, and the momentum balance, Eq. 5, using the effective viscosity μ, Eq. 6. The turbulent flow will be modeled with a k-ε-Modell. The turbulent viscosity μ_t is determined by Eq. 7 as a ratio of the turbulent kinetic energy k and the dissipation ε which are the described by two transport equations, Eq. 11 and 12, using the turbulent production P. The temperature T is calculated from the energy balance, Eq. 8, assuming ideal gas behavior, Eq. 10, and heat transfer coefficient defined by Eq. 9. Finally, the humidity can be calculated with a transport equation, Eq. 13, using a diffusion coefficient D_ϕ. The equations – structure as well as fluid – are solved using the Open Source CFD-code Open-Foam.

EQ. 4 $$\nabla \cdot (\rho u) = 0$$

EQ. 5 $$\nabla \cdot (\rho u u) = \nabla \cdot [\mu(\nabla u + \nabla u^T) - \tfrac{2}{3}\,\mu\nabla \cdot (u) I] - \nabla p + S_i$$

EQ. 6 $$\mu = \mu_l + \mu_t$$

EQ. 7 $$\mu_t = \frac{c_\mu\, \rho k^2}{\varepsilon}$$

EQ. 8 $$\nabla \cdot (\rho u c_p T) - \nabla \cdot [\alpha \nabla T] - u \cdot \nabla p = 0$$

EQ. 9 $$\alpha = \alpha_l + \alpha_t$$

EQ. 10 $$p = \rho R\, T$$

EQ. 11 $$\nabla \cdot (\rho u k) = \nabla \cdot \left[\left(\mu_l + \frac{\mu_t}{\sigma_k}\right)\nabla k\right] + P - \rho\varepsilon$$

EQ. 12 $$\nabla \cdot (\rho u \varepsilon) = \nabla \cdot \left[\left(\mu_l + \frac{\mu_t}{\sigma_\varepsilon}\right)\nabla \varepsilon\right] + C_{1\varepsilon}\frac{\varepsilon}{k}P - C_{2\varepsilon}\rho\frac{\varepsilon^2}{k}$$

EQ. 13 $$\nabla \cdot (\rho u \phi) = \nabla \cdot (D_\phi\, \nabla \phi)$$

2.4.3 STRESS-POROSITY RELATIONSHIP

Different kinds of foams with different bulk densities, permeabilities and hardness were used in this study. A detailed description of the complex structure of the foam in the CFD model fails due to the required numerical resolution. The foam will be modeled as a homogeneous material in the structural as well as in the fluid simulations. The mechanical properties of the foam are determined by compression tests and modeled by a linear-elastic behavior represented by Young's modulus E and the transversal contraction υ. Based on these values structural simulations predict the displacement and stresses in the foam. The local porosity can be estimated based on the local stress influencing the pressure drop which is implemented in the CFD code by a source term in the momentum equation, Eq. 5. The pressure-flow velocity correlations for different porosities have been obtained by extensive test on a flow bench.

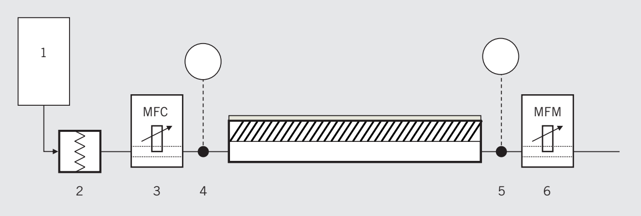

❸ Experimental setup

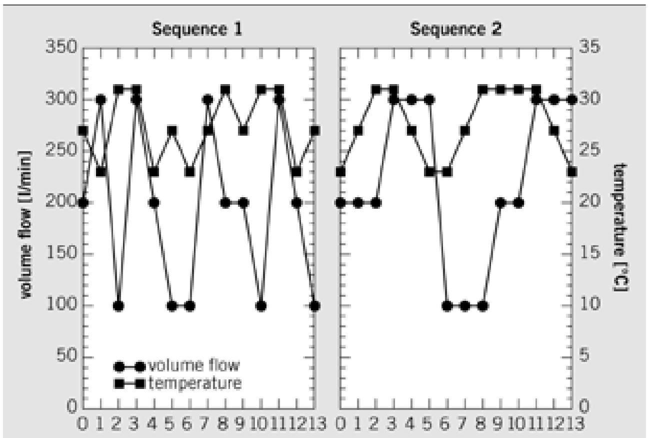

❹ Experimental test conditions

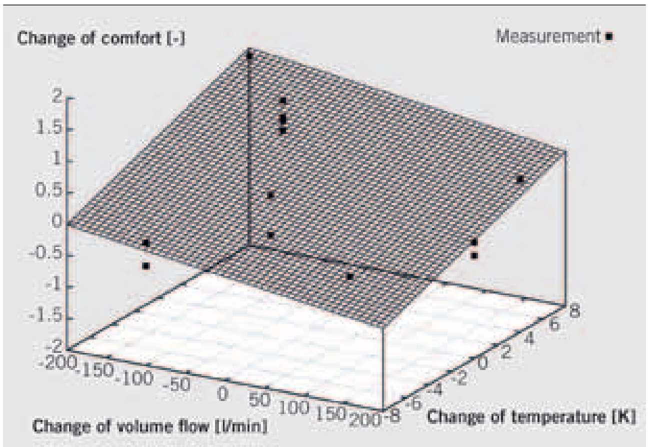

❺ Change of discomfort ΔC for different changes of temperature and volume flows for foam 1, test procedure 1

3 EXPERIMENTS

To obtain a correlation between measurable values (values like velocity, temperature) and the subjective impression of the discomfort behavior, extensive measurements were made. The experimental setup, the procedure of the experiments as well as the experimental results will be described in the next sections.

3.1 EXPERIMENTAL SETUP

The experimental setup is shown in ❸. Heated air will be supplied by the pressurized vessel (1) and the heater (2) which enters the armrest on the right side. The mass flow is controlled by a mass

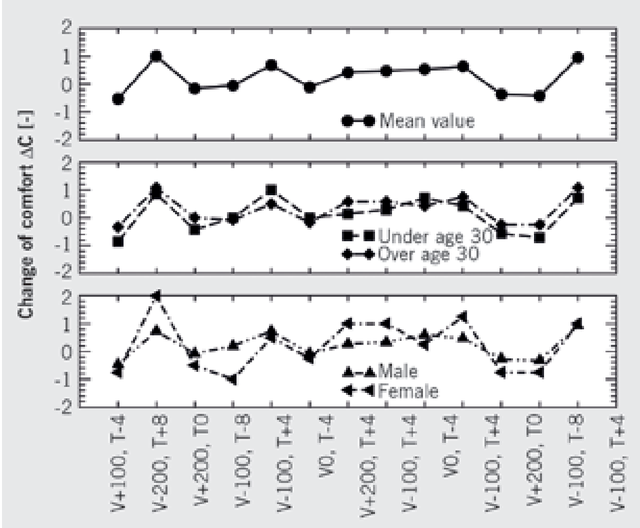

❻ Change of discomfort ΔC for foam 1, procedure 1 for different test conditions

flow controller (3) at the inlet and a mass flow meter (6) at the outlet. The air will be distributed homogeneously over the cross section by a static mixer and flows through the porous foam. The arm is placed in the middle of the armrest on a cloth. A part of the volume flow goes through the cloth whereas the most part enters the armrest on the right side. Temperatures and pressure values are measured at different positions (4) and (5) shown in ③.

3.2 PROCEDURE OF THE EXPERIMENTS

For a statistical evaluation of the results, different test procedures have been used. Every test procedure has 13 different conditions, i.e. temperatures and volume flows. ❹ shows the two different procedures which have been used. Each test person has to evaluate, starting from the first reference state, if the next state is much more comfortable (+2), less comfortable (-2) or nothing has changed (0). Values in between (-1, +1) were also possible. In order to check the reliability of the measurement two sequences in the test procedure are identical (3-5 and 11-13). The results will be confident, if the reliability factor R, Eq. 14, is smaller than 5. The factor R is defined by the values of comfort change ΔC_i for the different operation points i.

3.3 EXPERIMENTAL RESULTS

The values for the change of comfort are shown in the following section as functions of the temperature and volume flow at the inlet of the experimental setup. In the 3D graphs a quadratic interpolation of the measured values is shown for a better visualization of the data. In total more than 50 people were tested. The age of the test persons ranged from 20 to 52 years.

❺ shows the change of discomfort ΔC_i plotted against the temperature and volume flow at the inlet for foam 1 and test procedure 1. An increase of the temperature has a dominating effect on the positive change of discomfort ΔC. Also a reduction of the volume flow leads to an increase of ΔC_i.

❻ shows the results for foam 1 and test procedure 1 plotted against the changes from step to step. The same behavior like in the 3D graph can be seen for the 2D plot. A comparison of the results for test persons under and above 30 years shows no significant differences, i.e.

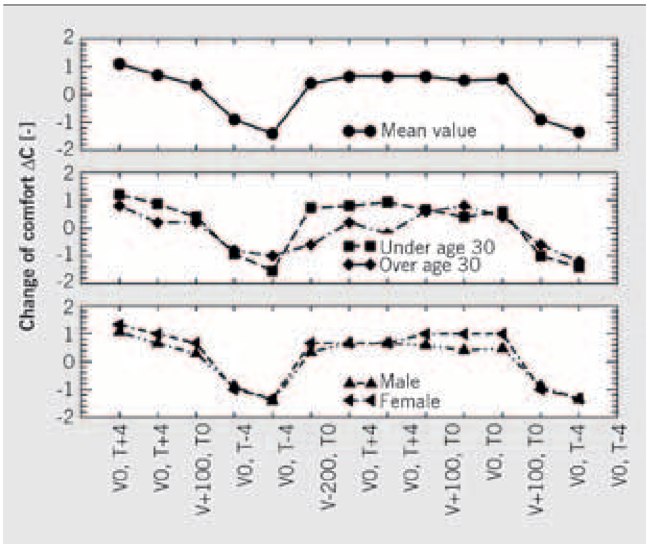

❼ Change of discomfort ΔC for different changes of temperature and volume flows for foam 1, test procedure 2

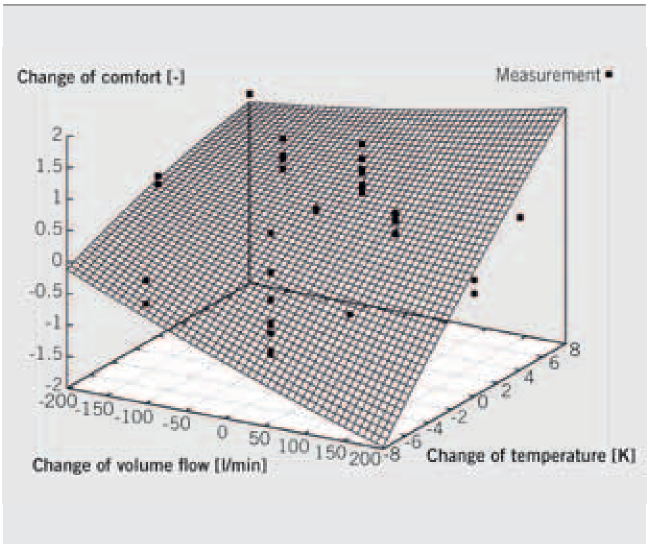

❽ Experimental results for all foams and procedures

the discomfort behavior is independent of the age of the test persons. A comparison of the male and female test persons show a few differences regarding the absolute value but not in respect of the trends. ❼ shows the identical graphs for foam 1 but using the slightly modified test procedure 2. The same experimental findings can be obtained whereas the differences between male and female test persons are smaller than for procedure 1. Test procedure 2 uses a test point with no modification of temperature and mass flow giving a value of 0.5. Therefore the experimental results in a range of ±0.5 can be regarded as identical. ❽ shows the 3D visualization of all experiments showing the identical tendencies, i.e.:

: dominating effect on a positive ΔC is an increase of temperature
: lower volume flows lead to an increase of ΔC
: no influence of the age of the test persons
: no influence of foam
: no influence of sex of the test persons.

The values for the change of discomfort ΔC can be approximated by a quadratic function, Eq. 15, leading to a set of coefficients ai shown below:

$a_0 = 0{,}166932$
$a_1 = 0{,}146816\ K^{-1}$
$a_2 = -0{,}00171476\ K^{-2}$
$a_3 = -0{,}00122757\ min \cdot l^{-1}$
$a_4 = 1{,}88203 \cdot 10^{-6}\ min^2 \cdot l^{-2}$
$a_5 = 0{,}000424689\ min \cdot l^{-1} \cdot K^{-1}$.

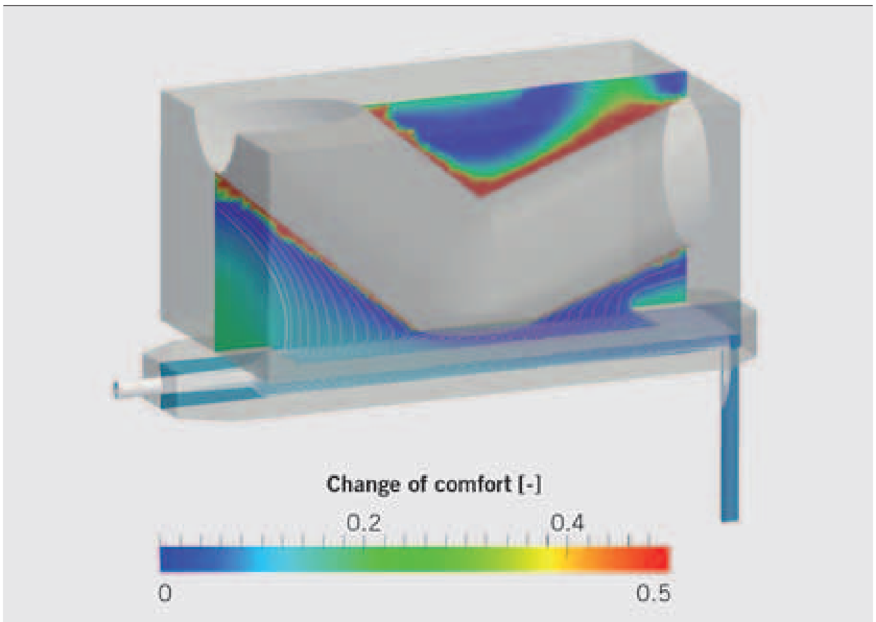

❾ Streamlines and discomfort ΔC in cross section of the armrest

These values are the basis of correlating the flow properties (velocity, temperature) obtained in CFD simulations to changes of the discomfort behavior.

GL. 15	$\nabla C = a_0 + a_1 \cdot T + a_2 \cdot T^2 + a_3 \cdot \dot{V} + a_4 \cdot \dot{V}^2 + a_5 \cdot \dot{V} \cdot T$

4 NUMERICAL RESULTS

❾ shows the streamlines and the change of discomfort ΔC in the simulation model using the parameters for the foam 1 and a volume flow of 200 l/min and a temperature of 27 °C at the inlet. By evaluating the discomfort behavior the flow and temperature distributions can be changed to optimize the virtual prototype.

5 CONCLUSIONS

A simulation environment was developed to predict the discomfort behavior in virtual prototypes for armrests. A coupled solution of the structural behavior of the foam structure and the fluid flow allows the determination of the local conditions. The discomfort behavior is estimated by a correlation matrix of experimental values. Extensive experiments were made to gain the correlation matrix for the discomfort behavior which could be given as a function of velocity and volume flow. In further steps, this method will be extended to other applications where a contact between a body and a support takes place.

REFERENCES

[1] Murphy, T.; Oliver, M. L.: Development and design of a dynamic armrest for hydraulic-actuation joystick controlled mobile machines. In: Applied Ergonomics 39 (2008), Nr. 3, S. 316-324

[2] Catalina, T.; Virgone, J.; Kuznik, F.: Evaluation of thermal comfort using combined CFD and experimentation study in a test room equipped with a cooling ceiling. In: Building and Environment 44 (2009), Nr. 8, S. 1740-1750

[3] Tanabe, S.; Kobayashi, K.; Nakano, J.; Ozeki, Y.; Konishi, M.: Evaluation of thermal comfort using combined multi-node thermoregulation (65MN) and radiation models and computational fluid dynamics (CFD). In: Energy and Buildings 34 (2002), Nr. 6, S. 637-646

[4] Lin, Z.; Chow, T. T.; Fong, K. F.; Wang, Q.; Li, Y.: Comparison of performances of displacement and mixing ventilations. Part I: thermal comfort. In: International Journal of Refrigeration 28 (2005), Nr. 2, S. 276-287

[5] Mezrhab, A.; Bouzidi, M.: Computation of thermal comfort inside a passenger car compartment. In: Applied Thermal Engineering 26 (2006), Nr. 14-15, S. 1697-1704

[6] Zhang, H.; Dai, L.; Xu, G.; Li, Y.; Chen, W.; Tao, W.: Studies of air-flow and temperature fields inside a passenger compartment for improving thermal comfort and saving energy. Part II: Simulation results and discussion. In: Applied Thermal Engineering 29 (2009), Nr. 10, S. 2028-2036

[7] Cengiz, T. G.; Babalik, F. C.: An on-the-road experiment into the thermal comfort of car seats. In: Applied Ergonomics 38 (2007), Nr. 3, S. 337-347

[8] Zhang, H.; Arens, E.; Huizenga, C.; Han, T.: Thermal sensation and comfort models for non-uniform and transient environments: Part I: Local sensation of individual body parts. In: Building and Environment 45 (2010), Nr. 2, S. 380-388

[9] Fiala, D.: Dynamic Simulation of Human Heat Transfer and Thermal Comfort, Leicester, De Montfort University, PhD Thesis, 1998

[10] Zhang, L.; Helander, M. G.; Drury, C. G.: Identifying Factors of Comfort and Discomfort in Sitting. In: Human Factors 38 (1996), Nr. 3, S. 377-389

THANKS

The financial support of the Federal Ministry of Economics and Technology is gratefully acknowledged. We want to thank the Arbeitsgemeinschaft industrieller Forschungsvereinigungen (AIF), Berlin for the support during the project.

The support of Dipl.-Ing. (FH) Andreas Grimm, Dipl.-Ing. (FH) Dietmar Ingelfinger, Dipl.-Ing. (BA) Andreas Albert, Dipl.-Ing. (FH) Klaus Schächtele and Dipl.-Ing. (FH) Peter Gratz of Gratz Engineering GmbH in Weinsberg is gratefully acknowledged. The support of the president of the Baden-Wuerttemberg Cooperative State University Mosbach Prof. Geilsdörfer, Andreas Lang, Dipl.-Ing. (BA) Achim Hantschel and Dipl.-Ing. Marius Friedrich is gratefully acknowledged.

Finally, we want to thank Dr.-Ing. Klaus Mager, Mager Consultants, Bad Dürrheim for the administrative support.

AUTHORS

UNIV.-PROF. DR.-ING. LUTZ ECKSTEIN is Head of the Institut für Kraftfahrzeuge (ika) at RWTH Aachen University (Germany).

DIPL.-ING. RENÉ GÖBBELS is Scientific Assistant in the Body Department of the Institut für Kraftfahrzeuge (ika) at RWTH Aachen University (Germany).

DR.-ING. MARTIN GOEDE is Head of the Vehicle Lightweight Design at Volkswagen Group Research in Wolfsburg (Germany) and Chairman of the FAT Research Group "Lightweight Design".

DIPL.-ING. TINO LAUE is Project Manager for Vehicle Lightweight Design and Energy Efficiency at Volkswagen Group Research in Wolfsburg (Germany).

DIPL.-ING. DIPL.-WIRT.-ING. ROLAND WOHLECKER is Teamleader Structural Analysis and Benchmarking of the Forschungsgesellschaft Kraftfahrwesen mbH Aachen (fka) (Germany).

ANALYSIS OF SECONDARY WEIGHT REDUCTION POTENTIALS IN VEHICLES

The research project, which is supported by the Forschungsvereinigung für Automobiltechnik (FAT), contains the development of a classification system for the analytical determination of the secondary weight reduction in vehicles. Based on defined selection criteria, all components with weight reduction potential of the vehicle areas body, drive train, chassis, electronics and interior are identified at first. Based on this, empirical and analytical relationships between component properties and weights are developed for the calculation of the secondary weight reduction.

THE SEAL OF APPROVAL FOR SCIENTIFIC ARTICLES IN ATZ.
ATZ PEER REVIEW
RECEIVED 2010-06-08
REVIEWED 2010-07-04
ACCEPTED 2010-08-23
REVIEWED BY EXPERTS FROM RESEARCH AND INDUSTRY.

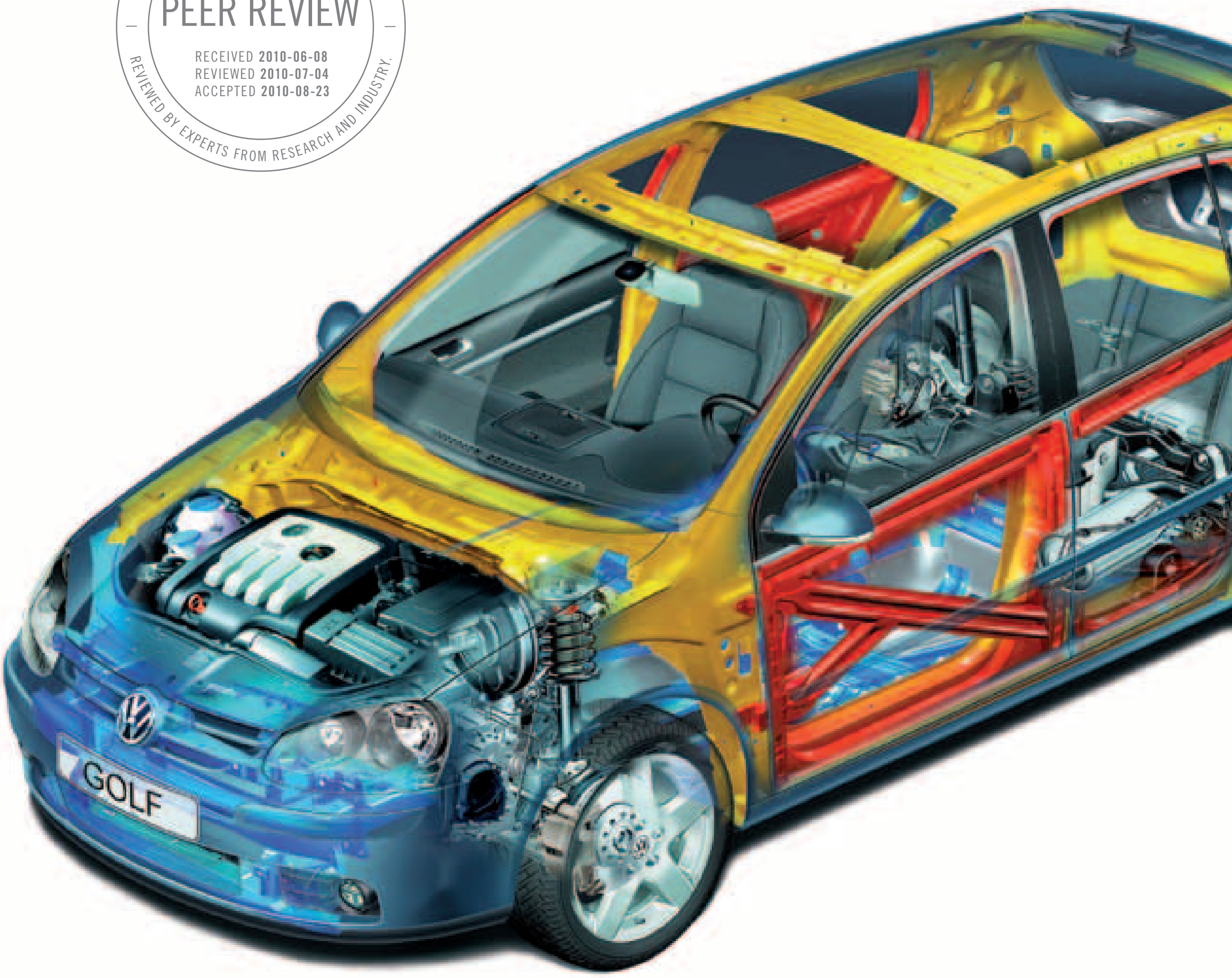

1 INTRODUCTION
2 IDENTIFICATION OF COMPONENTS WITH SECONDARY WEIGHT REDUCTION POTENTIALS
3 ANALYSIS OF THE SECONDARY WEIGHT REDUCTION OF THE BODY
4 ANALYSIS OF THE SECONDARY WEIGHT REDUCTION OF THE DRIVE TRAIN
5 ANALYSIS OF THE SECONDARY WEIGHT REDUCTION OF THE CHASSIS
6 APPLICATION OF THE SYSTEMATIC
7 SUMMARY

1 INTRODUCTION

The efficient use of existing energy resources and the associated resource conservation represent a major challenge for the automotive industry. In this context, the reduction of fuel consumption and CO_2 emissions are important objectives. In addition to the aspects drive train optimisation and energy management, the automotive lightweight design contributes to the reduction of CO_2. The weight of individual components can be reduced by different lightweight design measures such as material, concept or manufacturing lightweight design. The use of these primary measures enables to perform additional secondary measures for weight reduction. Within the scope of these measures, for example, the drive train, the brakes, the tank system etc. can be adapted in its dimensions to keep the properties of the entire vehicle on a comparison level.

2 IDENTIFICATION OF COMPONENTS WITH SECONDARY WEIGHT REDUCTION POTENTIALS

The components of the vehicle areas body, drive train, chassis, interior and electronics have to meet different requirements and layout criteria. One requirement of the drive train components consists, e. g., in transferring the driving power or the driving torque to the wheels. By reducing the torque, it is possible to optimize the dimensions of the engine speed converter, the torque converter, the transfer gearbox and of the drive shaft. At the same time, a decrease of the driving power leads to a reduction of fuel consumption, which leads to the downsizing of the fuel tank at constant range.

The layout of the body occurs in consideration of legal crash requirements (e. g. frontal, rear and side crash). Therefore the absorption of the crash energy at a defined intrusion is important. Forces and loads arising during driving operations represent essential variables for the chassis conception, which depends on the gross vehicle weight.

According to that, components whose dimensioning depends on the total vehicle weight, the driving power, the driving torque, the inertia forces, the fuel consumption and the energy absorption,

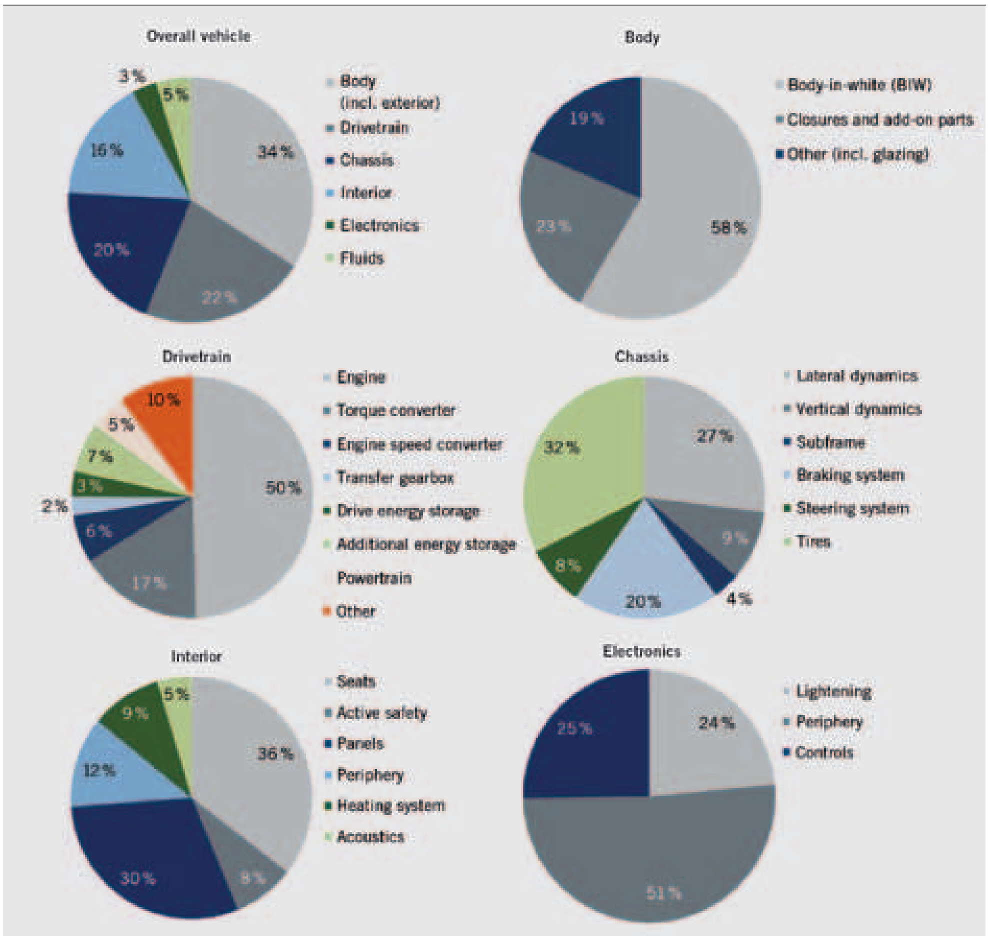

❶ Weight distribution of a compact class vehicle

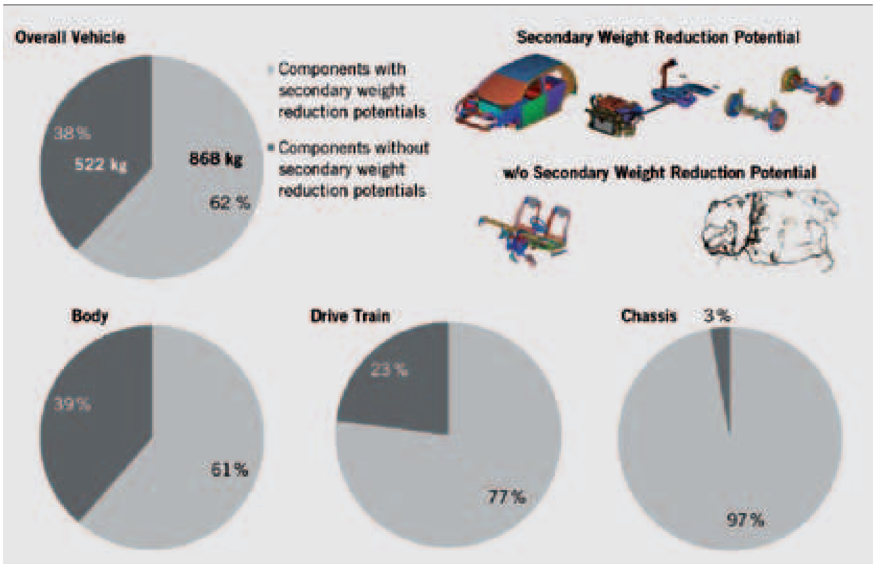

❷ Overview of the vehicle areas with secondary weight reduction potential

have potentials for secondary weight reduction. In consideration of the selection criteria, components of the vehicle areas, shown in ❶, determine the secondary weight reduction potentials, ❷. Thus the vehicle areas electronics and interior do not have any secondary weight reduction potentials.

3 ANALYSIS OF THE SECONDARY WEIGHT REDUCTION OF THE BODY

The secondary weight reduction potential of the body is determined by FE-simulations. For it a reference model based on a VW Golf V is used. For the analysis of the crash behaviour, the load cases EuroNCAP frontal and side impact as well as a rear impact in accordance to FMVSS 301 are conducted, ❸.

For the determination of the secondary weight reduction, body components with the highest energy absorption are determined. With the assumption of a primary weight reduction of 100 kg, the sheet metal thicknesses of these body components are reduced until reaching the same crash properties of the reference vehicle and the primarily 100 kg weight-reduced vehicle in terms of constant component intrusions.

During the EuroNCAP frontal impact, 20 % of the kinetic energy is absorbed by the upper and lower longitudinal beams as well as the bumper system. The component weights of the right and left longitudinal beams (above and down), the right and left crash boxes and the front cross member can be reduced from 19.97 kg to 12.82 kg at identical intrusions, ❹.

At the EuroNCAP side impact with deformable barrier, a total of 26 % of the introduced kinetic energy is absorbed by the external and internal B-pillar, the sill, the side panel, the seat cross members and the floor. By a reduction of the vehicle weight of 100 kg, the weight of these body components can be reduced from 58.2 kg to 57.26 kg, ❺.

During the rear impact with rigid barrier in accordance to FMVSS 301, 54 % of the introduced kinetic energy is absorbed by the rear longitudinal beams, the rear bumper system and the rear floor. The weight of these body components can be lowered by primary weight reduction from 28.47 kg to 26.95 kg, ❻. For a vehicle with a kerb weight of 1390 kg, the weight of the body can secondarily be reduced by 9.61 kg, if a primary weight reduction of 100 kg is considered.

4 ANALYSIS OF THE SECONDARY WEIGHT REDUCTION OF THE DRIVE TRAIN

The dimensioning of the individual assemblies of the drive train (engine, torque converter, engine speed converter, transfer gearbox, additional energy storage (AES) and power train) depends primarily on the

❸ Reference model and relevant crash load cases [1, 2, 3]

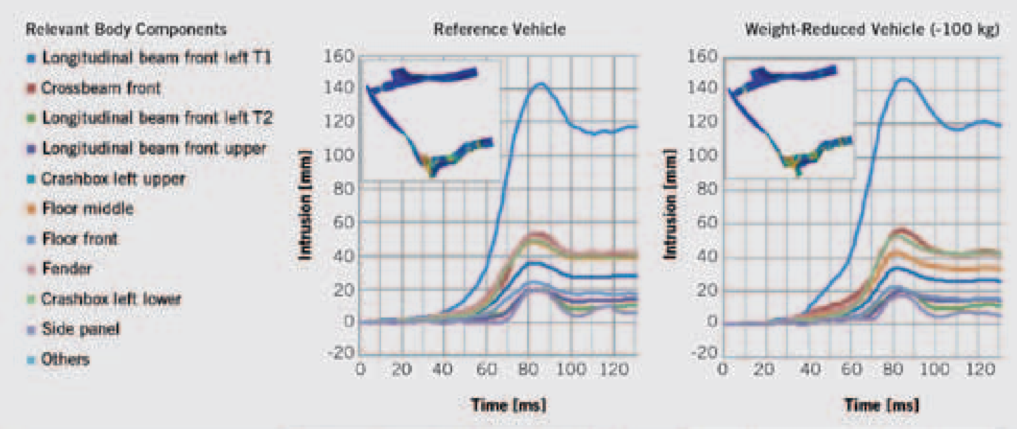

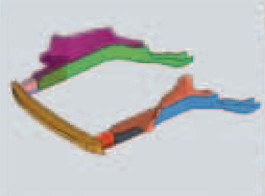

Component	Weight [kg]		Component	Weight [kg]
Longitudinal beam (r.)	7.31	-7.15 kg	Longitudinal beam (r.)	4.78
Longitudinal beam (l.)	7.29		Longitudinal beam (l.)	4.71
Crashbox (r.)	0.61		Crashbox (r.)	0.34
Crashbox (l.)	0.61		Crashbox (l.)	0.34
Crossbeam	4.15		Crossbeam	2.65

❹ Secondary weight reduction potentials in the front structure (frontal impact)

driving power and the driving torque. The layout of the individual assemblies of the drive train therefore requires the knowledge of the driving torque, which results from the driving resistances. The NEDC (without gradient resistance) represents the basis of the calculation. The driving resistances can thus be calculated in accordance with Eq. 1.

EQ. 1
$$P_{Bed} = (F_R + F_L + F_B) \cdot v_{Fzg} = F_{Bed} \cdot v_{Fzg}$$

Taking into account the speed-torque characteristics of the engine, the gearbox ratio (i_n) and the differential ratio (i_{Diff}), the following relation for engine speed, driving torque and vehicle speed can be defined:

EQ. 2
$$n_{Antr.} = \frac{v_{Fzg} \cdot i_n \cdot i_{Diff}}{2\pi \cdot r_{dyn}} = \frac{P_{Antr.}}{2\pi \cdot M_{Antr.}}$$

As a basis for determining the secondary weight reduction, it is assumed that the reference vehicle and the 100 kg weight-reduced vehicle have equal handling characteristics in terms of constant accelerations. Thereby, the available excess power shall be used

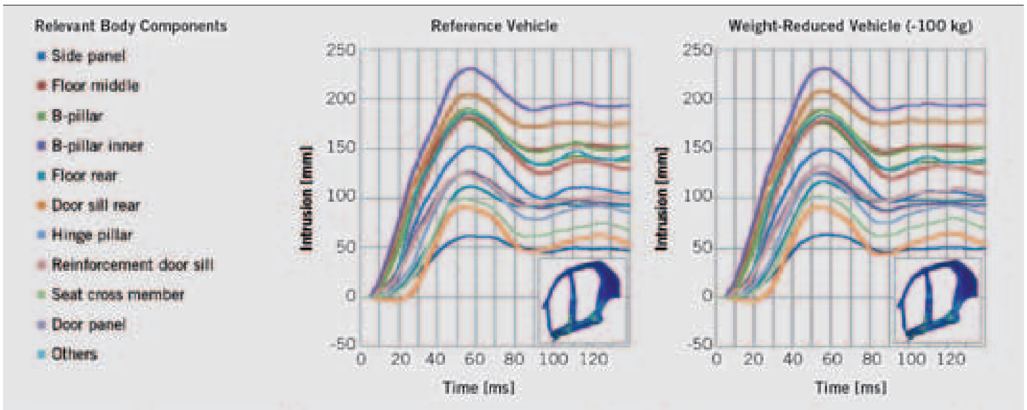

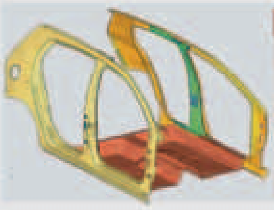

Component	Weight [kg]		Component	Weight [kg]
B-pillar (r.)	10.37	-0.94 kg	B-pillar (r.)	10.67
B-pillar (l.)	10.37		B-pillar (l.)	10.67
Side panel (r.)	11.35		Side panel (r.)	11.04
Side panel (l.)	11.43		Side panel (l.)	11.12
Floor (middle)	14.68		Floor (middle)	13.76

❺ Secondary weight reduction potentials in the passenger cell (side impact)

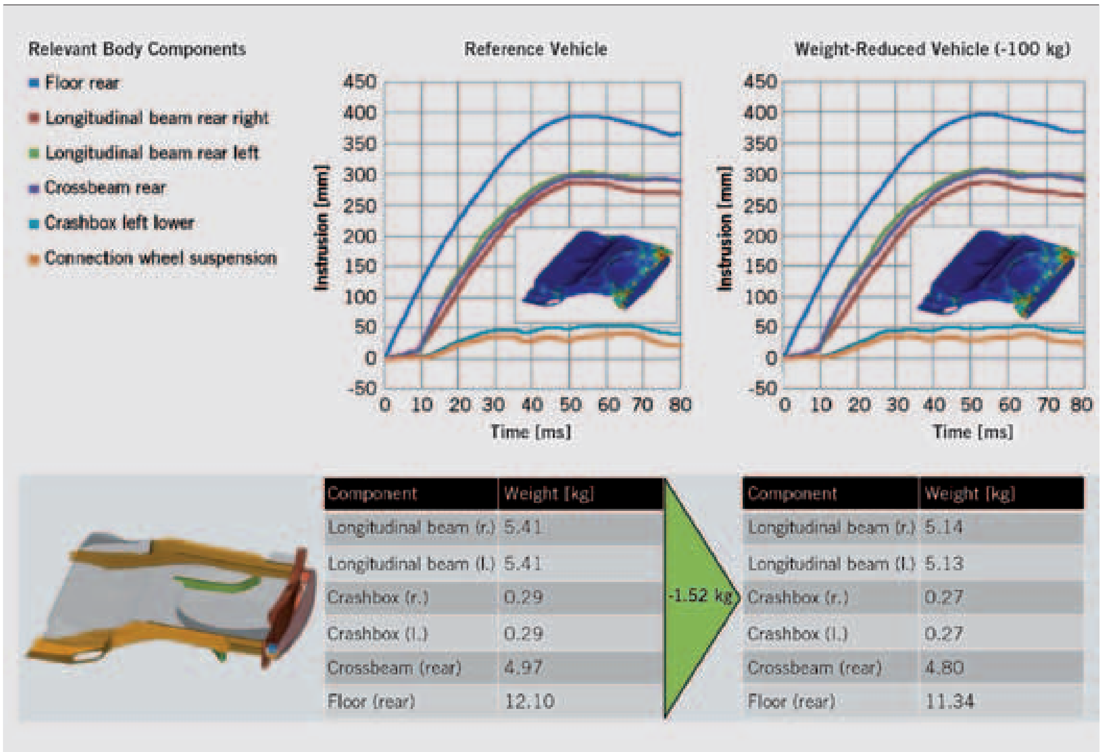

❻ Secondary weight reduction potentials in the rear structure (rear impact)

completely for the acceleration of the vehicle. Taking into account the primary weight reduction and constant accelerations, a new engine map can be calculated for the weight-reduced vehicle, ❼. Considering the NEDC operation, the resulting difference between the driving torques of the reference and the weight-reduced vehicle can be determined as the basis for the layout of the drive train components, Eq. 2.

For the dimensioning of the torque converter (manual five- and six-speed transmission), the shaft centre distance between the gearbox input shaft (GIS) and output shaft (GOS) is calculated based on the ratio of the first gear and the constant gearbox layout factors Z_i and K_i, Eq. 3. The gear wheel ratios are determined depending on the gearbox-ratio spread $i_{G,ges}$ with the help of the progressive ratio φ_1 and the progression factor φ_2, Eq. 4 and Eq. 5.

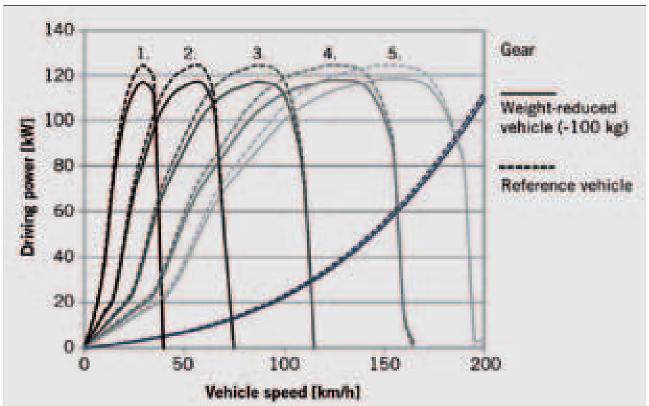

❼ Determination of the driving-power difference

Based on the calculated ratios, gear wheel ($d_{z,n}$) and pinion diameters ($d_{r,n}$) can be determined, Eq. 6 and Eq. 7.

EQ. 3

$$a = \sqrt[3]{\frac{M_{Antr.}\cdot(i_1+1)^4}{4\cdot i_1\cdot\frac{b}{d_1}}}\cdot\sqrt[3]{\frac{(Z_{B/D}Z_HZ_EZ_\varepsilon Z_\beta S_H)^2\cdot(K_AK_VK_{H\beta}K_{H\alpha})}{(\sigma_{H.lim}Z_{NT}Z_LZ_RZ_VZ_WZ_X)^2}}$$

EQ. 4

$$\varphi_1 = \sqrt[z-1]{\frac{i_{G,ges}}{\varphi_2^{0.5\cdot(z-1)\cdot(z-2)}}}$$

EQ. 5

$$i_n = i_z\cdot\varphi_1^{(z-n)}\cdot\varphi_2^{0.5\cdot(z-n)\cdot(z-n-1)}$$

EQ. 6

$$d_{r,n} = \frac{2\cdot a}{1+i_n}$$

EQ. 7

$$d_{z,n} = (2\cdot a) - d_{r,n}$$

The gearbox length is calculated by the summation of the widths and the number of the gear wheels ($b_{r,i}$ respectively (z+1)), the bearings (b_L respectively A_L) and detents (b_{SK} respectively B_S), Eq. 8.

On this basis, the calculation of the gearbox housing (diameter d) takes place, for which a hollow cylinder with a constant thickness of 11 mm is assumed, Eq. 9. Afterwards the determination of the component weights of the gear wheels and the gear shafts are conducted (e. g. for the pinions of the gears, Eq. 10).

Including other component weights (e. g. electronics, gear shift control etc.), the total weight of the torque converter is calculated under summation of the individual component weights.

EQ. 8	$l = \left((z+1) \cdot b_{r,i}\right) + (A_L \cdot b_L) + (B_S \cdot b_{Sk})$

EQ. 9	$d = a + 0.5 \cdot d_{r,1} + 0.5 \cdot d_{z,1}$

EQ. 10	$G_{r,i} = (d_{r,i}^{\,2} - d_{GEW,min}^{\,2}) \cdot \frac{\pi}{4} \cdot b_{r,i} \cdot \rho_{Stahl}$

For the dimensioning of the transfer gearbox, it is assumed for reasons of simplification that the differential is a gearbox with only one gear ratio. Against this background, the calculation of the differential weight takes place in accordance with Eq. 3 to Eq. 10.

To layout the drive shafts and the cardan shaft, the shafts and joints are regarded separately. With consideration of the ratios i_1 and i_{Diff} as well as the torsion fatigue strength $\tau_{b,W}$ and the reliability factor S_{AW} and S_{KW}, the calculation of the shaft diameter depends on the amount of the driving torque to be transferred, Eq. 11 and Eq. 12. It is taken into account that the drive shaft is designed as solid shaft and the cardan shaft generally as hollow shaft with the thickness t_{KW}. Therefore a value of 3 mm is accepted.

EQ. 11	$d_{AW} \geq \sqrt[3]{\frac{16 \cdot S_{AW} \cdot M_{Antr.} \cdot i_1 \cdot i_{Diff}}{\pi \cdot \tau_{b,W}}}$

EQ. 12	$t_{KW} \cdot d_{KW} \geq \frac{2 \cdot S_{KW} \cdot M_{Antr.} \cdot i_1}{\pi \cdot \tau_{b,W}}$

The weight of the drive and cardan shaft is the result of the diameter in combination with the respective lengths l_{AW} and l_{KW}, which depends on the vehicle package. It has to be considered that, based on real vehicle data, for the joints of the drive and cardan shafts, a total weight of 1.5 kg respectively 4 kg has to be added to Eq. 13 and Eq. 14.

EQ. 13	$G_{AW} = l_{AW} \cdot \pi \cdot \left(\frac{d_{AW}}{2}\right)^2 \cdot \rho_{Stahl}$

EQ. 14	$G_{KW} = l_{KW} \cdot \pi \cdot \left(\left(\frac{d_{KW}}{2}\right)^2 - \left(\frac{d_{KW}}{2} - t_{KW}\right)\right) \cdot \rho_{Stahl}$

For the dimensioning of the engine, the engine speed converter, the cooling system, the fluids and the AES, empirical relations for the component weight are defined depending on the driving torque by means of approx. 100 real vehicle specifications.

For the engine, there is a relation between the driving torque and the engine weight G_{AEW} as shown in Eq. 15. Thereby the assemblies, shown in ❽, are considered.

EQ. 15	$G_{AEW} = 0.2998 \cdot M_{Antr.} + 59.24$

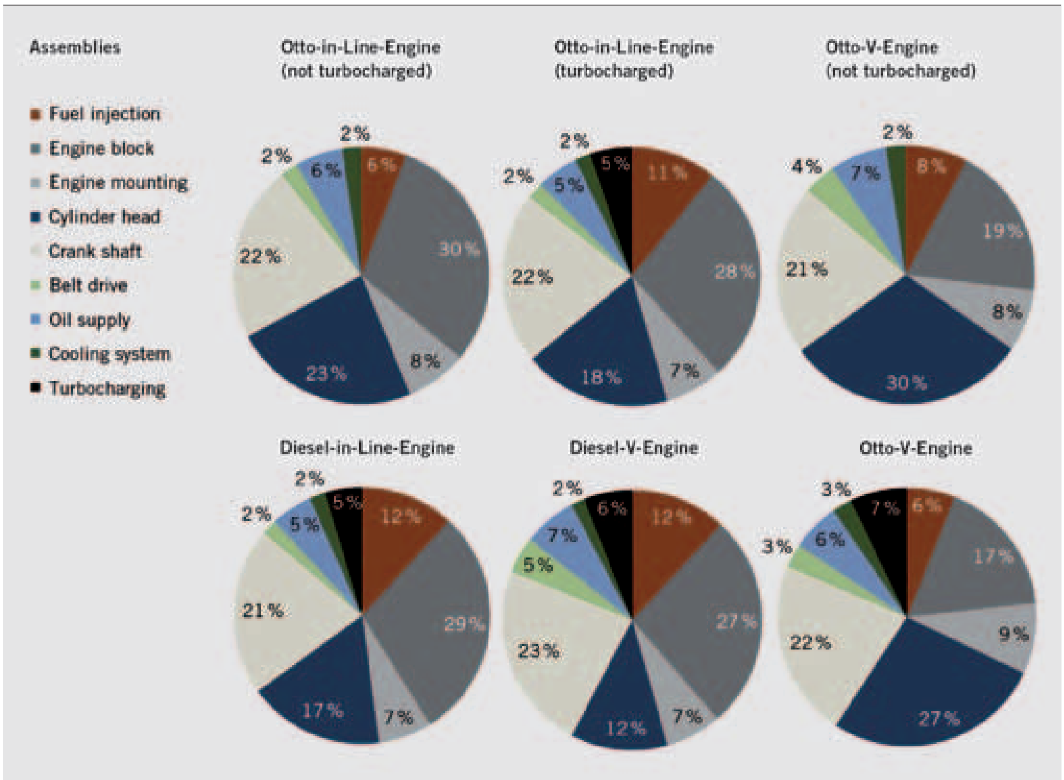

❽ Weight distribution of the individual assemblies of the engine

With regard to the engine speed converter, the assemblies flywheel (SR), clutch pressure plate (KDP) and clutch disc (KS) are considered. The component weight can be determined according to Eq. 16 to Eq. 18.

EQ. 16
$$G_{DZW,SR} = 0.0309 \cdot M_{Antr.} + 3.5157$$

EQ. 17
$$G_{DZW,KS} = 0.001 \cdot M_{Antr.} + 0.792$$

EQ. 18
$$G_{DZW,KDP} = 0.0098 \cdot M_{Antr.} + 1.8785$$

The dimensioning of the AES depends on the resisting torque of the engine during the starting process and the number of auxiliary consumers. Thereby, the starter battery weight increases almost linearly with the increasing driving torque respectively the engine weight, and increasing number of auxiliary consumers. For Otto and Diesel engines, the weight of the starter battery can be empirically determined according to Eq. 19 and Eq. 20.

EQ. 19
$$G_{ZES,OM} = 0.1298 \cdot G_{AEW} + 1.2152$$

EQ. 20
$$G_{ZES,DM} = 0.0935 \cdot G_{AEW} + 4.872$$

The weight of the cooling system G_K, consisting of the assemblies cooler, cooling hoses above and below as well as fan and fan motor, the empirical relation between driving torque and weights is given by Eq. 21. The weight of the fluids (engine oil (MÖ) and cooling water (KW)) can be calculated according to Eq. 22 and Eq. 23.

EQ. 21
$$G_K = 0.0177 \cdot M_{Antr.} + 2.6902$$

EQ. 22
$$G_{F,KW} = 0.0171 \cdot M_{Antr.} + 2.2155$$

EQ. 23
$$G_{F,MÖ} = 0.0092 \cdot M_{Antr.} + 1.8953$$

The size of the drive energy storage is determined at defined range by the vehicle consumption. Thus, the calculation of the fuel consumption is necessary in order to determine the size of the fuel tank. The Willans methodology [4] is chosen for the estimation of consumption. This assumes that the fuel consumption of a vehicle can be divided into the parts zero-power consumption V_{Null} and effective power consumption V_{Pe}, Eq. 24.

EQ. 24
$$V = V_{Null} + V_{P_e}$$

The zero-power consumption can be calculated using Eq. 25. The constants a_V, b_V and c_V for Otto engines are 0.076, 0.17 and 0.2 and for Diesel engines 0.08, 0.075 and 0.1. V_H represents the engine capacity and v_{Fzg} the vehicle speed.

EQ. 25
$$V_{Null} = \left(a_V \cdot \frac{v_{Fzg}^2}{v_{1000}^2} + b_V \cdot \frac{v_{Fzg}}{v_{1000}} + c_V \right) \cdot V_H$$

The consumption share V_{Pe} can be calculated with Eq. 26. For the constant coefficient z_{Pe}, a value of 0.264 l/kWh can be assumed for Otto engines and 0.208 l/kWh for diesel engines.

EQ. 26
$$V_{P_e} = z_{P_e} \cdot P_e$$

Given that the fuel tank volume $V_{KT,Ref.}$ is known, the range of the reference vehicle $S_{Ref.}$ can be calculated via the fuel consumption $V_{Ref.}$ and the average speed of the NEDC Δv_{NEDC} as shown in Eq. 27. The fuel tank volume of the weight-reduced vehicle results according to Eq. 28. The weight of the fuel tank can be calculated with Eq. 29.

EQ. 27
$$S_{Ref.} = \frac{V_{KT,Ref.}}{V_{Ref.}} \cdot \Delta v_{NEDC}$$

EQ. 28
$$V_{KT,gew.red.} = \frac{V_{gew.red.} \cdot S_{Ref.}}{\Delta v_{NEDC}}$$

EQ. 29
$$G_{KT} = 2.1942 \cdot e^{0{,}0227 \cdot V_{KT}}$$

5 ANALYSIS OF THE SECONDARY WEIGHT REDUCTION OF THE CHASSIS

The dimensioning of the chassis (lateral dynamics, vertical dynamics, subframe, braking system and steering system) depends primarily on the gross vehicle weight. The gross vehicle weight subsequently serves as input for the layout of the chassis components.

The lateral dynamics covers all components which are responsible for the wheel guidance of the vehicle. The front axle (McPherson) and the rear axle (control blade suspension) are regarded separately. FE-simulations are performed for the analysis of the secondary weight reduction. On the basis of the simulation results of the reference vehicle, all loads and stiffnesses are reduced by 10 %. Subsequently, an adjustment of the sheet metal thicknesses takes place until the stress of the components of the reference vehicle correspond to those of the weight-reduced vehicle. ❾ shows that with a primary weight reduction of 100 kg, the weight of the front and rear axle can be reduced by 0.92 kg.

The vertical dynamics comprises the components spring and damper. In the following, wheel-guiding spring/damper systems (McPherson struts) for the front axle (VA) and non-wheel-guiding systems for multi-link axles for the rear axle (HA) are regarded. Depending on the gross vehicle weight, based on the component weights of more than 100 real vehicles, the following empirical correlations are defined for the weight of the vertical dynamics, Eq. 30 and Eq. 31. The weight of the rear subframe $G_{SF,HA}$ is determined according to Eq. 32.

EQ. 30	$G_{VD,VA} = 0.0031 \cdot G_{Fzg.,zul.} + 1.7258$

EQ. 31	$G_{VD,HA} = 0.0045 \cdot G_{Fzg.,zul.} - 3.9097$

EQ. 32	$G_{SF,HA} = 0.0113 \cdot G_{Fzg.,zul.} - 3.141$

The starting point for the calculation of the breaking system is the definition of the braking distance s at 100 km/h and the resulting deceleration a_{Br}, Eq. 33. The braking distance is constant for the reference vehicle and the weight-reduced vehicle.

EQ. 33	$a_{Br} = 0.5 \cdot \frac{\Delta v^2}{s_{100km/h}}$

Afterwards, the wheel loads of the front ($F_{R,Z,v}$) and rear axle ($F_{R,Z,h}$) are determined with the help of the mean deceleration and the vehicle centre of gravity. l designates the wheel base, h the height of the centre of gravity as well as l_h and l_v the distance between the centre of gravity and the rear respectively the front axle, Eq. 34 and Eq. 35.

EQ. 34	$F_{R,Z,v} = \frac{G_{Fzg.,zul.} \cdot g \cdot \frac{l_h}{l} + G_{Fzg.,zul.} \cdot a_{Br,100km/h} \cdot \frac{h}{l}}{2}$

EQ. 35	$F_{R,Z,h} = \frac{G_{Fzg.,zul.} \cdot g \cdot \frac{l_v}{l} + G_{Fzg.,zul.} \cdot a_{Br,100km/h} \cdot \frac{h}{l}}{2}$

Taking into account the coefficient of static friction of the street μ_{Str}, the maximum braking power at the front $F_{Br,v}$ and at the rear wheel $F_{Br,h}$ can be calculated using Eq. 36 and Eq. 37.

EQ. 36	$F_{Br,v} = \mu_{Str.} \cdot F_{R,Z,v}$

EQ. 37	$F_{Br,h} = \mu_{Str.} \cdot F_{R,Z,h}$

Assuming a known effective diameter of the break disc in the front $D_{Br,S,v}$ and in the rear $D_{Br,S,h}$ as well as a dynamic wheel radius r_{dyn} of the reference vehicle, the braking power at the effective diameter in the front $F_{Br,S,v}$ and in the rear $F_{Br,S,v}$ can be calculated as follows:

EQ. 38	$F_{Br,S,v} = F_{Br,v} \cdot \frac{2 \cdot r_{dyn}}{D_{Br,S,v}}$

EQ. 39	$F_{Br,S,h} = F_{Br,h} \cdot \frac{2 \cdot r_{dyn}}{D_{Br,S,h}}$

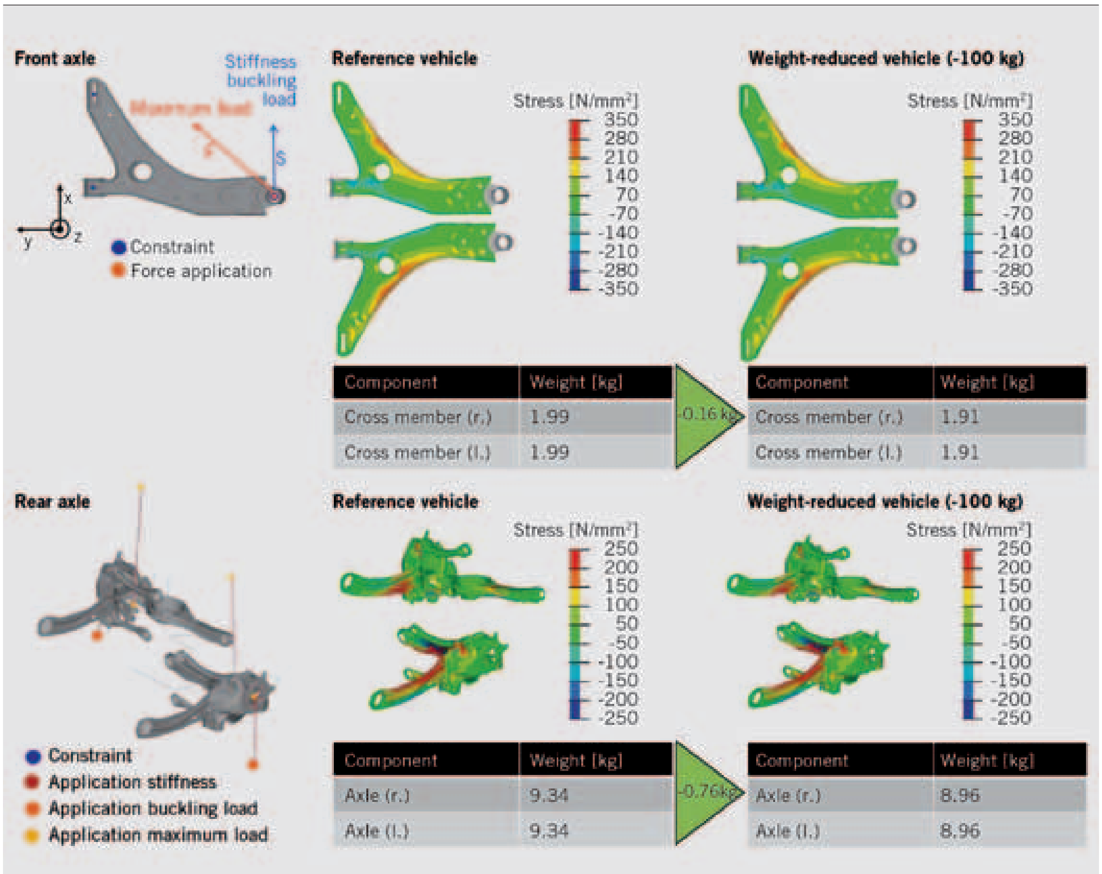

9 Secondary weight reduction potentials of the assembly lateral dynamics (chassis)

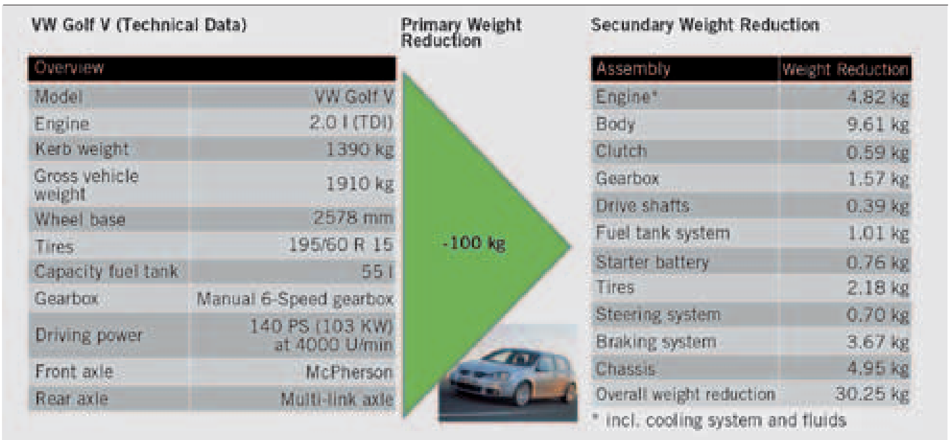

Overview	
Model	VW Golf V
Engine	2.0 l (TDI)
Kerb weight	1390 kg
Gross vehicle weight	1910 kg
Wheel base	2578 mm
Tires	195/60 R 15
Capacity fuel tank	55 l
Gearbox	Manual 6-Speed gearbox
Driving power	140 PS (103 KW) at 4000 U/min
Front axle	McPherson
Rear axle	Multi-link axle

Assembly	Weight Reduction
Engine*	4.82 kg
Body	9.61 kg
Clutch	0.59 kg
Gearbox	1.57 kg
Drive shafts	0.39 kg
Fuel tank system	1.01 kg
Starter battery	0.76 kg
Tires	2.18 kg
Steering system	0.70 kg
Braking system	3.67 kg
Chassis	4.95 kg
Overall weight reduction	30.25 kg

* incl. cooling system and fluids

⑩ Secondary weight reduction potentials (VW Golf V)

In the following, it is assumed that the braking power at the effect diameter of the weight-reduced vehicle matches in the front and in the rear to the one of the reference vehicle.

At a constant, dynamic wheel radius r_{dyn}, the effective diameter of the brake disc in the front $D_{Br,S,v,gew.red}$ and in the rear $D_{Br,S,h,gew.red}$ is calculated at constant braking acceleration a_{Br} and adapted wheel loads according to Eq. 40 and Eq. 41.

EQ. 40
$$D_{Br,S,v,gew.red.} = F_{Br,v,gew.red.} \cdot \frac{2 \cdot r_{dyn}}{F_{Br,S,v}}$$

EQ. 41
$$D_{Br,S,v,gew.red.} = F_{Br,v,gew.red.} \cdot \frac{2 \cdot r_{dyn}}{F_{Br,S,h}}$$

As shown in Eq. 42 to Eq. 45, the weight of the brake discs is determined depending on the diameter by means of real vehicle data.

EQ. 42
$$G_{FW,Br,S,innenbel.,v} = 0.5443 \cdot e^{0.0089 \cdot D_{Br,S,außen,v,i}}$$

EQ. 43
$$G_{FW,Br,S,massiv,v} = 0.0554 \cdot D_{Br,S,außen,v,i} - 9.7911$$

EQ. 44
$$G_{FW,Br,S,innenbel.,h} = 0.0008 \cdot D_{Br,S,außen,h,i}^{1.5745}$$

EQ. 45
$$G_{FW,Br,S,massiv,h} = 0.0238 \cdot D_{Br,S,außen,h,i} - 2.0143$$

According to Eq. 46, the layout of the steering system takes place basing on an empirical correlation between the gross vehicle weight and the steering system weight for over 100 real vehicles.

EQ. 46
$$G_{LS} = 0.006 \cdot G_{Fzg.,zul.} + 10.923$$

6 APPLICATION OF THE SYSTEMATIC

For the VW Golf V with an unloaded weight of 1390 kg, represented in ⑩, a potential secondary weight reduction of 30.25 kg in the case of a primary weight reduction of 100 kg can be assumed. By taking into consideration the iteration loops, a maximum secondary weight reduction of 45.54 kg is possible.

Within the scope of a fuel consumption simulation, it is determined that the fuel consumption can be lowered from 5.87 l/100 km to 5.68 l/100 km by using primary measures. In consideration of the secondary weight reduction, a consumption of 5.66 l/100 km is possible. Thus, the CO_2 emissions can be lowered from 155.48 g/km to 150.6 g/km respectively 149.99 g/km.

7 SUMMARY

Within the scope of the FAT research project, a methodology was developed for the calculation of the secondary weight reduction. All components in the passenger car with secondary weight saving potentials were identified. Analytical as well as empirical correlations between the component properties and the component weights of the vehicle areas body, chassis and drive train were compiled. FE-simulations were performed to determine the weight reduction of the body and the front and rear axle. For the derivation of empirical formulas, real component weights of over 100 vehicles were considered.

It turned out that with a primary weight reduction of 100 kg, a total of 30.25 kg can secondarily be saved. If iteration loops are taken into account, the secondary weight reduction reaches a maximum of 45.54 kg. The fuel consumption could be reduced by the primary and secondary weight reduction by 0.21 l/100 km and the CO_2 emissions by 5.49 g/km.

REFERENCES

[1] EuroNCAP Frontal Impact Test Protocol. http://www.euroncap.com, February 2010
[2] EuroNCAP Side Barrier Impact Test Protocol. http://www.euroncap.com, February 2010
[3] Federal Motor Vehicle Safety Standards and Regulations – U.S. Department for Transportation – Part 571.301 (rigid barrier). http://www.fmcsa.dot.gov, September 2006
[4] Rhode-Brandenburger, K.: Verfahren zur einfachen und sicheren Abschätzung von Kraftstoffverbrauchspotenzialen. Conference 'Einfluss von Gesamtfahrzeug-Parametern auf Fahrverhalten/Fahrleistung und Kraftstoffverbrauch', Haus der Technik Essen, 19th/20th November 1996